Post-reproductive inhibition of the autophagic vesicle nucleation complex extends *C. elegans* lifespan through the neurons

Dissertation zur Erlangung des Grades

"Doktor der Naturwissenschaften"

am Fachbereich Biologie

der Johannes Gutenberg-Universität in Mainz

Thomas Wilhelm

geb. am 06.01.1985 in Saarbrücken, Deutschland

Mainz, 2017

[redacted]


JG|U
JOHANNES GUTENBERG
UNIVERSITÄT MAINZ


imb
Institut für
Molekulare Biologie

Summary

Autophagy represents an ubiquitous intracellular catabolic process that delivers cytoplasmatic components to the lysosome for degradation. This study shows that key autophagy genes are detrimental in late life and shorten lifespan. This is in stark contrast to previous reports, which linked autophagy almost exclusively to cytoprotective and longevity-promoting effects. While autophagy is still positive in young worms, negative effects were only observed with advanced age. This finding is in accordance with the antagonistic pleiotropy hypothesis of aging, which predicts that some genes mediate beneficial effects early in life when natural selection is strong, but are detrimental late in life when natural selection is weak.

Specifically, post-reproductive inactivation of genes governing the early autophagic step of vesicle nucleation such as *bec-1*, *unc-51* and *epg-8* strongly extend *C.elegans* lifespan. In contrast, no longevity was observed upon post-reproductive inactivation of autophagy flux genes past the step of vesicle nucleation. The here presented data supports an age-related impairment of autophagy, which is likely at the root of its harmful effects in late life.

This study further uncovers that post-reproductive inhibition of autophagosome nucleation extends lifespan primarily through neurons. Notably, this neuronal mediated lifespan extension is accompanied by improved neuronal health, reduced sarcopenia and improved mobility.

The obtained results collectively hold the potential to become paradigm defining in regards to how autophagy modulates health as well as lifespan across aging. Moreover, targeting the process of vesicle nucleation

may prove to be a potential therapeutic avenue in treating humans with age-related neurodegenerative diseases.

Zusammenfassung

Autophagie ist ein ubiquitäres intrazelluläres katabolisches System, das zytoplasmatische Komponenten für den Abbau zum Lysosom liefert. Diese Studie zeigt, dass essentielle Gene der Autophagie im Alter schädlich sind und die Lebenspanne verkürzen. Dies steht im Gegensatz zu früheren Studien, die Autophagie fast ausschließlich mit zytoprotektiven und langlebigkeitsfördernden Effekten verknüpfen. Autophagie hat zwar einen positiven Einfluss auf die Lebensspanne in jungen Würmern, mit fortgeschrittenem Alter sind jedoch negative Effekte festzustellen. Dies stimmt mit der Hypothese der antagonistischen Pleiotropie des Alterns überein, welche besagt, dass hoher Selektionsdruck früh im Leben Allele selektiert, die die Fitness in der Jugend verbessern, aber die Gesundheit und Überlebenschancen im Alter bei geringen Selektionsdruck verschlechtern.

Die hier vorgestellten Ergebnisse zeigen, dass die post-reproduktive Inaktivierung von Genen, welche den frühen autophagischen Schritt der Vesikelnukleation vermitteln (wie *bec-1*, *unc-51* und *epg-8*) , die Lebensspanne stark verlängert. Im Gegensatz dazu hat die post-reproduktive Inaktivierung von Genen, welche Schritte des autophagischen Fluxes nach der Vesikelnukleation kontrollieren, keine positiven Effekte auf die Lebensdauer.

Diese Ergebnisse unterstützen die Hypothese einer altersbedingten Beeinträchtigung der Autophagie, welche wahrscheinlich den negativen Auswirkungen der Autophagie im Alter zugrunde liegt.

Interessanterweise verlängert die post-reproduktive Hemmung der Vesikelnukleation die Lebensdauer primär durch Neuronen, was mit einer Verbesserung des neuronalen Netzwerks, reduzierter Sarkopenie und einer verbesserten Mobilität einhergeht.

Diese neuen Erkenstnisse erweitern unser Verständnis wie Autophagie die Gesundheit und den Alterungsprozess über die Lebensspanne hinweg beeinflusst. Darüber hinaus könnte eine gezielte Inhibierung der autophagischen Vesikelnukleation eine neue Behandlungsmöglichkeit für altersbedingte neurodegenerative Krankheiten im Menschen darstellen.

Preface

The research described in this thesis was conducted at the Institute of Molecular Biology (IMB) in Mainz (Germany) within the working group of Dr Holger Richly. The presented work is my PhD project that I carried out as a student of the International PhD Programme (IPP) on gene regulation, epigenetics, and genome stability that awards the doctoral degree through the Johannes Gutenberg University Mainz.

I have written this thesis independently and without the help of others. The content of this thesis is based solely on experiments that I designed and performed myself unless otherwise indicated. The research presented here was part of a larger study, which was carried out by Jonathan Byrne and myself in the course of our respective PhD studies. Within this larger study, Jonathan and I worked on separate sub-projects that we coordinated in order to build a larger and more comprehensive report that would be suitable for publication in a high-quality scientific journal. Within our separate sub-projects, we independently designed, evaluated, and interpreted our experiments. In order to give the reader a more complete picture and better understanding of the contextual framework of my work, I have also included a few experiments that were carried out by Jonathan Byrne and discussed them within the context of my data. Moreover, I present one figure that was produced under my supervision by Johannes Geisinger in the course of his Master's studies within the working group of Holger Richly. It is indicated within the figure's legend whether the presented data originates from either Jonathan Byrne or Johannes Geisinger. Briefly, the 24-well post-reproductive screen (Figure 18), its validation (Figure 19), timed knockdown of the top candidates *pha-4* and

bec-1 across *C. elegans* lifespan (Figure 20), PHA-4::GFP, as well as BEC-1::RFP western blots to check knockdown efficiency (Figure 24, A and B), and qPCR data to compare *pha-4* and *bec-1* knockdowns in WT and *rrf-3* mutants (Figure 34) originate from Jonathan Byrne. Healthspan scoring of worms with neuron-specific inactivation of *bec-1* (Figure 38) was carried out by Johannes Geisinger.

Table of Contents

List of Abbreviations

AGE-1: ageing alteration-1

AKT-1: serine/threonine kinase 1

AP: antagonistic pleiotropy

ATG-1,2,5, ... : autophagy-related 1,2,5, ...

BCL-2: B-cell lymphoma 2

BEC-1/BECN: beclin-1 orthologs

CDL-1: histone RNA hairpin-binding protein 1

CMA: chaperone-mediated autophagy

CUP-5: coelomocyte uptake-defective 5

cyk-3: cytokinesis defect 3

DAF-2, 16: abnormal dauer formation 2, 16

DCP-66: deacetylase complex protein 66

DMSO: dimethyl sulfoxide

DOT-1.1: DOT1 histone methyltransferase 1.1

DRH-3: dicer related helicase 3

dsRNA: double-stranded RNA

DRO-1: DR1 (One) transcription factor 1

E1-like: ubiquitin-activating enzyme like

E2-like: ubiquitin-conjugating enzyme like

EDTA: ethylenediaminetetraacetic acid

EGO-1: enhancer of glp-1

EGTA: ethylene-bis(oxyethylenenitrilo)tetraacetic acid

EPC-1: enhancer of polycomb-like 1

EPG-5,8: ectopic P granules 5, 8

ER: endoplasmic reticulum

ERI-1: enhanced RNAi

EV: empty vector

FOXA: forkhead box A transcription factor

FuDR: 5-fluorodeoxyuridine

GFP: green fluorescent protein

GNA-2: glucosamine phosphate N-Acetyl transferase 2

HAT: histone acetyltransferase

HDAC: histone deacetylase

HLH-30: helix loop helix 30

HTS: high throughput screening

IGF-1: insulin-like growth factor 1

IPTG: isopropyl β-D-1-thiogalactopyranoside

JMJD-1.1: jumonji (transcription factor) domain protein 1.1

Jnk-1: c-jun N-terminal kinase-1

LC3: microtubule-associated protein light chain 3

LET-363, 716: lethal 363, 716

LGG-1, 2: LC3 ortholog 1, 2

LIN-29: abnormal cell lineage 29

MCOLN1: mucolipin-1

MIG-32: abnormal cell migration 32

MEC-3: mechanosensory abnormality 3

MSP-56, 76: major sperm protein 56, 76

MTL: mean treated lifespan

NA: numerical aperture

NaAz: sodium azide

NRDE-1: nuclear RNAi defective 1

NTL-9: NOT-Like (yeast CCR4/NOT complex component) 9

p62: nucleoporin p62

PAS: pre-autophagosomal structure

PBST: phosphate buffered saline with tween-20

PHA-4: defective pharynx development 4

PI3K: phosphatidylinositol 3-kinase

PI3P: phosphatidylinositol (3,4,5)-trisphosphate

PKA: Ras/cAMP-dependent protein kinase A

PLK-1: polo-like serine/threonine-protein kinase 1

PRG-2: piwi related gene 2

RBR-2: retinoblastoma binding protein related 2

RDE-1: RNAi defective 1

RFP: red fluorescent protein

RFP-1: ring finger protein 1

RNAi: RNA interference

RRF-3: RNA-dependent RNA polymerase 3

RT: room temperature

S6K: ribosomal protein S6 kinase

SDS-PAGE: sodium dodecyl sulfate polyacrylamide gel electrophoresis

SEM: standard error of the mean

SID-1,2: systemic RNA interference defective 1, 2

SPT-4: SPT transcription factor family 4

SQST-1: sequestosome related 1

CW STED: Continuous Wave Stimulated Emission Depletion

TAF-4: TAF (TBP-associated transcription factor) 4

TFEB: transcription factor EB

TOR: target of rapamycin

ULK1,2: unc-51-like kinase 1, 2

UNC-51, 119: uncoordinated 51, 119

UTX-1: human UTX (Ubiquitously transcribed TPR on X) homolog 1

VHA-13,15: vacuolar H ATPase 13, 15

VPS-15,34: related to yeast Vacuolar Protein Sorting factor 15, 34

WT: wild type

ZFP-1: zinc finger protein 1

Introduction

Autophagy

Autophagy comes from the Greek "auto" meaning self and "phagy" meaning eating - thus "eating of self". As such, autophagy refers to the process in which the cell self-digests and recycles is own components, such as misfolded proteins and damaged or obsolete organelles. Metabolites that result from this degradation process are then recycled and reused by the cell to build new macromolecules and organelles. Besides this canonical role of autophagy, it becomes increasingly clear that it is also involved in other processes such as cell death (Liu et al., 2005; Yu et al., 2006), antigen representation (Schmid and Münz, 2007; Schmid et al., 2007), and the clearance of invading microorganisms (Nakagawa et al., 2004; Ogawa et al., 2005). Autophagy is also linked with the pathogenesis of many diseases such as cancer (Mathew et al., 2007) and neurodegenerative disorders (Nixon, 2013). Moreover, autophagy-related genes (Atg) have also been shown to be involved in other membrane-trafficking processes such as endocytosis (Ruck et al., 2011). The 2016 Nobel Prize in Physiology and Medicine was awarded to Yoshinori Ohsumi for his groundbreaking work in the field of autophagy, a fact which highlights the importance of this biological process for both our understanding of molecular cell biology and its implications in modern medicine.

Types of autophagy

There are three major types of autophagy, namely macroautophagy, microautophagy and chaperone-mediated autophagy (CMA). As the name implies, CMA uses chaperone-mediated recognition of a pentapeptide motif

and directly translocates its protein targets across the lysosomal membrane for degradation (Majeski and Fred Dice, 2004). In contrast, both microautophagy and macroautophagy are able to deliver larger structures to the lysosome through membrane encapsulation. Microautophagy directly engulfs cytoplasmatic components at the surface of the lysosomal membrane via invagination (Boya et al., 2013). Macroautophagy is usually referred to as "autophagy", as it represents the best-studied form of autophagy. As a specialised organelle, the autophagosome mediates the process of macroautophagy. Macroautophagy is generally thought of as a non-selective form of autophagy, as the autophagosome engulfs a whole section of the cytoplasmatic components and delivers them to the lysosome for degradation (Mizushima, 2007). Since macroautophagy substrates are generally not proximal to the autophagosomal membrane, there is no direct recognition process. However, recent studies suggest that autophagy is quite a selective process after all (Bjørkøy et al., 2006; Zhang et al., 2009; Von Muhlinen et al., 2010). Autophagic cargo receptor proteins, such as p62/SQST-1, often contain motives that mediate Atg8/LC3/LGG-1 recognition and binding (Johansen and Lamark, 2011). Hence, cargo receptor proteins act as molecular bridges that allow substrate as well as autophagosomal membrane recognition and thereby increase the selectivity of macroautophagy. As this study exclusively focuses on macroautophagy, from now on it will be referred to as "autophagy".

The autophagic machinery

Autophagy is a ubiquitous catabolic process, which causes cellular bulk degradation through vesicular engulfment of cytoplasmic components. Autophagy consists of several sequential steps that are referred to as the

autophagic flux (Figure 1, Table 1). This section describes the autophagic flux by focusing on *C. elegans* autophagy proteins. Several key transcription factors, such as PHA-4 and HLH-30, regulate the expression of autophagy genes upon different stimuli.

These upstream stimuli also lead to the phosphorylation and activation of ATG-13, which in turn stabilizes the autophagy-initiating kinase UNC-51 (Hosokawa et al., 2009). Subsequently, UNC-51 phosphorylates BEC-1 and in doing so initiates the autophagic cascade. This phosphorylation step is crucial for the formation of the VPS-34/BEC-1/EPG-8 class III phosphatidylinositol 3-kinase (PI3K) complex (Russell et al., 2013). This complex generates phosphatidylinositol 3-phosphate (PI3P) (Kihara et al., 2001), and recruits additional ATG proteins to the pre-autophagosomal structure (PAS). The VPS-34/BEC-1/EPG-8 complex is specifically linked to the process of autophagic vesicle nucleation and hence often referred to as the autophagic vesicle nucleation complex (Yang and Zhang, 2011). Since the step of vesicle nucleation is essential for autophagy initiation, the vesicle nucleation complex must be tightly regulated. In order to form the phagophore at the PAS, ATG-9 recruits a membrane to its formation site (Yamamoto et al., 2012). Upon phagophore formation, the two ubiquitin-like conjugating systems ATG-12 (consisting of ATG-12, ATG-5, and ATG-16.2) and LGG-1 (consisting of LGG-1, ATG-3, and ATG-7) mediate vesicle expansion and vesicle completion (Suzuki et al., 2007). As the phagophore increases in size, it engulfs cytoplasmatic components with its double membrane. Upon complete sequestration, the vesicular structure closes and creates the autophagosome. Next, ATG-9 performs an additional role in retrieving components of the outer autophagosomal membrane for re-usage at the PAS in the process of

autophagosome maturation (Reggiori et al., 2004). The process of autophagosome maturation is further characterised by a movement of the vesicle along the microtubule network towards the lysosome and by cleavage and recycling of LGG-1 from the outer autophagosomal membrane (Tanida et al., 2005). In contrast, LGG-1 remains in the inner membrane and is degraded together with the autophagic substrate as the autophagosome fuses with the lysosome after maturation is complete (Kimura et al., 2007; Palmisano and Meléndez, 2016). In the autolysosome, which was formed through the fusion of autophagosome and lysosome, macromolecules are degraded to monomeric units that are subsequently exported into the cytosol for the build-up of new macromolecules.

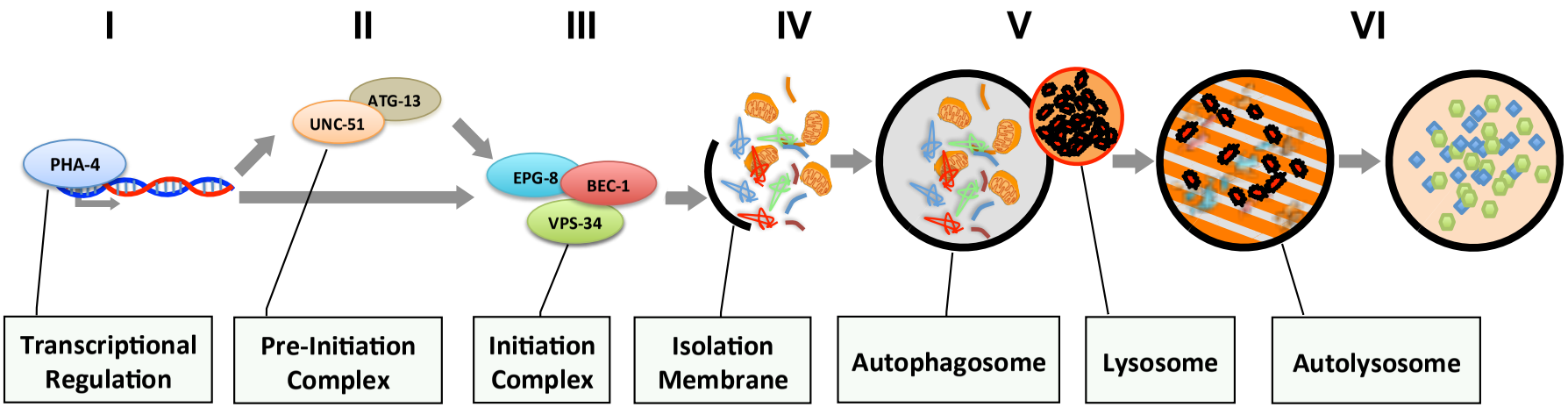

Figure 1: The autophagic flux. Schematic depiction of the macroautophagy process in *C.elegans*. Autophagy is orchestrated in a multi-step cascade that includes: (I) transcriptional regulation, (II) induction, (III) vesicle nucleation, (IV) vesicle expansion and maturation, (V) lysosomal fusion of the autophagosome, and (VI) degradation within the autolysosome. Monomeric biomolecules generated in this process are finally recycled back to the cytoplasm. In *C.elegans*, autophagosomes are relatively small with a diameter of 300-500 nm. Autophagosomes in *S. cerevisiae* and in mammals measure about 400-500 nm and 500-2000 nm, respectively.

I: Regulation			Function
Yeast	**Worm**	**Human/Mouse**	
-	hlh-30	*TFEB*	Transcription factor regulating several autophagy-related genes (Settembre et al., 2011; Lapierre et al., 2013; Guo et al., 2014).
-	pha-4	*FOXA*	Transcription factor regulating several autophagy-related genes (Panowski et al., 2007a; Lehmann, 2008; Sheaffer et al., 2008a).
II: Induction			
Atg1	unc-51	*ULK1,2*	Serine/Threonine protein kinase that recruits autophagy proteins to the PAS (Matsuura et al., 1997; Meléndez et al., 2003).
Atg13	atg-13	*ATG13*	Regulatory subunit of UNC-51, which is activated through phosphorylation via TOR and PKA (Chang and Neufeld, 2009; Hosokawa et al., 2009; Stephan et al., 2009).
III: Vesicle nucleation			
Vps34	*vps-34*	*VPS34*	PI3K of the VPS-34 complex that is needed for autophagic vesicle nucleation (Roggo et al., 2002). Also involved in endocytic retrograde transport (Ruck et al., 2011).
Atg6	*bec-1*	*BECN1*	VPS-34 PI3K complex component that is needed for localising autophagy protein to the PAS (Meléndez et al., 2003). Also involved in endocytic retrograde transport (Ruck et al., 2011).
Atg14	*epg-8*	*ATG14*	Autophagy-specific subunit of the VPS34 PI3K complex. Required for localizing additional ATG proteins to the PAS (Kametaka et al., 1998; Suzuki et al., 2007). In contrast to the VPS-34/VPS-15/BEC-1 complex, the VPS-34/BEC-1/EPG-8 complex is exclusively involved in autophagy (Yang and Zhang, 2011)
Vps15	*vps-15*	*VPS15*	Serine/threonine protein kinase that is part of the VPS34 PI3K complex that is needed to recruit ATG8 (Stack et al., 1993). In *C. elegans* the VPS-34/VPS-15/BEC-1 complex is linked to endosome

			formation rather than to autophagy (Ruck et al., 2011; Lee et al., 2012; Law et al., 2017).
Atg9	*atg-9*	*Atg9*	Transmembrane protein that guides membrane to the phagophore (Mari et al., 2010)
III: Vesicle expansion/maturation			
Atg3	*atg-3*	*ATG3*	E2-like enzyme that conjugates PE with Atg8 (Ichimura et al., 2000; Tanida et al., 2002)
Atg4	*atg-4.1*	*ATG4*	Cysteine protease that cleaves Atg8 C-terminus (Kirisako et al., 2000)
Atg5	*atg-5*	*ATG5*	Complexes with Atg12 through lysine conjugation (Kametaka et al., 1996)
Atg7	*atg-7*	*ATG7*	E1-like enzyme that activates Atg8 and Atg12 (Kim et al., 1999; Meléndez et al., 2003; Jia and Levine, 2007)
Atg8	*lgg-1*	*GABARAP*	Ubiquitin-like protein that is conjugated to PE (Kirisako et al., 2000; Meléndez et al., 2003; Jenzer et al., 2014; Manil-Ségalen et al., 2014)
-	*lgg-2*	*MAP1LC3 (LC3)*	Atg8 ortholog, lgg-2 is a homolog of and acts synergistically with lgg-1 (Alberti et al., 2010; Manil-Ségalen et al., 2014)
Atg10	*atg-10*	*ATG10*	E2-like enzyme that conjugates Atg5 and Atg12 (Shintani et al., 1999)
Atg12	*lgg-3*	*ATG12*	Ubiquitin-like protein that is conjugated to Atg5 (Mizushima et al., 1998; Hars et al., 2007)
Atg16	*atg-16.2*	ATG16L	Forms a complex with Atg5 and Atg12 (Mizushima et al., 1999)
IV: Lysosomal fusion			
-	*epg-5*	*EPG5*	Tethers and determines the fusion specificity of autophagosomes with lysosomes (Tian et al., 2010; Wang et al., 2016)
V: Lysosomal degradation			
-	cup-5	*MCOLN1*	Regulates lysosome biogenesis and mutants are impaired in lysosomal maturation (Fares and Greenwald, 2001; Sun et al., 2011)

VI: Recycling			
Atg9	atg-9	ATG9	Transmembrane protein that interacts with Atg2 (Noda et al., 2000)
Atg2	atg-2	ATG2	Membrane associated protein that interacts with Atg9 (Shintani et al., 2001; Wang et al., 2001)
Atg18	atg-18	WIPI1	Membrane associated protein that interacts that binds PI3P and PI(3,4)P (Barth et al., 2001; Meléndez et al., 2003)

Table 1: Autophagy related genes at different steps of the autophagic flux. Flux steps I-VI in Figure 6 match the respective sub-categories in this table: (I) transcriptional regulation, (II) induction, (III) vesicle nucleation, (IV) vesicle expansion and maturation, (V) lysosomal fusion of the autophagosome, and (VI) degradation within the autolysosome. Gene names and functions are given for the following species: *S. cerevisiae* (yeast), *C. elegans* (worm), and *Homo sapiens*/*mus musculus* (human/mouse). The list is not exhaustive but aims to give a rough overview of the genes involved in the autophagic cascade.

Regulation of autophagy

Autophagy is a tightly regulated process that responds to different stimuli. One can consider two working modes of autophagy, namely "basal" and "induced" autophagy (Mizushima, 2005). The former is constantly active for the routine turnover of cytoplasmatic components, whereas the latter describes an enhanced autophagic turnover that is transiently activated by certain stimuli. These stimuli include: lack of nutrients, growth factor deprivation, pathogen infection, and ER stress (He and Klionsky, 2009). Serum starvation induces autophagy in many cell culture systems (Mizushima, 2007). Since individual cells within a body do not necessary sense certain stressors, it is conceivable that autophagy is also regulated at an organismal level. During starvation this occurs through the endocrine system, whereby insulin suppresses autophagy and glucagon enhances it (Mortimore and Pösö, 1987; Scott et al., 2004). Further, amino acid sensing and insulin growth factor signals converge on the target of rapamycin (TOR), which represents a master regulator of nutrient signalling. Inhibition of TOR has been shown to induce autophagy in yeast (Noda and Ohsumi, 1998), flies (Ravikumar et al., 2004), worms (Hansen et al., 2008a), and mammals (Ravikumar et al., 2004). Conversely, in nutrient-rich conditions, TOR directly inhibits the kinase activity of Atg1/Ulk1/UNC-51 via its phosphorylation (Chang and Neufeld, 2009; Nazio et al., 2013) and thereby reduces the induction of autophagosomes. Another major autophagy regulator is the glucose-sensing Ras/cAMP-dependent protein kinase A (PKA) pathway. Active PKA inactivates Atg1/Ulk1/UNC-51 via phosphorylation (Budovskaya et al., 2004, 2005) and appears to modulate autophagy in parallel to TOR signalling (Yorimitsu et al., 2007). Furthermore, autophagy is activated through

the AMP-activated protein kinase (AMPK) (Kim et al., 2011). AMPK is activated trough decreasing ATP levels due to poor nutrition and directly leads to Atg1/Ulk1/UNC-51 activation (Egan et al., 2010; Kim et al., 2011). The activity of the Atg1/Ulk1/UNC-51 complex is critical for the recruitment of the VPS34 complex to the phagophore (Itakura and Mizushima, 2010; Matsunaga et al., 2010), which represents the first step in the autophagic cascade. Another mechanism that regulates autophagy is the interaction between Atg6/Beclin 1/BEC-1 and the apoptosis-related protein Atg9/Bcl-2/ATG9. It has been shown that starvation or ER stress activates c-Jun N-terminal kinase-1 (Jnk-1), which phosphorylates Bcl-2 and thereby disrupts its interaction with Beclin 1 (Ogata et al., 2006; Wei et al., 2008). This frees up Beclin 1 to induce autophagic vesicle nucleation. Therefore, in mammals Bcl-2 inhibits Beclin 1 dependent autophagy (Pattingre et al., 2005). However, the exact biological function of this apoptosis-autophagy crosstalk is still a matter of debate. Although BEC-1 depletion triggers apoptosis in *C. elegans*, it has yet to be established if ATG-9 functions as a suppressor of autophagy in worms (Takacs-Vellai et al., 2005).

The role of autophagy in health and longevity

During adulthood autophagy slows down the ageing process and its activity is required for lifespan extension through germline removal, TOR inhibition, reduced insulin/IGF-1 signalling, reduced mitochondria respiration, as well as through dietary restriction (Gelino and Hansen, 2012). These findings indicate that enhanced autophagy has a cytoprotective and health-promoting function. Further, the formation of dauer larvae, which constitutes a long-lived larval arrest stage that can survive harsh conditions, is dependent on autophagy

(Meléndez et al., 2003). Similarly, the formation of stress-resistant yeast spores in response to nutrient depletion is abolished by defects in the autophagic machinery (Tsukada and Ohsumi, 1993). Pharmacological treatments that extend lifespan in different model organisms, such as resveratrol, spermidine, and rapamycin have been shown to depend on autophagy (Figure 2). The polyamine spermidine increases lifespan in yeast, worms, and flies by autophagy induction though inhibition of histone acetyltransferase (HATs) (Eisenberg et al., 2009). Specifically, decreased chromatin acetylation levels via spermidine treatment lead to a transcriptional

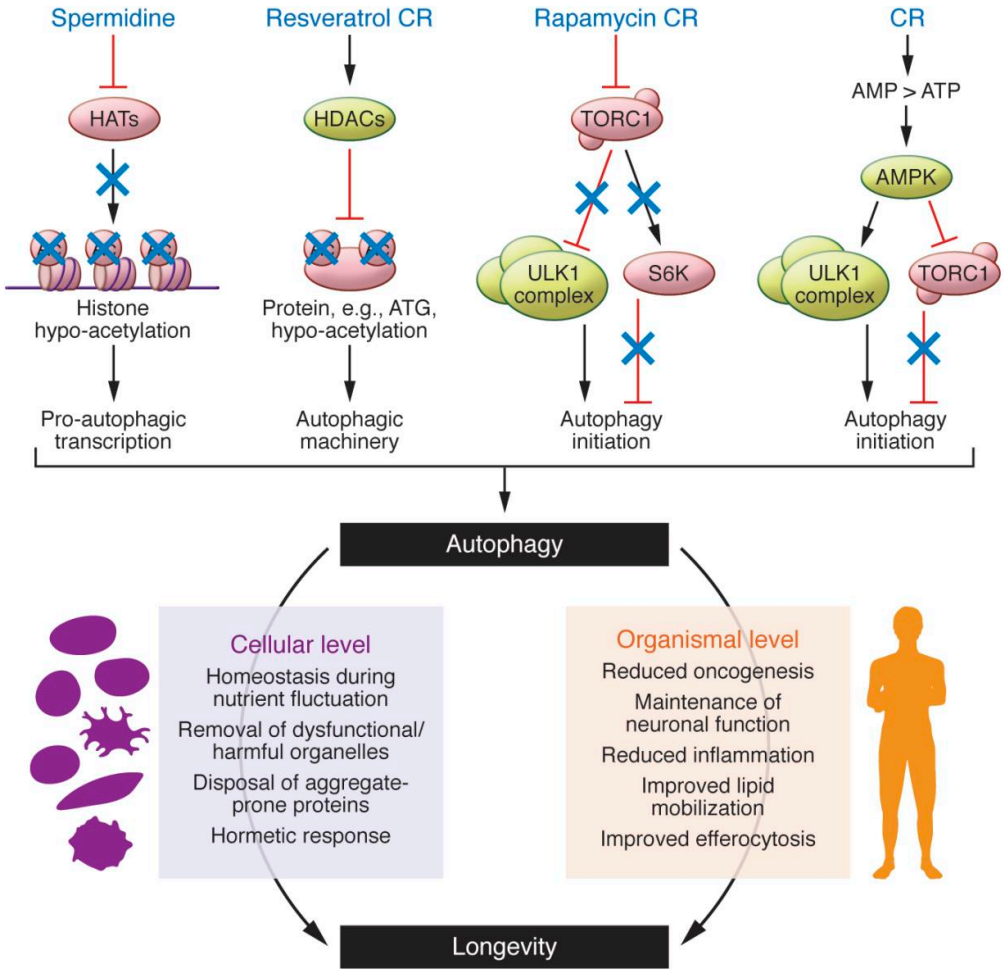

Figure 2: Pharmacological and nutritional regimens induce autophagy and prolong lifespan. Pharmacological treatments as well as caloric restriction regimens have been shown to induce autophagy and thereby mediate health- and lifespan-promoting effects. This figure is reproduced from Madeo and colleagues (Madeo et al., 2015).

upregulation of many autophagy-related genes that trigger autophagy (Eisenberg et al., 2009). The natural phenol resveratrol induces autophagy and increases lifespan via the activation of histone deacetylases (HDACs) (Morselli et al., 2010). Activation of the histone deacetylase SIRT1 seems to especially activate key autophagy genes such as ATG5, ATG7, and ATG8 via deacetylation (Lee et al., 2008).

Further, autophagy seems to mediate the positive effects of hormesis, a process whereby mild stress results in improved health and survival. Longevity that is mediated through hormetic heat stress has been linked to increased autophagy and a decrease in protein aggregates (Kumsta et al., 2017). Autophagy also plays a role in the hormetic effects of ischemic preconditioning. Here, a short ischemic event that enhances cellular autophagy is a primary contributor to decreasing the death rate of preconditioned heart muscle cells in a myocardial infarction (Huang et al., 2010). Intriguingly, the activation of autophagy alone seems to be sufficient to promote longevity. For example, transgenic overexpression of ATG5 in mice leads to extended lifespan dependant on autophagy (Pyo et al., 2013). Similarly, overexpression of the transcription factor HLH-30/TFEB, which targets many autophagy-related genes, increases lifespan in *C. elegans* (Lapierre et al., 2013). Enhanced neuronal expression of Atg8a in *Drosophila melanogaster* leads to increased lifespan and reduces the presence of ubiquitinated and oxidized proteins in aged animals (Simonsen et al., 2008). Conversely, loss-of-function mutations in autophagy genes reduce lifespan in worms as well as flies (Simonsen et al., 2008; Toth et al., 2008; Lee et al., 2010a).

Autophagy in ageing and neurodegeneration

Autophagy is classically described as a protection mechanism against diverse pathologies that include age-associated illnesses such as cancer and cardiovascular and neurodegenerative diseases (Lee et al., 2010b; Kaushik and Cuervo, 2015). In fact, genetic inhibitions of autophagy lead to abnormal protein aggregate accumulation that often mimic age-associated pathologies (Rubinsztein et al., 2011). Especially in post-mitotic or slowly-dividing cells such as hepatocytes and neurons, autophagic impairment leads to the formation of protein aggregates and to cellular degeneration (Komatsu et al., 2005; Hara et al., 2006; Nakai et al., 2007). This is because these tissues, compared to fast-dividing cell types, are more dependent on thorough protein turnover to avoid the accumulation of harmful protein aggregates and damaged organelles.

When elderly animals are increasingly challenged by large protein aggregates that are poor substrates to proteasome, autophagy should become increasingly important. Yet, decreased autophagic activity is closely linked to ageing (Rubinsztein et al., 2011; Kaushik and Cuervo, 2015). In particular, the age-associated decline of intracellular recycling systems, including autophagy, has been proposed as the main reason for the late life onset of many neurodegenerative pathologies (Cuervo et al., 2005). In line with this, different studies have shown that autophagic degradation becomes less efficient as neurons age (Cuervo and Dice, 2000; Lynch and Bi, 2003) and that the reactivation of autophagy ameliorates neurodegeneration. (Nah et al., 2015). Further, dysfunctional autophagy has been observed in cell culture (Larsen et al., 2002; Boland et al., 2008; Sadasivan et al., 2010) and in animal models of neurodegenerative diseases (Wang et al., 2006; Knöferle et al., 2010; Font-

nieves et al., 2011; Zhang et al., 2011). Brain sections of patients with Alzheimer's, Parkinson's, and Huntington's disease show the accumulation of dysfunctional autophagic vesicles (Nixon, 2013). Build-up of these structures is generally linked to a dysfunction of the late autophagic flux at the step of lysosomal degradation. Further, many studies documented an excessive number of autophagic vesicles in damaged neurons from tissue samples of patients with neurodegenerative diseases (Viscomi and D'Amelio, 2012).

Underlying causes for these detrimental effects are diverse and include: harmful accumulation of autophagosomes and autolysosomes, defective retrograde transport, increased ROS production, ineffective organelle clearance, cell death through leakage of lysosomal enzymes, and incomplete degradation as a source of cytotoxic products (Wong and Cuervo, 2010; Nixon, 2013). However, the exact mechanism that links the impaired late autophagic flux to neurodegeneration is still a matter of debate and seems to largely depend on the disease context (Nixon, 2013). Intriguingly, the inhibition of autophagosome formation has been shown to counteract neurodegeneration under conditions of pathologic vesicle accumulation (Yang et al., 2007; Lee and Gao, 2009). Moreover, in diseases that feature defective autophagy, a further induction of the system could be linked to accelerated neurodegeneration (Zhang et al., 2011). Overall, it becomes increasingly clear that autophagy acts as a double-edged sword that is positive when functional but harmful when deregulated (Shintani and Klionsky, 2004).

Evolution of Ageing

Darwin's theory of evolution describes the incremental changes in inheritable traits within a population. The driving force of evolution is twofold. Firstly,

variable traits within a population due to different alleles are caused by mutations. Secondly, natural selection favours individuals with traits that provide greater evolutionary fitness. An individual is fitter when it possesses favourable traits that allow for its reproduction in greater numbers, compared to a less fit individual. Hence, the abundance of favourable fitness-promoting alleles in the population's gene pool increases over time.

Evolutionary theories of ageing regard the ageing process as a trait that is shaped through natural selection like any other organismal characteristic. The scientific debate that aims to understand how natural selection moulds lifespan was sparked in the late 19th century and remains ongoing today. This chapter provides an abbreviated historic introduction to the evolutionary theories of ageing. Key figures and their contribution to the current understanding of the evolution of ageing are discussed below.

I. Weismann & Wallace: Natural Selection of Ageing

In 1891, the German scientist August Friedrich Leopold Weismann first published that ageing is shaped through the evolutionary force of natural selection (Weismann, 1891). He rejected the common belief that organismal lifespan is solely determined ‘by the constitution of the animal's body’ as an analogue to a molecular machine that inevitably accumulates damage over its lifetime. In contrast Weismann proposed that the ‘duration of life is not exclusively determined by the size of the animal, the complexity of its structure, and the rate of its metabolism.’ He exemplified this by comparing the long-lived ant queen and the very short-lived male ant (Weismann, 1891). According to his view, the duration of life is predefined as a result of the evolutionary adaption to external conditions and the species’ inherent needs.

Thus, he regarded lifespan as a trait that is as similarly shaped by natural selection as by other structures and functions of an organism. In order to promote fitness, lifespan must be long enough that an individual can maintain its species through reproduction and by feeding and protecting its offspring. Once the individual has accomplished these tasks, Weismann stated, natural selection is blind towards its subsequent performance and its total lifespan. From that observation, he deduced that lifespan does not greatly exceed the period of reproduction, except in those species that tend their offspring. He further hypothesized that lifespan is modulated by the time period in which an individual must produce offspring to ensure the perturbation of its species. This reproductive period is determined by external conditions acting on the organism. Weismann assigned the largest influence on lifespan to different causes of death such as hunger, cold, heat, droughts, floods, epidemics, predation, and parasites. He argued that higher occurrences of these environmentally caused deaths would result in the need for each individual to quickly reach maturity and to reproduce in large numbers. As many more individuals die from these causes than by natural death, he concluded that natural selection does not promote longevity. Rather, natural selection would tend to shorten the reproductive period and thereby also the lifespan of the species (Weismann, 1891). The latter he reasoned from the principle that as soon as natural selection ceases to operate upon any characteristic, even longevity, it begins to disappear. His converse argumentation was that, ‘Duration of life, like every other characteristic of an organism, is subject to individual fluctuations.’ and that, ‘As soon as the long-lived individuals in a species obtain some advantage in the struggle for existence, they will gradually become dominant, and those with the shortest lives will be exterminated.’

(Weismann, 1891). Further, Weismann hypothesised that immortal individuals would be unable to avoid slight injuries that would eventually accumulate. Therefore, such an individual would be crippled over time and unable to fulfil the purpose of its species, and hence be less valuable to the species than its offspring. Moreover, such an immortal organism would compete for resources that would be better invested in its progeny. Natural selection therefore would shorten its life to provide perfect conditions for large numbers of vigorous successors. (Weismann, 1891).

We also must acknowledge Alfred Russell Wallace, who independently formulated similar ideas to Weismann on the evolution of ageing, although never actively publishing them. Wallace stated that natural selection would eliminate individuals that have provided numerous offspring, as they would only compete with their successors for resources. Wallace's note on 'The Action of Natural Selection in Producing Old Age, Decay, and Death' was written some time between 1965 and 1870 and published by Weismann's editor in the book "Essays Upon Heredity and Kindred Biological Problems" on page 23 (Weismann, 1891).

II. Haldane: Declining Force of Natural Selection

John Burdon Sanderson Haldane was a British-born Indian scientist that tackled many questions on evolutionary genetics through mathematical models. In contrast to previous thinking, including that of Weismann and Wallace, he realised that that evolution does not select groups or species but acts only on the fitness of the individual. Haldane proved the former line of argumentation, namely that evolution selects for ageing and death to make room for offspring, to be incorrect. He argued that when reproductive output

can be sustained, it would not be beneficial to the species to install ageing and death mechanisms. Haldane proposed that, at the level of an individual, natural selection becomes inefficient at maintaining organismal function and health during old age (Haldane, 1943). He came to this insight through observing the disease progression of the heritable human disease Huntington's Chorea, which is caused by a dominant allele. Huntington's disease is characterized by its late onset, with initial symptoms only showing after the age of 30, and a subsequent fatal disease progression. According to Haldane, although it is a devastating heritable disease, Huntington's Chorea is not eradicated through natural selection because it occurs after the peak age for reproduction (Haldane, 1943). Through this critical clue, he realized that the force of natural selection declines as a function of age (Figure 3). Consequently, disease-causing mutations that act late in life cannot be ‘seen’ by natural selection, which creates a ‘selection shadow’ for aged individuals (Figure 3).

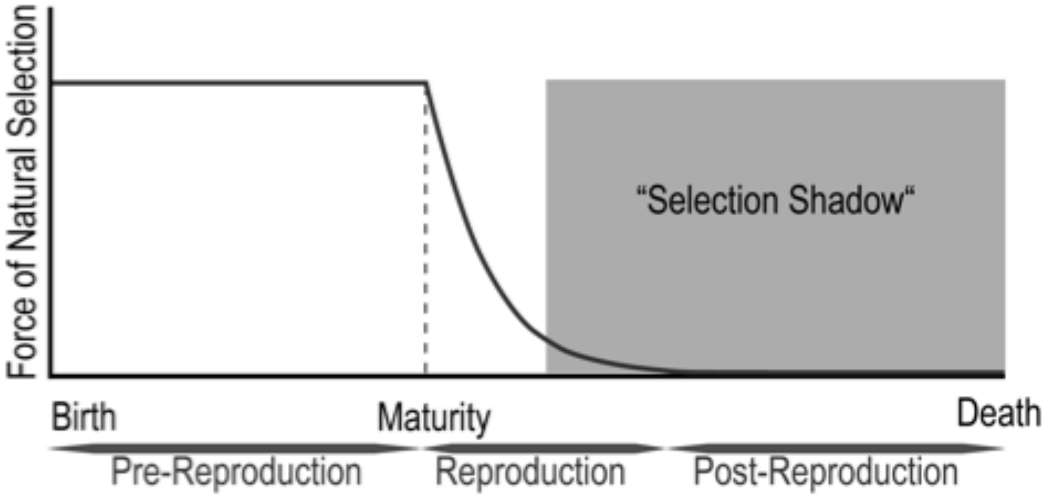

Figure 3: Force of Natural selection over age. The force of natural selection is at its maximal level during before the onset of the reproductive period of life. As soon as offspring is produced, the selection force sharply declines reaching its minimal strength post-reproduction. This creates a so called "selection shadow" during late-life (grey region), which is "blind" towards harmful mutant alleles that show their

III. Medawar and Williams:

Sir Peter Brian Medawar and George Christopher Williams further developed Haldane's idea. In his publications ‘Old Age and Natural Death’ and ‘An Unsolved Problem of Biology’ (Medawar, 1946, 1952), Medawar provided a verbal and graphical model on the evolution of ageing. As organisms in their natural habitat normally die at early ages due to external factors, there is little force to select against late-acting detrimental mutations after reproduction. Medawar proposed that these harmful mutations can accumulate in the genome and thereby promote ageing (Medawar, 1952). This model is known as the mutation accumulation theory of ageing (Figure 4). In 1957 George C. Williams formulated the antagonistic pleiotropy (AP) theory of ageing, which is related to the mutation accumulation theory (Williams, 1957). However, Williams developed his ideas without prior knowledge of Medawar's or Haldane's publications (Rose et al., 2008).

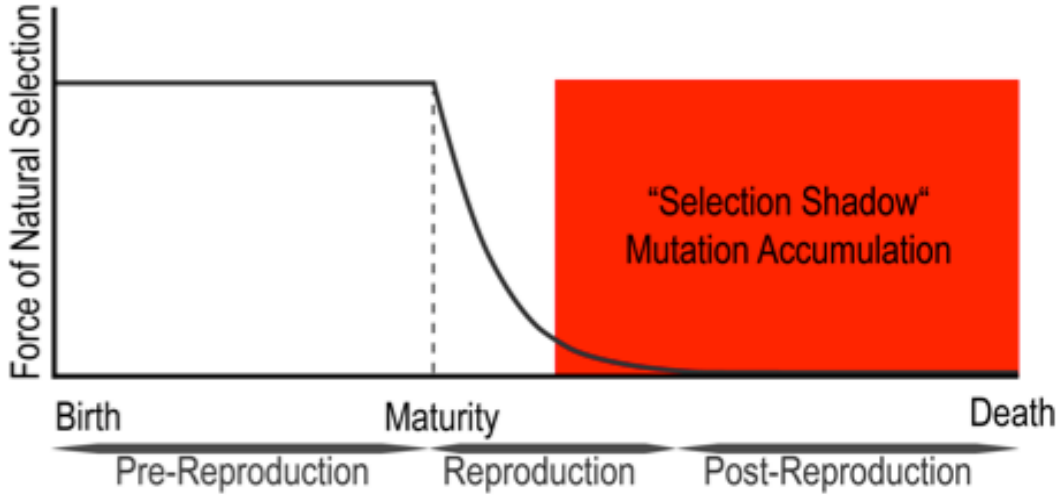

Figure 4: Mutation Accumulation Theory. The force of natural selection declines as a function of age. As soon as offspring is produced, the selection force sharply declines reaching its minimal strength post-reproduction. This creates a so called "selection shadow" during late-life which allows for the accumulation of late-acting detrimental mutations (red region). Accumulation of these negative late-acting alleles in the population leads to an evolution of ageing.

The AP theory is based on two assumptions: first, that one gene controls more than one trait and secondly that these pleiotropic effects can have opposing consequences on the organismal health or survival. This evolutionarily-based hypothesis predicts that strong natural selection enriches genes that mediate fitness early in life, at the expense of accumulating their harmful effects late in life, when natural selection is weak (Figure 5). Therefore, antagonistic pleiotropy is also known as the 'pay later' theory, which illustrates the trade-off between early fitness and detrimental late-life effects that both originate from the same allele. Antagonistic pleiotropy actively selects for fitness-promoting genes in early life that exhibit pleiotropic deletions effects later in life. This is in contrast to the accidental accumulation of these harmful alleles, which is proposed by Medawar's mutation accumulation theory. The AP hypothesis explains the inter-species variation of lifespan that can be observed in the animal kingdom. William postulated that, according to his theory, species with earlier reproductive onset and large

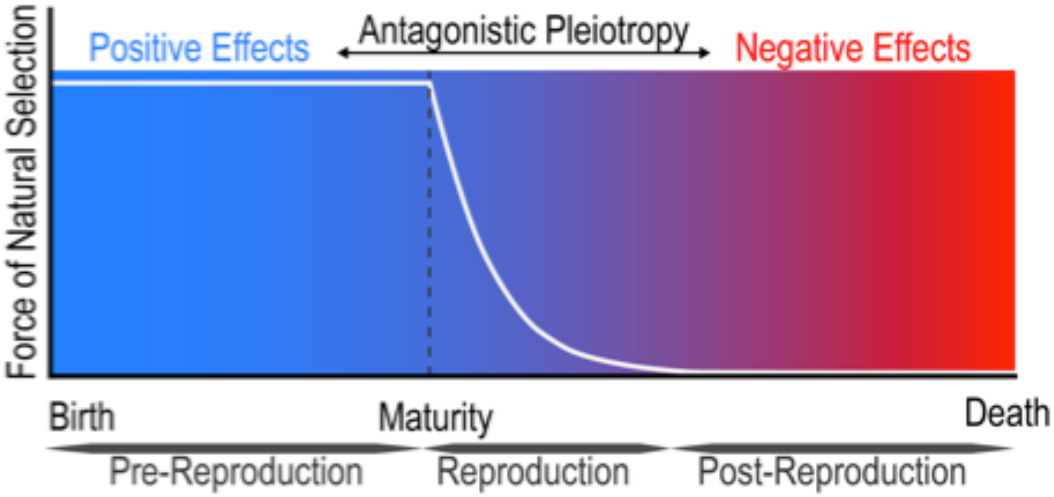

Figure 5: Antagonist Pleiotropy Theory. The force of natural selection declines over age. Antagonistic pleiotropy genes have positive fitness effects (blue region) early in life and negative effects (red region) late in life.

numbers of offspring are expected to have shorter lifespans (Williams, 1957). Interestingly, Williams himself did not use the term antagonistic pleiotropy for this genetic trade-off; Michael R. Rose coined this widely-accepted term later (Rose, 1982).

IV. Fisher and Hamilton: Mathematical Support

Haldane, Medawar, and Williams intuitively understood that the selection pressure on early-acting genes is higher than the selection pressure on late-acting genes. However, a mathematical description of the declining force in natural selection was lacking until William Donald Hamilton's publication in 1966 (Hamilton, 1966). Hamilton built his work on that of Sir Ronald Aylmer Fisher, who introduced key concepts of the 'Malthusian parameter' and 'reproductive value' in 1930 (Fisher, 1930). In his mathematical equations, Fisher assumed a sexually reproducing and age-structured population. In his hypothetical population, individuals survive to age *x* with a probability of *l (x)* and have a reproduction rate at age *x* of same sex offspring of *m (x)*. Fisher showed that such a population would reach an asymptotic exponential rate of population increase *r*, which he named the Malthusian parameter. The Malthusian parameter is given by the single real root of his equation (Equation 1) (Fisher, 1930; Hughes and Reynolds, 2005; Rose et al., 2008).

(1)

$$\sum_{0}^{\infty} e^{-rx}\, l(x) m(x) dx = 1$$

x: age class

r: intrinsic rate of population increase/"Malthusian parameter"

$l(x)$: survivorship at age x

$m(x)$: fecundity at age x

Hamilton derived the first partial derivative to quantitatively describe the effect of the chance of survival on Fisher's Malthusian parameter *r*, which he used as a parameter for Darwinian fitness. Hamilton described a population that is stable in size and has one real *r*, which is determined by the combination of an age-specific survival function *l(y)* and an age-specific fecundity function *m(y)*. With his equation, he mathematically predicted how a mutation that acts at a specific age influences the fitness of an individual. Hamilton's partial derivative shows that, due to the age-specific decrease in the survival probability, the effect of a mutation on fitness *r* also declines with age (Equation 2). Hence, the force of natural selection acting on a mutation also decreases as the organism ages. He further proposed that the impact of a mutation allele on fitness, which corresponds to its specific change in *r*, determines whether or not this allele will spread within the population's gene pool (Hamilton, 1966). The fitness impact of an individual at a given time point, based on its chance of survival is given by *s(x)/T*. *T* represents a measure for generation time and can considered to be constant over short time periods. Hence this denominator can be ignored, leading Hamilton to the following equation:

(2)

$$s(x) = \sum_{y=x+1} e^{-ry}\, l(y)m(y)$$

x: age class

y: all ages after age x

r: intrinsic rate of population increase/"Malthusian parameter"

$l(y)$: survivorship at all ages after age x

$m(y)$: fecundity at all ages after age x

$s(x)$: strength of natural selection on mortality at age x

Before reproduction, *m(y)* is zero and cannot affect *s(x)*, which remains at its maximum of one. As soon as the organism starts reproducing, *s(x)* decreases. This is because older individuals have a smaller reproductive potential that is given by a decreasing *l(y)*. Even if fecundity *m(y)* increases with age, this would not stop the decline in fitness but only slow it down. After reproduction the individual ceases to have a reproduction potential and *s* equals zero (Hamilton, 1966; Hughes and Reynolds, 2005; Rose et al., 2008). The strength of natural selection on age-specific mortality is described by *s(x)*. A similar function *s'(x)* describes the strength of natural selection on age-specific fecundity (Equation 3). The intrinsic growth rate *r* of a population must be positive to ensure the survival of a population. Therefore, *s'(x)* realistically decreases constantly over life.

(3) $$s'(x) = e^{-rx} l(x)$$

x: **age class**

r: **intrinsic rate of population increase/"Malthusian parameter"**

$l(x)$: **survivorship at age** x

$s'(x)$: **strength of natural selection on fecundity at age** x

Figure 6 shows the sensitivity of *r* against age-specific changes in mortality and fecundity plotted against age. In contrast to *s(x)*, the age-specific force of natural selection on fecundity *s'(x)* can increase or decrease before the reproduction commences (Charlesworth, 1994) (Figure 6). In his influential article, 'The Moulding of Senescence by Natural Selection', Hamilton stated that 'senescence is an inevitable outcome of evolution' (Hamilton, 1966). Further, his model shows that '...higher fertility will be a primary factor leading

to the evolution of higher rates of senescence unless the resulting extra mortality is confined to the immature period' (Hamilton, 1966).

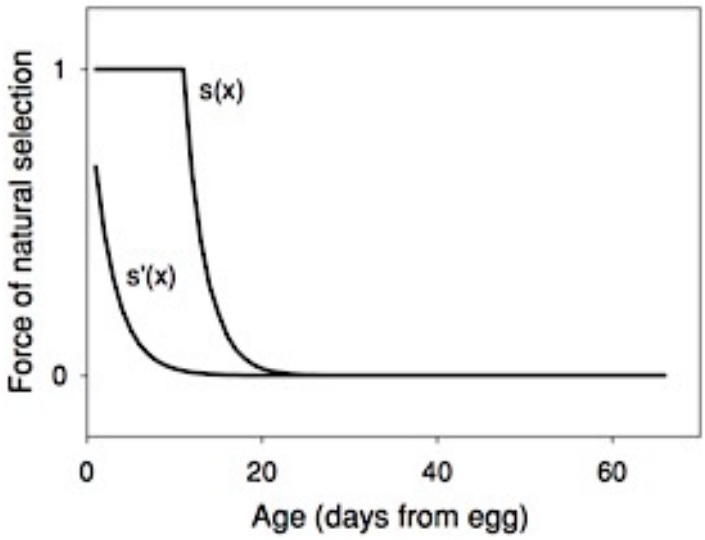

Figure 6: Age-specific strength of natural selection on mortality ($s(x)$) and fecundity ($s'(x)$). A cohort of 1111 female Drosophila melanogaster from population CO_1 from Rauser et al. (Rauser et al., 2006) was used to calculate age-specific survival and fecundity values. (This figure is reproduced from Rose and colleagues (Rose et al., 2007)).

IV. Charlesworth and Rose: Population Genetics Support

Hamilton's mathematical analysis on the evolution of ageing predicted in which way and at which time the decline in natural selection leads to ageing. He argued that senescence is inherent to age-structured population (Hamilton, 1966). However, Hamilton's mathematical analysis was based on verbally reasoned scenarios for evolutionary effects on genes within a population. In contrast, Charlesworth used precise population genetic models and extended cases of sex differences, non-random mating, density-dependent effects, and environmental fluctuations to complement Hamilton's work (Rose et al., 2007). Beginning in 1970 Charlesworth published many papers that cumulatively made mathematical formulations of earlier verbal suggestions on

the evolution of ageing possible (Charlesworth, 1970, 1973; Charlesworth and Giesel, 1972; Charlesworth and Williamson, 1975). Further, Charlesworth's work mathematically proved Medawar's ‘mutation accumulation’ theory of ageing (Charlesworth and Williamson, 1975; Charlesworth, 1994). He also corroborated that the effects of an allele on the Malthusian parameter indeed represent the best measurement of its likelihood to be an evolutionary selection (Rose et al., 2007). Michael Robertson Rose, a former PhD student of Charlesworth, mathematically proved William's ‘antagonistic pleiotropy’ theory of ageing (Rose, 1985). In his analysis Rose showed that natural selection indeed favours alleles that are beneficial to the organism early in life even when those same alleles are detrimental late in life.

V. Sokal, Mueller, Rose, & others: Experimental Support

Based on Hamilton's functions, predictions can be made that are experimentally testable. This can be done by manipulating the force of natural selection over the lifetime of an organism and subsequently quantifying the effects of ageing patterns and longevity. By eliminating chances of reproduction later in life one would expect to shift the ‘selection shadow’ (see Figure 3) to a younger age and ultimately shorten the lifespan. Conversely, increasing the chances of reproduction at older but not at younger ages would shift the ‘selection shadow’ to an older age and thereby extend lifespan. These experiments were suggested as early as 1968 by Edney and Gill (Edney and Gill, 1968). On this basis, the Austrian-American biostatistician and entomologist Robert Reuven Sokal was the first to carry out deliberate laboratory experiments to manipulate the evolution of ageing. For this purpose, Sokal restricted the reproduction time of the flour beetle *Tribolium*

castaneum to a very short period in early life for 40 generations, while control animals were allowed to reproduce freely. After 40 generations the selected beetles showed a significantly reduced median lifespan compared to the control beetles (Sokal, 1970). This finding supports Haldane's force of natural selection and is compatible with the mutation accumulation as well as the antagonistic pleiotropy hypothesis of ageing.

Similar findings were made by Laurence D. Mueller, who tested heterosis effects across the lifespan of *Drosophila melanogaster* (Mueller, 1987). Mueller selected flies for over one hundred generations to reproduce very early but not later in life. Moreover, due to a small population size and genetic drift, these animals were highly inbred at the end of this selection protocol. This regime let to the creation of flies that had reduced fecundity in late life. The mutation accumulation theory explains this phenomenon with an earlier accumulation of deleterious mutation, caused by a shift of the 'selection shadow' to younger ages. These deleterious late-life mutations exert their negative effects due to their homozygosity in the highly inbred fly population. Based on this presumption, Mueller tested for mutation accumulation by crossing two inbred strains that were selected for early reproduction. He observed significant hybrid vigour effects for fecundity at later ages. Conversely, he did not detect similar hybrid vigour effects when crossing inbred fly populations that were not selected for early reproduction. He accounted this to the random accumulation of deleterious alleles in the early reproducing flies and the 'cure' due to heterzougousity of these deleterious alleles after crossing. A pure antagonistic pleiotropy, in contrast, should have led to the fixation of the same alleles and no hybrid vigour effects (Mueller, 1987). Although Mueller's results argue for the mutation

accumulation theory, they do not exclude the presence of antagonistic pleiotropy effects (Rauser and Mueller, 2009).

The opposite approach was to postpone reproduction to late life by discarding eggs that are laid during young adulthood. As discussed before, such a regime is expected to shift the 'selection shadow' to an older age and thereby extend the organism's lifespan by experimentally strengthening natural selection at later ages. Jean Marie Wattiaux carried out experiments in *Drosophila subobscura* to characterise the effects on offspring caused by continuous reproduction at late ages. He found that 'repeated reproduction with old flies ... reduced sexual activity of the males, gave better longevity and resulted in a different chromosomal polymorphism' (Wattiaux, 1968a, 1968b). Later, Rose and Charlesworth showed that a selection for late reproductive potential in *Drosophila melanogaster* leads to: a decrease in early-life reproduction, an overall decline in reproduction, and a prolonged lifespan (Rose and Charlesworth, 1980, 1981). These findings strongly corroborate Williams' antagonistic pleiotropy theory of ageing, stating, '...senescence in *Drosophila* is due to the late-acting deleterious effects of genes which are favoured by natural selection because of beneficial effects at early ages' (Rose and Charlesworth, 1980). However, these experiments sparked debates on their validity due to poor experimental design. Only later studies conducted by Rose and Luckinbill used properly replicated experiments that unequivocally showed laboratory evolution of postponed ageing (Figure 7), which corroborated the evolutionary theory of ageing (Luckinbill et al., 1984; Rose, 1984). Interestingly, these findings were also reproduced in mice (Nagai et al., 1995).

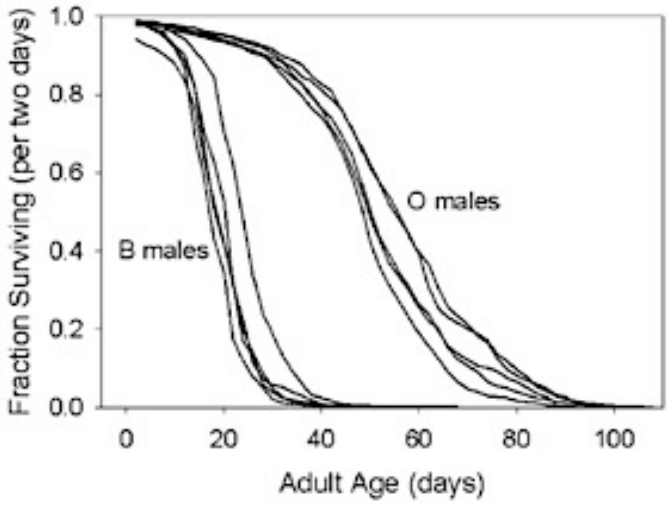

Figure 7: Survival of early and late reproducing male Drosophila melanogaster across age. Survival of early reproducing population (B males) and late reproducing population (O males) is plotted against the fly age. Flies were subjected to over 100 generations of laboratory evolution as in early or late reproducing regimes, with a difference of 55 days between their day of last reproduction. (This figure shows data from Rose and colleagues (Rose et al., 2002) and is reproduced from Rose and colleagues (Rose et al., 2008))

Although the two key mechanisms of the evolution of ageing, namely mutation accumulation and antagonistic pleiotropy, are not mutually exclusive, there is more experimental evidence at hand in support of the antagonistic pleiotropic theory of ageing (Rose et al., 2007). This is because most experimental interventions to prolong lifespan in model organisms come with a 'trade-off', by reducing one or more functional fitness characteristics in early life (e.g. fecundity) (Partridge et al., 2000; Van Voorhies et al., 2006). Still, a large body of evidence suggests that both mechanisms act in concert to shape the ageing process through evolution. In summary, the studies discussed show that ageing is not a pre-defined result of the interaction between an organism and the environment but that it is a trait like many others that is naturally modified by evolution.

Working hypothesis and experimental setup

Conventional Longevity Screens in C. elegans

The roundworm *C. elegans* is particularly suited for research on ageing due to its fast lifecycle (Figure 8) and its short lifetime, with a median lifespan of 25 days. The genome of this nematode was the first of any multicellular organism to be fully sequenced and is very well annotated (The *C. elegans* Sequencing Consortium, 1998). Further, *C. elegans* is amenable to genetic manipulation and in particular to gene knockdown via RNA interference (RNAi). Feeding worms with bacteria engineered to express dsRNA leads to a robust and quick RNAi response and represents a very cost- and time-effective gene inactivation method (Timmons et al., 2001). The availability of genome-wide RNAi feeding libraries (Kamath et al., 2003; Rual et al., 2004) has led to the identification of hundreds of longevity genes in *C. elegans* since the early 2000s (Ni and Lee, 2010). In fact, many genes that modulate ageing were first discovered in *C. elegans* (Uno and Nishida, 2016). Interestingly, practically all longevity genes that were identified in these studies converge on a small set of longevity pathways that include insulin-like growth factor-1 signalling as well as TOR signalling (Uno and Nishida, 2016). Common to these classical RNAi as well as mutagenesis screens for longevity in *C. elegans,* is that genes are inactivated during the whole lifespan through either permanent mutations or gene knockdown from early larval stages (Klass, 1983; Ni and Lee, 2010). Interestingly, heavy fitness costs in early life have been identified for many longevity mutants identified in these screens (Friedman and Johnson, 1988; Van Voorhies and Ward, 1999; Van Voorhies et al., 2006).

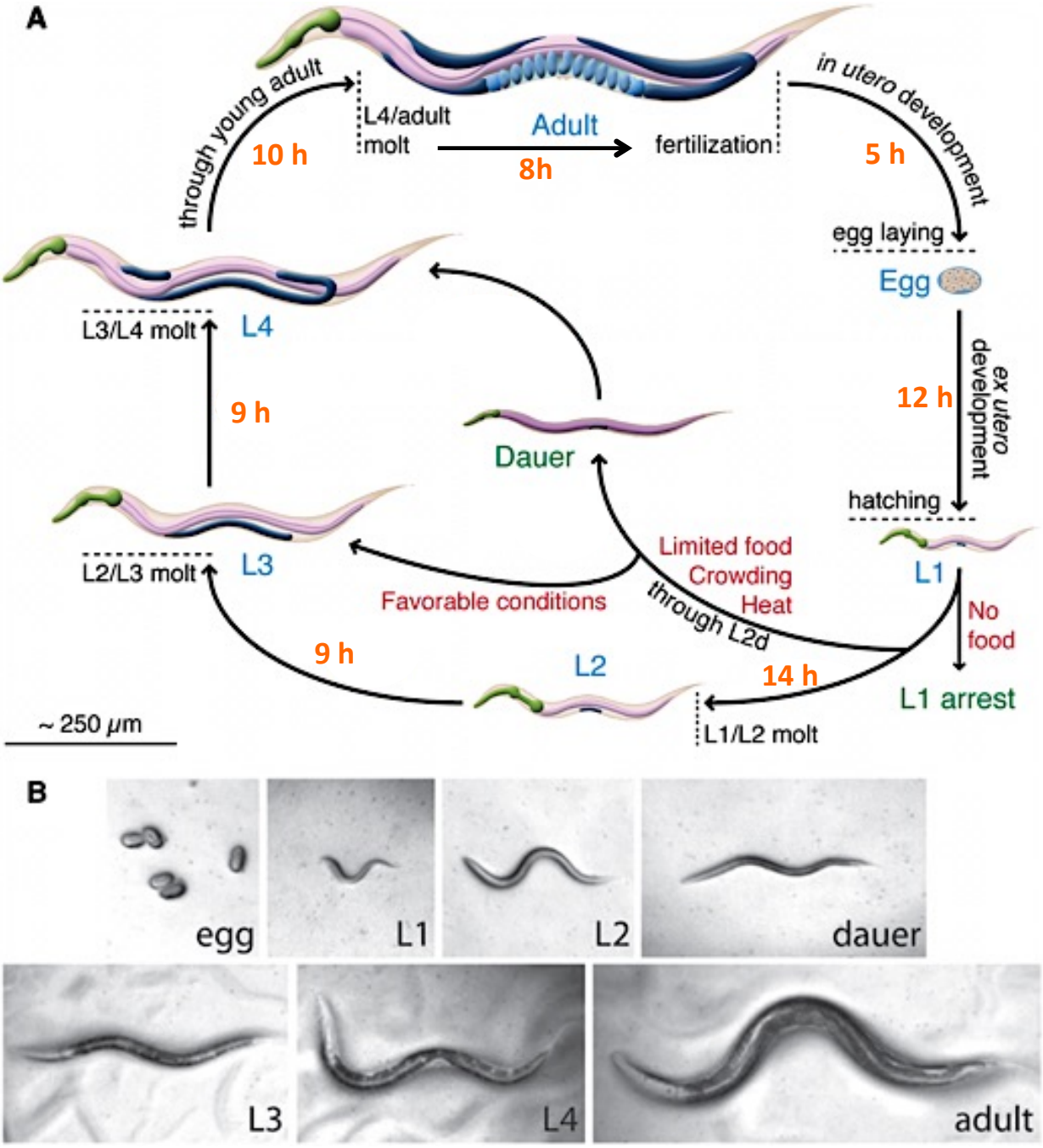

Figure 8: Lifecycle and development stages of *C. elegans*. (A) The lifecycle of *C. elegans* at 20°C. Stages in blue depict the normal developmental stages whereas arrest stages (due to stress or starvation) are labelled in green. Size of the depicted worms roughly matches the scale. Graphics originate from (Hall and Altun, 2012) and were modified from (Cihan, 2014). (B) Micrographs of *C. elegans* lifecycle on standard NGM agar plates, feeding on *E. coli* bacteria. Post-larval development inside the egg, worms develop through four larval stages (L1-L4) before reaching maturity. At 20°C worms are starting to reproduce roughly 2.5 days after they have existed as eggs. Micrographs originate from (Fielenbach and Antebi, 2008) and the panel is reproduced from Chian and colleagues (Cihan, 2014).

These observations are consistent with Williams' AP theory of ageing, which predicts that strong natural selection early in life enriches fitness-promoting alleles that cause harmful effects after reproduction, when natural selection is ineffectual (Williams, 1957). Hence, in conventional longevity screens, genes that are essential for early fitness and health but are detrimental and lifespan-shortening in late life remained undiscovered. Interestingly, two longevity screens that were initiated after larval development, during the late L4 stage (see Figure 8), identified over 60 genes that extend lifespan when inactivated post-developmentally (Chen et al., 2007; Curran and Ruvkun, 2007). However, these screens could only identify AP genes that are involved in development, as they were commenced early in life at the point of maximal selection pressure (Figure 9).

Late-life Longevity Screen in C. elegans

Based on the AP theory of ageing, we speculated that a post-reproductive RNAi screen that targets genes within 'selection shadow' should identify previously undiscovered longevity genes that modulate lifespan conversely over ageing. Post-reproductive inactivation of these genes should reduce their negative effects late in life while preserving their positive effects in early life (Figure 9). Mitigation of harmful late-life AP effects should theoretically improve health and result in an increased organismal lifespan, which can be detected as a screening readout (Figure 9). As discussed before, many potentially lifespan-extending AP genes should lead to severe fitness impairment when inactivated in early life; this would have made their discovery through traditional screens impossible. Therefore we speculated that a post-reproductive RNAi screen would not only identify genes that

behave according to the AP hypothesis but also uncover previously undiscovered regulators of ageing.

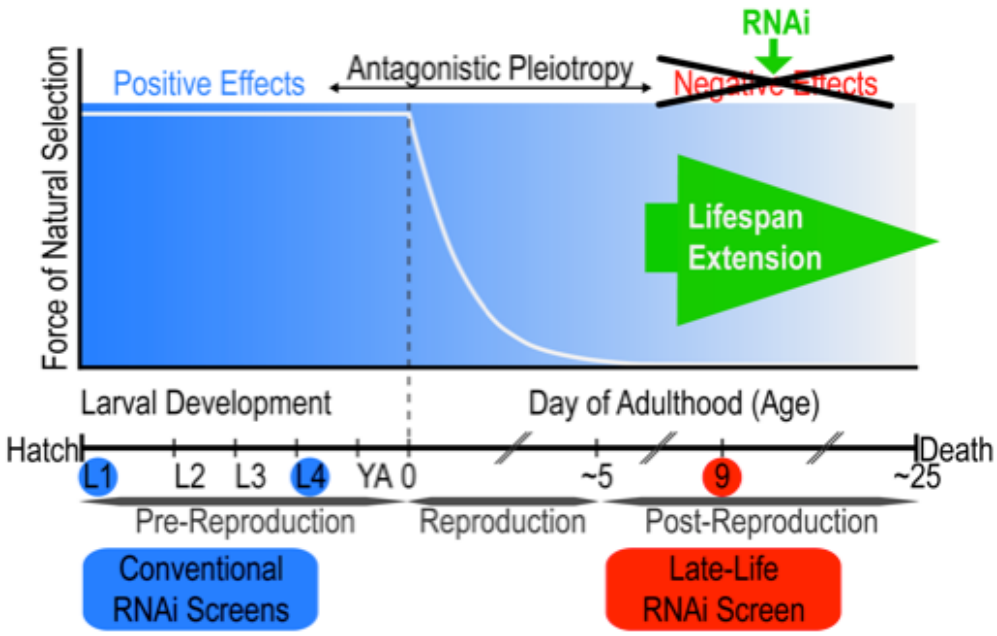

Figure 9: Antagonistic pleiotropy in *C. elegans*. (A) Strong natural selection at early ages favours alleles that are beneficial for survival and reproduction. These genes can exhibit pleiotropic deleterious effects late in life and thus lead to an evolution of ageing. The 'selection shadow' is depicted as a grey box. (B) By inactivating these detrimental genes late in life we aim to extend *C. elegans'* lifespan.

Results

Post-reproductive RNAi screen for AP genes

Excursion: Automated AP screen using 96-transwell plates

Due to the availability of genome-wide libraries and the ease of application and scaling, RNAi feeding represents the method of choice for genetic RNAi screens in *C. elegans*. Since a screening for AP genes requires a post-

reproductive initiation of gene inactivation, a major concern was that the reduced feeding rate of aged worms (Huang et al., 2004) could hinder efficient gene knockdown. To address this possibility, transgenic worms expressing GFP in their muscles were post-reproductively exposed to feeding RNAi that targets *gfp*. Despite reduced feeding of aged animals, post-reproductive RNAi led to a potent inactivation of GFP by day 10 which was even stronger by day 14 of adulthood (Figure 10).

This observation indicates that feeding of dsRNA-expressing bacteria in aged and post-reproductive *C. elegans* leads to effective gene inactivation, which is

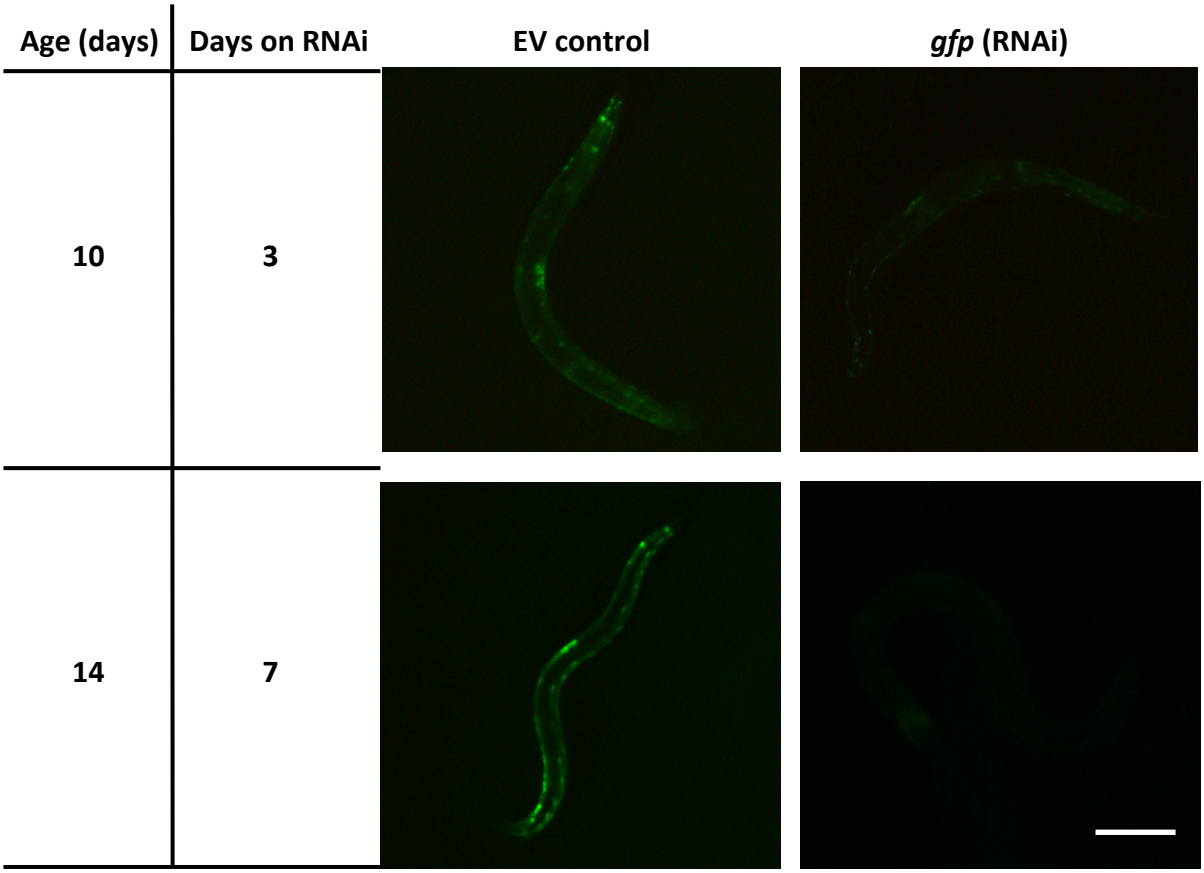

Figure 10: RNAi efficiency in aged *C.elegans*. Transgenic animals expressing GFP in the body wall muscles under the *myo-3* promoter were used to determine if RNAi via feeding is still effective at more advanced ages. Worms were treated from day seven with RNAi targeting GFP. Scale bar represents 250 µm.

a prerequisite for successful RNAi screening in post-reproductive worms.

Next, we developed a high-throughput and semi-automated RNAi screening platform for age-synchronized and post-reproductive *C. elegans* (Figure 11). The screening protocol starts by age-synchronizing fertile worms, which are grown in a liquid culture without the usage of 5-fluorodeoxyuridine (FUdR). FUdR treatment inhibits DNA synthesis and leads to parental sterility in *C. elegans*. The latter effect is commonly used in ageing studies as a straightforward method to age-synchronize cultured *C. elegans*. However, the use of FUdR for ageing studies is controversial, since the drug itself seems to have strong effects on *C. elegans'* lifespan (Aitlhadj and Stürzenbaum, 2010), which could potentially mask or lead to misinterpretation of the idenfied longevity effects. To avoid these potential caveats of FUdR treatment, we age-synchronized worms by separating adult worms from their offspring through repetitive sedimentation in liquid medium in combination with Percoll® density separation. This protocol was repeated daily until the worms stopped their egg production completely, roughly at day 9 of adulthood. Once the animals had entered their post-reproductive phase of life, 30 worms were sorted into each well of HTS Transwell®-96 well-permeable support plates with a large particle flow cytometer (Biosorter®, Union Biometrica) (Figure 11). Each of the wells harboured a different RNAi clone in liquid medium. The worms were now sitting on a transparent polyester membrane with 8 µm pores (Figure 12). Due to its small size, *Escherichia coli* can easily diffuse through these pores, which makes frequent feeding with freshly induced dsRNA expressing bacteria possible. Moreover, the permeable membrane system allows the performance of regular washes to avoid cloudiness and unwanted contamination in the wells. Using high-speed live microscopy of the 96-

transwell RNAi screening plates, pictures of the RNAi treated animals are obtained within two-day intervals until the end of their lifespan (see Figures 11 and 12).

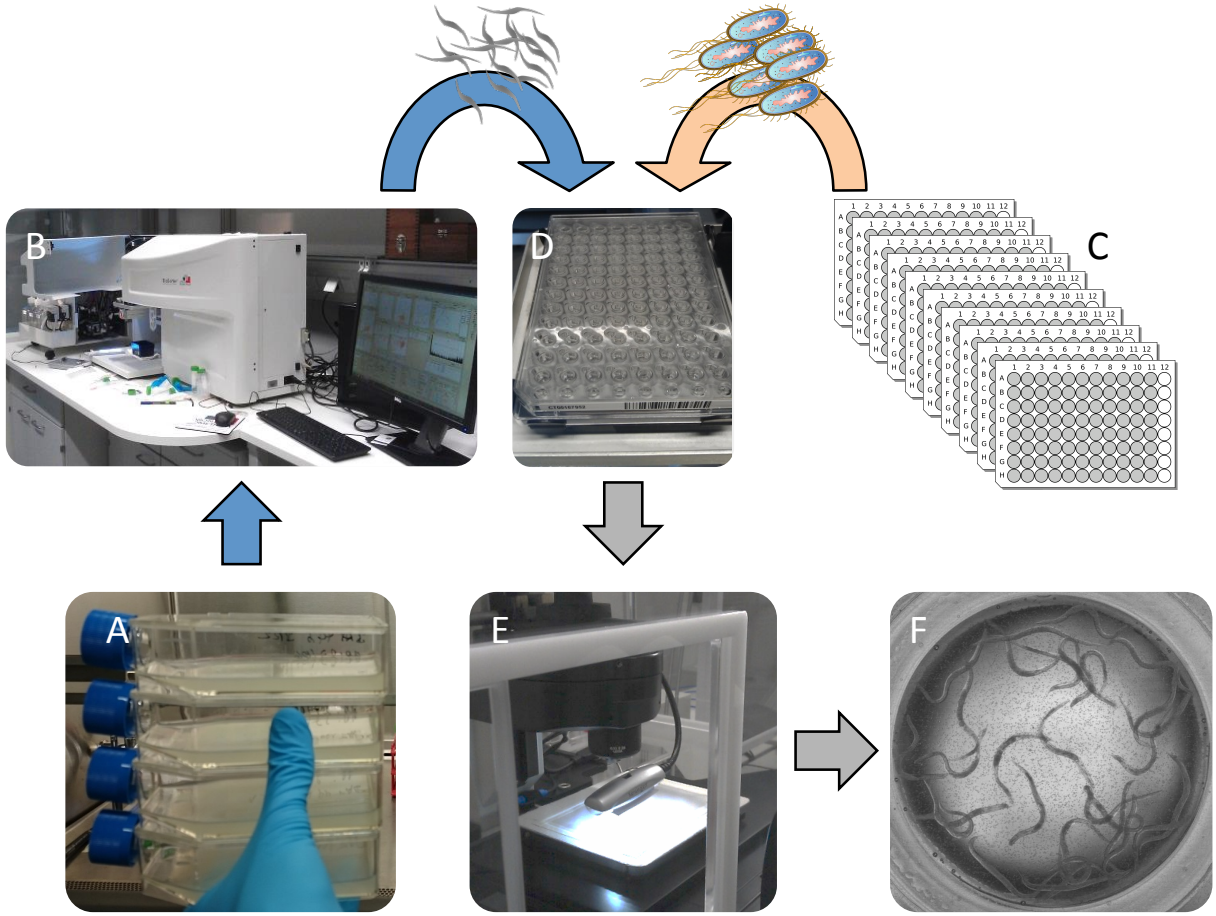

Figure 11: Semi-automated 96-transwell screen. (A) Age-synchronized worms were grown in liquid culture until day 9 of adulthood. (B) Post-reproductive day 9 old worms are sorted with a large particle flow cytometer (Biosorter®, Union Biometrica). (C) 96-well receiving plates were spotted with IPTG induced dsRNA expression bacteria of the RNAi library. (D) HTS Transwell®-96 well permeable support plates were inserted into the receiver plate and 30 worms were sorted onto the permeable membrane of each well and incubated at 20 °C. (E) The worms were imaged every second day using an automated microscopy screening platform. (F) Widefield images of each well were further processed to determine worm survival over time.

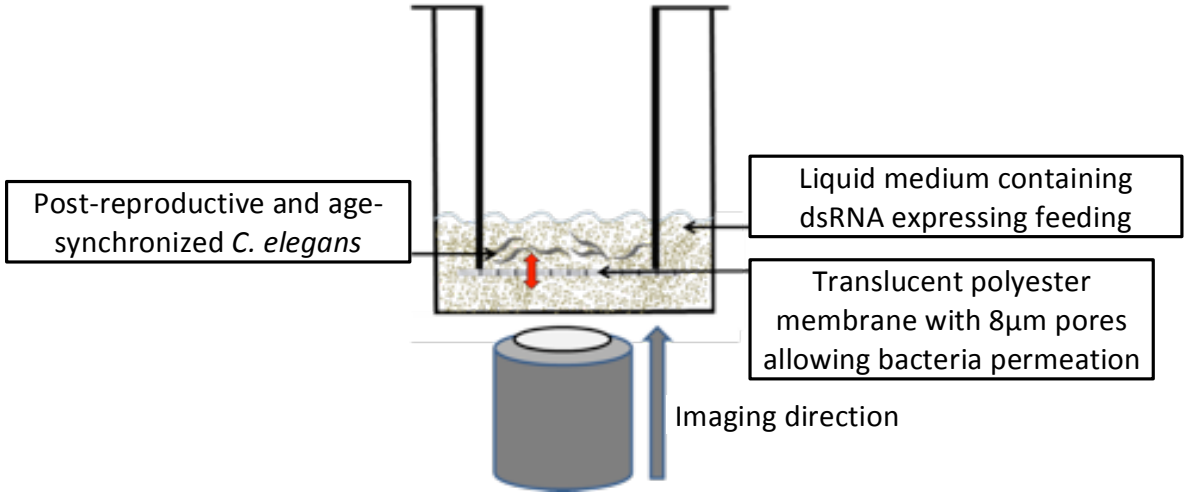

Figure 12: Imaging method using HTS Transwell®-96 well permeable support plates. The permeable support sits within a receiver well that contains NGM liquid medium and *E. coli* feeding bacteria. Post-reproductive and age-synchronized *C. elegans* are sorted on a translucent polyester membrane that has pores with an 8 µm diameter. These pores allow bacteria to freely permeate from the receiver well into the permeable support that carries the worms. Worms are microscopically imaged from below through the translucent membrane with a 1.25× objective.

A phenotypic measurement that can be employed to identify dead worms in liquid medium is a straightening of their body axis (Wählby et al., 2012). A worm population with individuals that have a normal lifespan typically experience a sharp increase in mortality after day 20 of adulthood. Hence, body straightening strongly increases when comparing worms at day 12 to worms at day 25 of adulthood (Figure 13). Using this criterion to differentiate living from dead worms, we manually scored a pilot screen to address the general feasibility of the screening protocol. This pilot screen enclosed *daf-2* and *utx-1* as known longevity genes (Dorman et al., 1995; Jin et al., 2011; Maures et al., 2011), as well as a non-targeting dsRNA (Ahringer library clone Y95B8A_84.g) (Tischler et al., 2006) and empty vector (ev) as negative controls. Manual scoring was carried out with micrographs of the screening

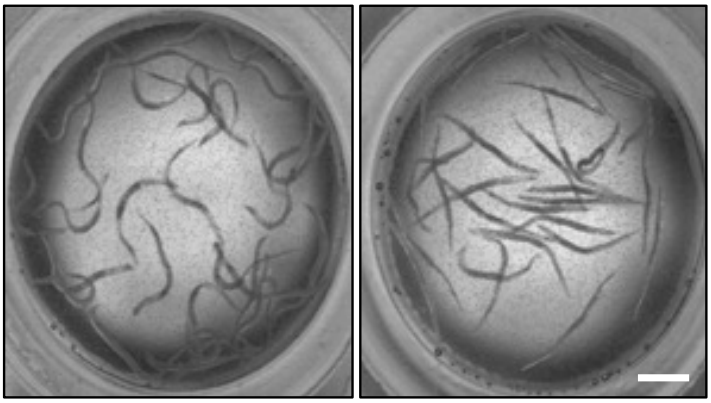

Age: day 16 day 25

Figure 13: Typical pictures acquired at day 16 (worms mostly alive) and day 25 of adulthood (worms mostly dead). At day 16 of adulthood the majority of the worms are still alive and show a curved body axis. In contrast, most of the worms are dead at day 25 of adulthood and have a straightened body axis. Straightening of the worm is a hallmark for death. Scale bar represents 500 µm.

plate that were obtained at day 30 of adulthood using a dedicated counting program that allows quick manual scoring of each worm as dead or alive. Scoring was carried out in two independent screening plates with respectively eight replicate wells per condition. Importantly, each condition was blindly scored to avoid any bias. By day 30 roughly 10% of the control worms were still alive in both replicate plates (Figure 14). In contrast, animals that were treated with *utx-1* or *daf-2* RNAi from day 9 were long-lived in both pilot screens, with around 20% to 25% worms alive at day 30 in both replicate plates. This increased survival upon *utx-1* or *daf-2* RNAi from day 9 recapitulated longevity phenotypes that were observed when these genes were inactivated in early life (Dorman et al., 1995; Jin et al., 2011; Maures et al., 2011). Hence, the inactivation of *utx-1* and *daf-2* seem to also extend lifespan when inactivated after reproduction. No other genes tested in the pilot screen showed a significant increase in survival at day 30 compared to the control conditions (Figure 14). However, the identification of two

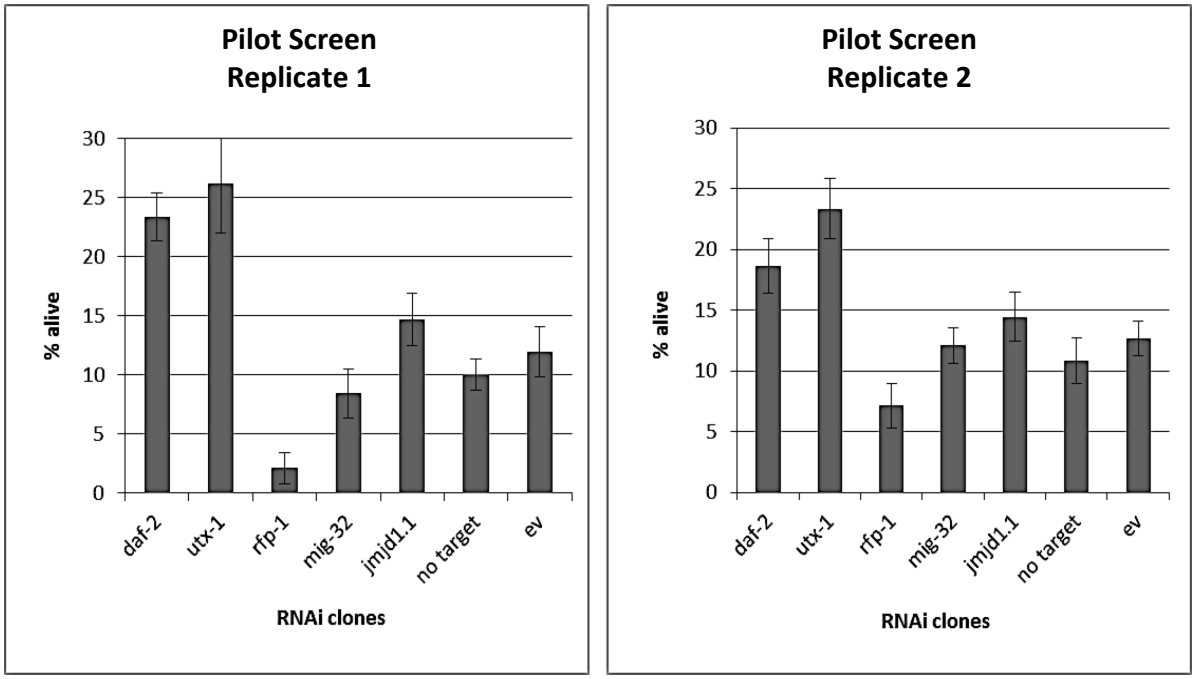

Figure 14: Pilot Transwell RNAi screen in post-reproductive *C. elegans*. The percentage of living worms was determined my manual counting in of each well of the HTS Transwell®-96 well permeable support plate. Scoring was performed at day 30 of adulthood. Each treatment was carried out in eight replicates and on a two independent plates in order to determine plate to plate variances.

previously published longevity phenotypes through the pilot screen supports the suitability of this novel screening methodology in detecting novel lifespan-regulating genes. Further, it can be seen that the readout of the two replicate plates largely mirror each other, arguing for a high reproducibility and robustness of the screening assay.

Next, different methodologies were assayed that would allow for an automated high-throughput identification of longevity genes using the 96-transwell system. The goal was to determine the dead-alive ratio of the worms within short intervals in order to generate individual lifespan curves for each imaged well.

As worms age, their mobility is strongly reduced (Huang et al., 2004). In fact, mobility as a marker for healthspan generally correlates with lifespan

(Huang et al., 2004). Hence, comparison between RNAi effects of the age-related decrease in mobility should allow for the identification of novel longevity genes. To measure *C. elegans* mobility, we acquired a short video of 30 frames for each well (Figure 15). A mean movement value was assigned to each well by quantifying and averaging movement between each successive frame of the obtained film. Similar to the bending of the body axis, we observed a strong reduction of movement between day 16 and day 25.

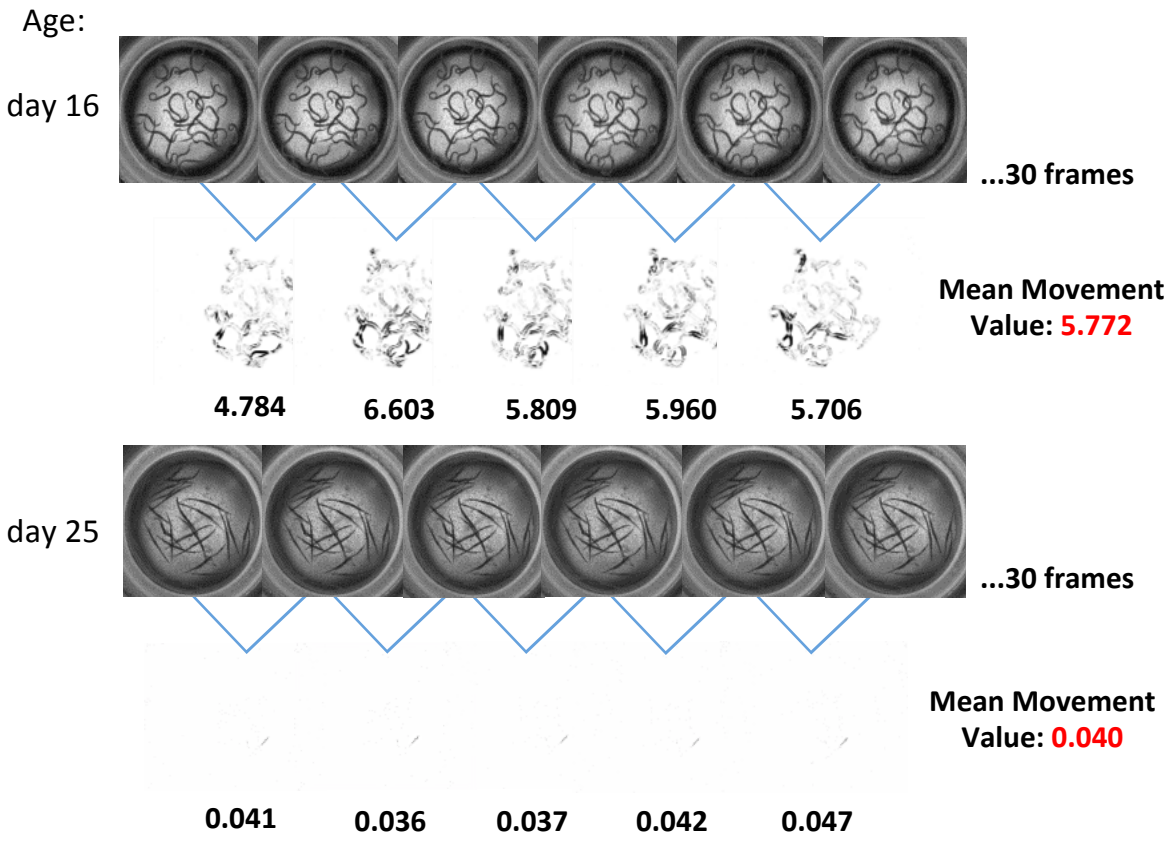

Figure 15: Automated movement scoring using frame differences. A short movie with 30 frames is acquired form each well and movement between each frame and the next is calculated through changes in the picture. The movement is averaged between all frame differences and gives the mean movement score as a parameter for relative movement in each well.

An additional option to determine the ratio between dead and live worms is the use of the dead cell stain SYTOX Orange. The fluorescent dye SYTOX Orange is excluded from living cells but enters and stains dead cells with damaged membranes where it binds to DNA (Roth et al., 1997). SYTOX staining has been previously described as a tool to discriminate living from dead *C. elegans* (Gill et al., 2003). We here show that SYTOX staining can additionally be employed to identify dead worms in our 96-transwell system (Figure 16). However, we also encountered a major caveat of this method

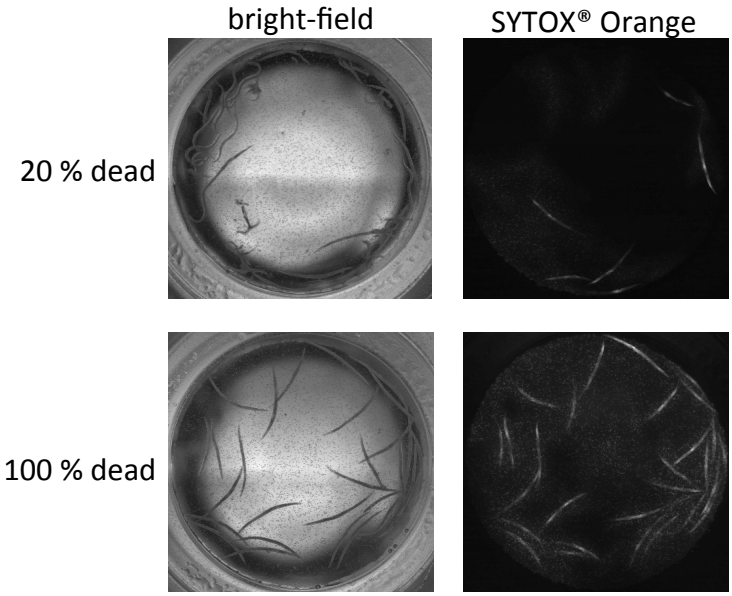

Figure 16: Dead/alive scoring using SYTOX® Orange dead cell stain. Age-synchronized day 9 old worms were sorted on a 96-transwell plate. Worms were killed through heat and sorted at different ratios together with alive worms.

when monitoring an ageing *C. elegans* population over time. This is because stained dead worms lose their bright staining over time before the cuticle degrades. Hence it is impossible to discriminate non-stained live worms from dead worms that have lost their staining over time. This limitation let us to not further use SYTOX staining as a marker for dead worms.

Following, we wanted to further investigate an automated method to identify dead worms based on the straightening of their body axis. For this we used a Cell Profiler based imaging toolbox for high-throughput *C. elegans* analysis, named Worm Toolbox (Wählby et al., 2012). Our goal was to use this toolbox to create an automated image-analysis pipeline with pictures obtained with our 96-transwell system. After training the Worm Toolbox on aged worms that were imaged in the transwell system, the software was able to identify worms in the pictures and determine whether their body axis was straight or bent (Figure 17). We extensively trained the Worm Toolbox pipeline on transwell pictures with post-reproductive worms to create a new worm model.

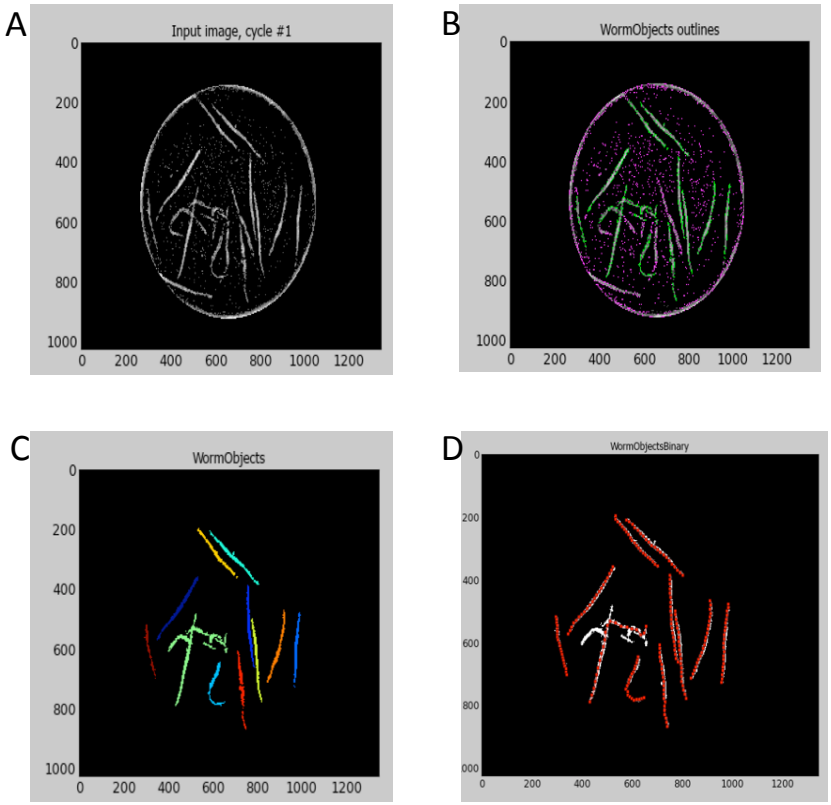

Figure 17: Worm Tool analysis of worms sitting in 96-transwell plates. (A) Removal of variations in illumination and separation of worm objects from background. (B) Identification of individual worms based on the trained worm model. (C) Identification of worms with separation of touching and tangled worms. (D) Identification and tracing of worm body axis.

Although this resulted in a robust recognition of worms in our transwell system, some worms could not be detected or were not completely untangled (Figure 17). Nonetheless, our trained image analysis pipeline correctly recognized most imaged worms and could be employed to automatically discriminate between a straightened and bent worm body axis. In summation, the quantification of straight body axis using the Worm Tool pipeline (Figure 17) as well as determining a well-specific movement score through short videos (Figure 15) represent the two most reliable automated methods to monitor health- and lifespan in our 96-transwell system. We decided to make use of both methods as a dual scoring system to screen for potential longevity genes in post-reproductive *C. elegans*. Given the expertise of our research group in transcriptional control and chromatin biology, we aimed to identify novel post-reproductive longevity genes that act in post-reproductive worms on chromatin. Hence, we compiled a RNAi sub-library of 280 genes that comprised chromatin modifiers and transcription factors that originated from the Ahringer *C. elegans* RNAi feeding library (Kamath et al., 2003). As these gene-regulatory factors are often associated with detrimental effects to organismal fitness, the identification of longevity effects in late-life would most likely be rooted in an AP mechanism. This gene-regulatory sub-library was screened using our 96-transwell system. RNAi was initiated at day 9 of adulthood and the worms were imaged every two days. The plates were washed every four days and subsequently exposed to new and freshly induced RNAi feeding bacteria.

Unfortunately, we encountered heavy bacterial contamination of the transwell plates within the first week of the assay. This contamination led to high die-off rates and clouded most of the wells, which made downstream

analysis impossible. This screening was repeated three more times but the contamination issue persisted, possibly due to a reoccurring bacillus contamination that was introduced while dispensing the worms with the Biosorter. We observed that the contaminant grew much more quickly in liquid medium than on plates, which led to the decision to carry out a simplified version of our screening protocol using 24-well agar plates. Although contamination issues forced us to abandon the 96-transwell screening system we believe that, once the contamination issue is solved, this methodology will allow for high-throughput longevity screening in post-reproductive *C. elegans* and potentially lead to the identification of a large set of genes that behave according to the AP hypothesis of ageing.

24-well screen for AP genes

Our originally compiled RNAi sub-library of chromatin factors and DNA binding proteins targeted 280 genes. For the 24-well screening, this library was extended, with the help of our collaboration partner Dr Baris Tursun from the Max Delbrück Centre for Molecular Medicine, to a comprehensive chromatin sub-library targeting roughly 800 genes. This extended library now contains histone variants and modifiers, as well as factors of the RNAi machinery, and the ubiquitin pathway. Due to the aforementioned contamination issues in the 96-transwell, we now used a simplified 24-well NGM agar plate system to screen for post-reproductive longevity. This simplified screening setup was inspired by longevity screens that were previously utilised by Gary Ruvkun's lab and required manual dead-alive scoring using a dissection scope (Hamilton et al., 2005; Curran and Ruvkun, 2007).

We employed this method to screen for genes that mediate longevity upon knockdown late in life. To increase the potency of the RNAi mediated gene knockdown we used *rrf-3* mutant worms, which are hypersensitive to RNAi (Simmer et al., 2002). In order to rapidly identify AP candidates, we age-synchronized *C. elegans* in liquid culture until day 9 of adulthood and subsequently sorted the animals on 24-well RNAi plates. At day 30 of adulthood we flooded the 24-well agar plates with M9 buffer liquid to trigger swimming movements of living worms. Subsequently, we manually scored the survival ratio of each well to detect longevity effects. Despite the lack of automation and a tedious scoring procedure, this screening identified numerous previously unknown genes that extend lifespan. In total, we uncovered 30 novel longevity genes (Figure 18). When examining the list of observed RNAi or mutant phenotypes of these genes on Wormbase (version WS258), we found that 19 out of these 30 genes are linked to detrimental

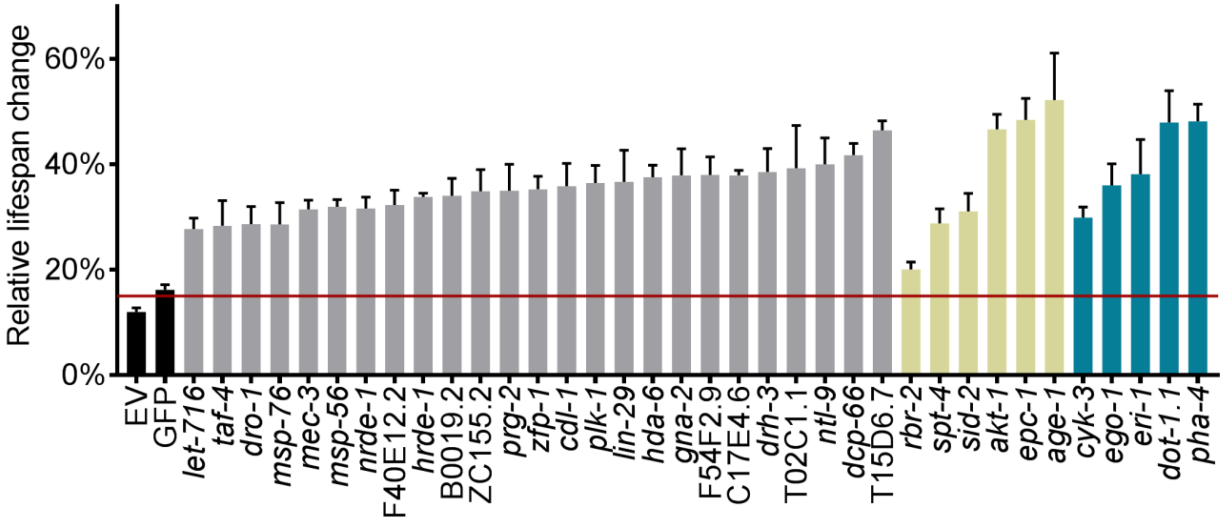

Figure 18: Potential post-reproductive longevity genes identified. Relative lifespan change indicated % of alive *rrf-3* worms at day 30 of adulthood. Non-targeting EV and GFP control conditions are shown in black. Potential novel post-reproductive longevity genes are shown in grey, with our top five candidates highlighted in green. Known longevity genes are shown in yellow. (Data created by Jonathan Byrne)

effects when inactivated in young worms. Hence, these genes likely extend lifespan due to AP mechanisms when inactivated after reproduction. Based on their harmful effects when inactivated in early life as well as robust lifespan extending effects in our screen we choose our top five AP candidate genes, namely *cyk-3*, *ego-1*, *eri-1*, *dot-1.1,* and *pha-4*. We validated these AP gene candidates through conventional lifespan assays, which involved the repeated assessment of dead and live worms that were transferred every second day to a fresh RNAi plate (Figure 19). We observed a mean treated lifespan (MTL) extension that ranged from 12% for *eri-1* to 33% for *pha-4*. Hence, *pha-4* which encodes for the forkhead box (FOX) A transcription factor represents the top candidate of our screen. PHA-4 is essential during development where it functions as an organ identity gene, targeting over 4000 genes (Zhong et al., 2010). Specifically, PHA-4 is essential for early pharynx and midgut development (Kiefer et al., 2007). Further, the PHA-4 transcription factor binds

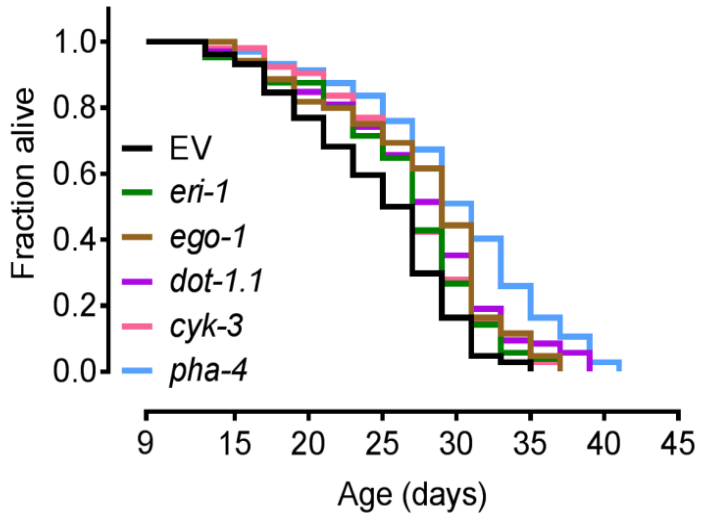

Figure 19: Post-reproductive inactivation top AP screening candidates significantly extend lifespan. Day 9 RNAi against *eri-1*, *dot-1.1*, *cyk-3*, *ego-1*, *pha-4*, and *bec-1* increase mean treated lifespan of post-reproductive worms, confirming our screening readout. (Data created by Jonathan Byrne)

key autophagy genes (Zhong et al., 2010) and is needed for autophagy induction and longevity upon caloric restriction and germline removal (Panowski et al., 2007b; Hansen et al., 2008b; Lapierre et al., 2011). Previous studies have shown that the inactivation of *pha-4* leads to lifespan shortening in young worms (Panowski et al., 2007b; Sheaffer et al., 2008b). The fact that PHA-4 positively regulates autophagy, which is generally associated with its positive effects on health and longevity (Rubinsztein et al., 2011), further peaked our interest to uncover potential AP functions of PHA-4 and downstream autophagy genes.

AP within the autophagic machinery

AP behaviour of pha-4 and downstream autophagy genes

In order to describe potential AP effects of *pha-4* across the lifespan, we commenced RNAi treatment from early larval development and at different time-points during adulthood (Figure 20). The inactivation of *pha-4* decreased lifespan when initiated during development and in young adulthood. Conversely, when inactivated later in life from day 5, 9, or 15 we observed a marked increase in lifespan. Hence, *pha-4* shows an AP phenotype as it modulates lifespan conversely across age. Notably, day 9 inactivation yielded the strongest longevity effect with a MTL extension of roughly 30%. To test whether autophagy is potentially involved in these opposing *pha-4* effects on lifespan, we inactivated the key autophagy gene *bec-1* at the same time-points across age (Figure 20). Similar to *pha-4*, the inactivation of *bec-1* from larval development and early adulthood reduced *C. elegans'* lifespan. When *bec-1*

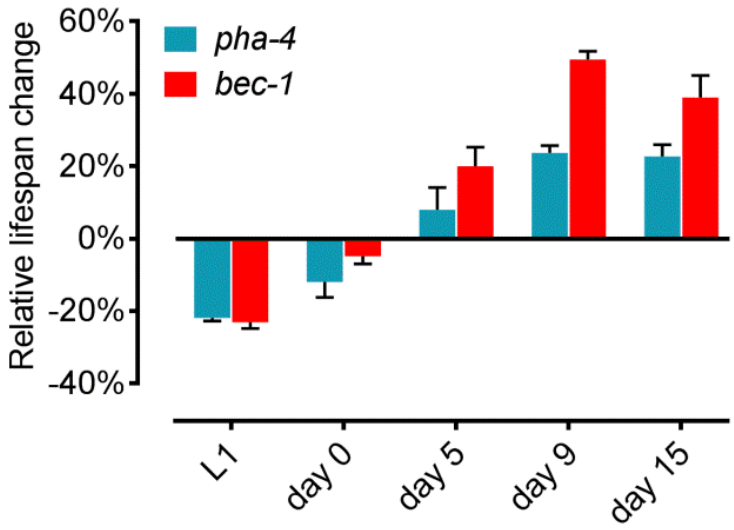

Figure 20: Inhibition of *pha-4* and *bec-1* modulate lifespan conversely across aging. RNAi targeting *pha-4* and *bec-1* leads to lifespan reduction during early larval development (L1) and young adulthood (day 0) but increase lifespan when commenced when adult worms are 5, 9 or 15 days old. (Data created by Jonathan Byrne)

was inactivated from day 5, 9 or day 15 we observed a marked increase in lifespan. Surprisingly, as compared to *pha-4*, post-reproductive inactivation of *bec-1* resulted in a greater lifespan extension. Specifically, day 9 inactivation of *bec-1* intervention caused a MTL extension of up to around 60%, twice that of *pha-4* inactivation from day 9. Yet, comparing the overall trend, *pha-4* and *bec-1* knockdowns exhibit matching AP effects across the lifespan. The inactivation of both genes results in the strongest lifespan reduction when initiated during early larval development, transitioning into positive effects on lifespan after reproduction that peak at day 9 of adulthood.

Longevity specific to autophagic nucleation complex inhibition

Since we observed strong lifespan extension on post-reproductive inactivation of the key autophagy gene *bec-1*, we set out to delineate the effects of the different members of the autophagic cascade on post-reproductive lifespan. As strong AP effects upon inactivation of the key autophagy BEC-1 complex

early and late in adult life were observed, we continued to investigate whether AP is a hallmark of all autophagy genes or exclusively for a specific subset. We inactivated several genes to specifically perturb the different steps of the autophagic flux at day 9 of adulthood. Following autophagy induction via the serine/threonine protein kinase UNC-51 and formation of the phagophore through the BEC-1/VPS-34/EPG-8 complex, the subsequent steps of the autophagic cascade include vesicle expansion and maturation, lysosomal fusion, autolysosomal degradation, and recycling (Figure 1, Table 1). Interestingly, we observed that BEC-1 complex members that build up the

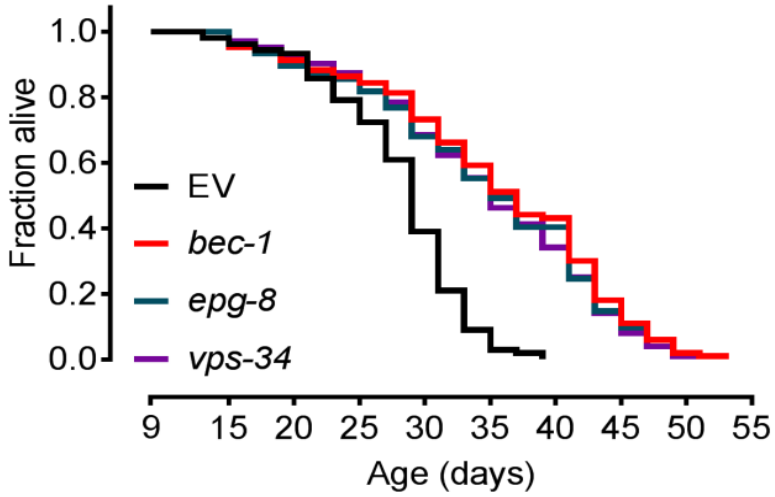

Figure 21: Inhibition of all three members of the autophagic vesicle nucleation complex equally extend *C.elegans* lifespan RNAi targeting *bec-1*, *epg-8*, and *vps-34* equally extend lifespan in rrf-3 mutant worms. - Lifespan assay was carried out in *rrf-3(pk1426)* worms; statistics are shown in supplemental table 1.

autophagic vesicle nucleation complex similarly and strongly extend lifespan upon their post-reproductive inactivation (Figure 21). Next, we inactivated several genes of the various autophagic flux steps from day 9 in order to investigate their effect on post-reproductive lifespan (Figure 22). Lifespan analysis revealed that the inhibition of this multistep process up to the point of vesicle nucleation strongly extends MTL. Conversely, genes that are involved in

the subsequent events of vesicle expansion, maturation, and recycling either did not change or reduced MTL upon inactivation. To test whether some of the observed discrepancies in the effect on lifespan may originate from insufficient knockdown of autophagy genes, we validated gene knockdown via real-time qPCR (Figure 23). We detected significant gene knockdown in the mRNA level for all RNAi targeted autophagy genes. Using western blotting, we also checked the reduction of LGG-1, BEC-1, as well as PHA-4 protein levels upon RNAi from day 9 (Figure 24). Notably, RNAi gene inactivation appeared to be more potent on the protein level than on the mRNA level. However, there was no correlation between the quantified mRNA reduction and lifespan effects of the genes. Surprisingly, day 9 inhibition of *lgg-1* significantly reduced lifespan whereas other autophagy genes presented in our study did not negatively affect lifespan. In addition to the significant lifespan shortening effects by *lgg-1* inactivation, we observed a very sick and sluggish worm phenotype within two days of *lgg-1* RNAi feeding (data not shown). As for the lifespan reduction, this sick phenotype was not observed for any other autophagy gene presented in our study. Overall, the negative phenotypes of *lgg-1* inhibition were independent of the treatment time-point and therefore did not exhibit AP behaviour. Combined, the strong discrepancies between lgg-1 and all other autophagic flux genes, including its homologue *lgg-2*, suggest a critical role for LGG-1 outside autophagy. To test this hypothesis, we simultaneously inactivated *bec-1* and *lgg-1* from day 9 of adulthood (Figure 25). Indeed, *lgg-1* inactivation from day 9 also shortens lifespan when autophagy is independently inactivated through simultaneous knockdown of *bec-1*.

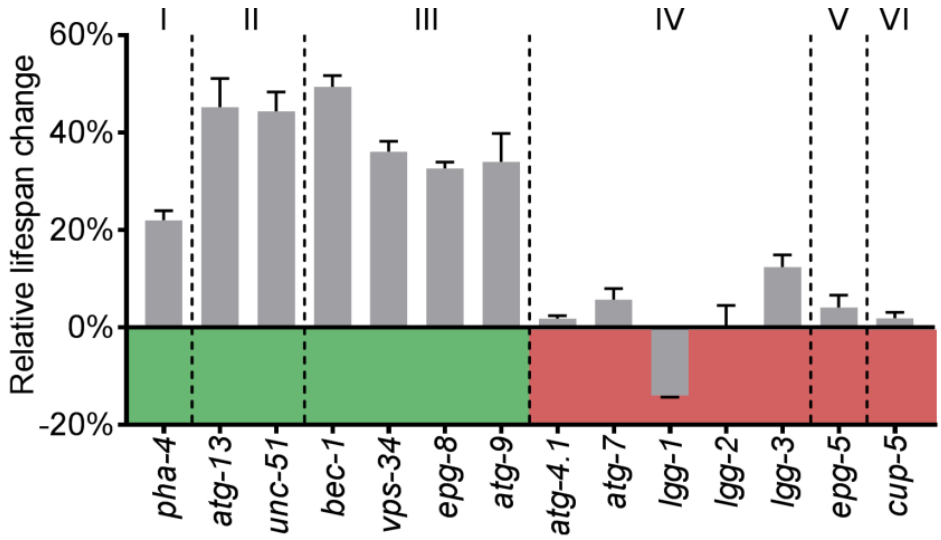

Figure 22: Post-reproductive inactivation of different autophagic flux genes. Day 9 RNAi targeting genes specific to the different steps of the autophagic cascade, including: regulation (I), induction (II), nucleation (III), expansion/maturation (IV), lysosomal fusion (V), and degradation (VI). Knockdown was carried out in *rrf-3* mutant worms. Showing relative percentage change in MTL +/- SEM compared to control. - Lifespan assay was carried out in *rrf-3(pk1426)* worms; statistics are shown in supplemental table 2.

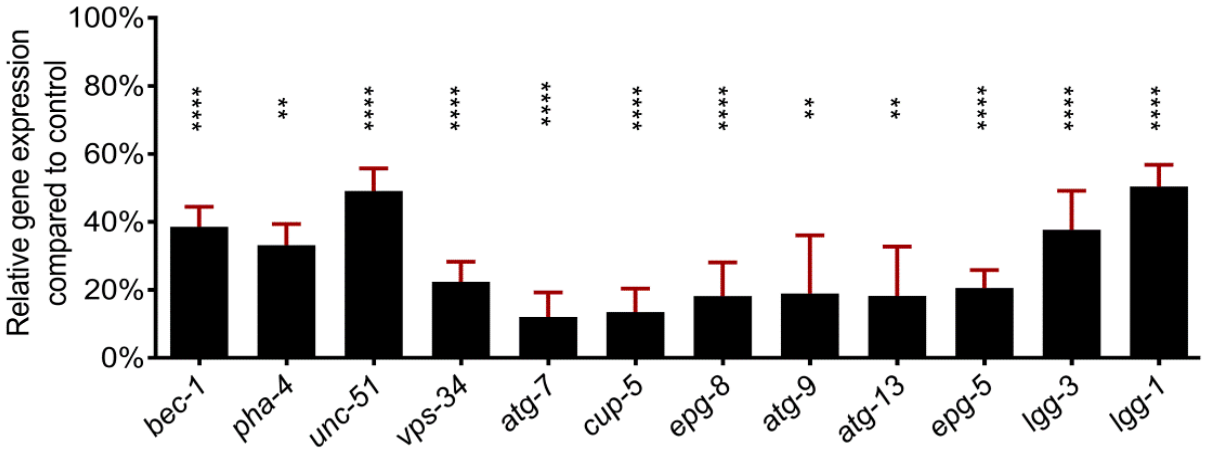

Figure 23: Real-time qPCR of autophagy flux gene expression upon day 9 RNAi. Relative gene expression (ΔΔCt) of day 12 old *rrf-3* mutant worms after initiation of RNAi from day 9.

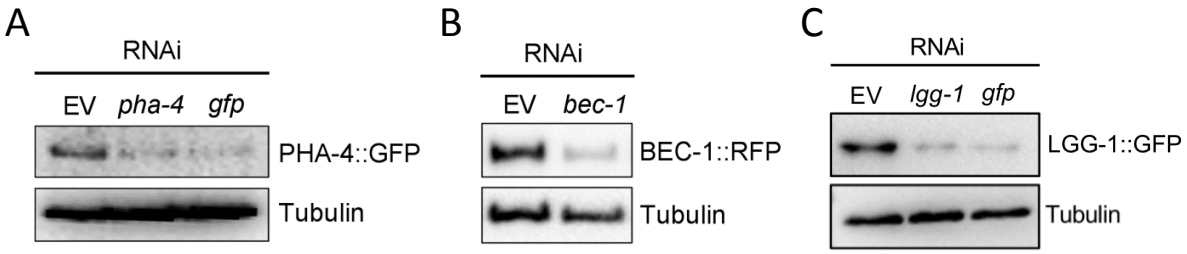

Figure 24: Representative western blot quantification of PHA-4, BEC-1, and LGG-1 upon day 9 RNAi. RNAi was initiated from day 9 and worms were harvested for western blot quantification at day 15 of adulthood. GFP-tagged PHA-4 and GFP were detected with an GFP antibody. RFP-tagged BEC-1 was detected with an RFP antibody.

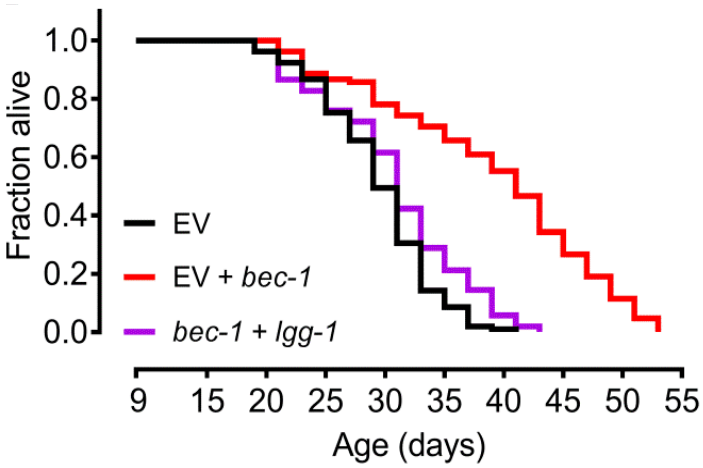

Figure 25: Combinatorial inactivation of *lgg-1* and *bec-1* from day 9 of adulthood. RNAi targeting *lgg-1* strongly reduces *bec-1* mediated longevity in post-reproductive worms. - Lifespan assay was carried out in *rrf-3(pk1426)* worms; statistics are shown in supplemental table 3.

Combined, our data suggests post-reproductive longevity is coupled to the early steps of the autophagic cascade up to and including the process of vesicle nucleation via the BEC-1/VPS-34/EPG-8 complex. However, inhibition of the later autophagic flux did not similarly result in longevity but had largely no effect on lifespan. The observed harmful effects mediated by the early autophagic flux as well as the apparent dispensability to a normal lifespan of

genes involved in the late autophagic flux, suggested a potential dysregulation or dysfunction of autophagy in aged *C. elegans*.

Dysfunctional autophagy in post-reproductive worms

When autophagosomes are formed, GFP::LGG-1 is recruited from its diffuse cytoplasmic localization to distinct foci that mark the autophagic double-membrane (Meléndez et al., 2003; Kang et al., 2007). When comparing young

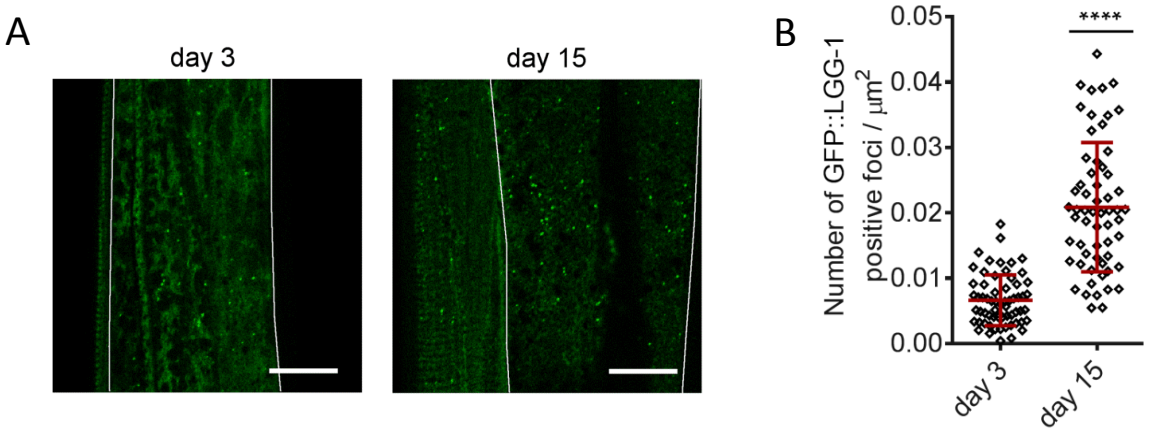

Figure 26: Age-related increase in autophagic structures. (A) Representative confocal image of GFP::LGG-1 marked autophagic structures within the hypodermis of young (day 3) and old (day 15) *rrf-3(pk1426); lgg-1p::GFP::lgg-1* worms. Scale bar represents 15 µm (B) Quantification of GFP::LGG-1 positive foci in the hypodermis of young (day 3) and old (day 15) worms; (**** = $p<0.0001$).

adult worms to aged post-reproductive worms, we observed a marked increase in LGG-1::GFP positive foci in the hypodermis (Figure 26). Using western blotting, we further detected a depletion of the two autophagic reporter protein GFP::LGG-1 and BEC-1::RFP pools with age (Figure 27, A and B). However, RNA sequencing results across *C. elegans* ageing did not mirror the age-related decline in autophagic proteins on the mRNA level (Figure 27C).

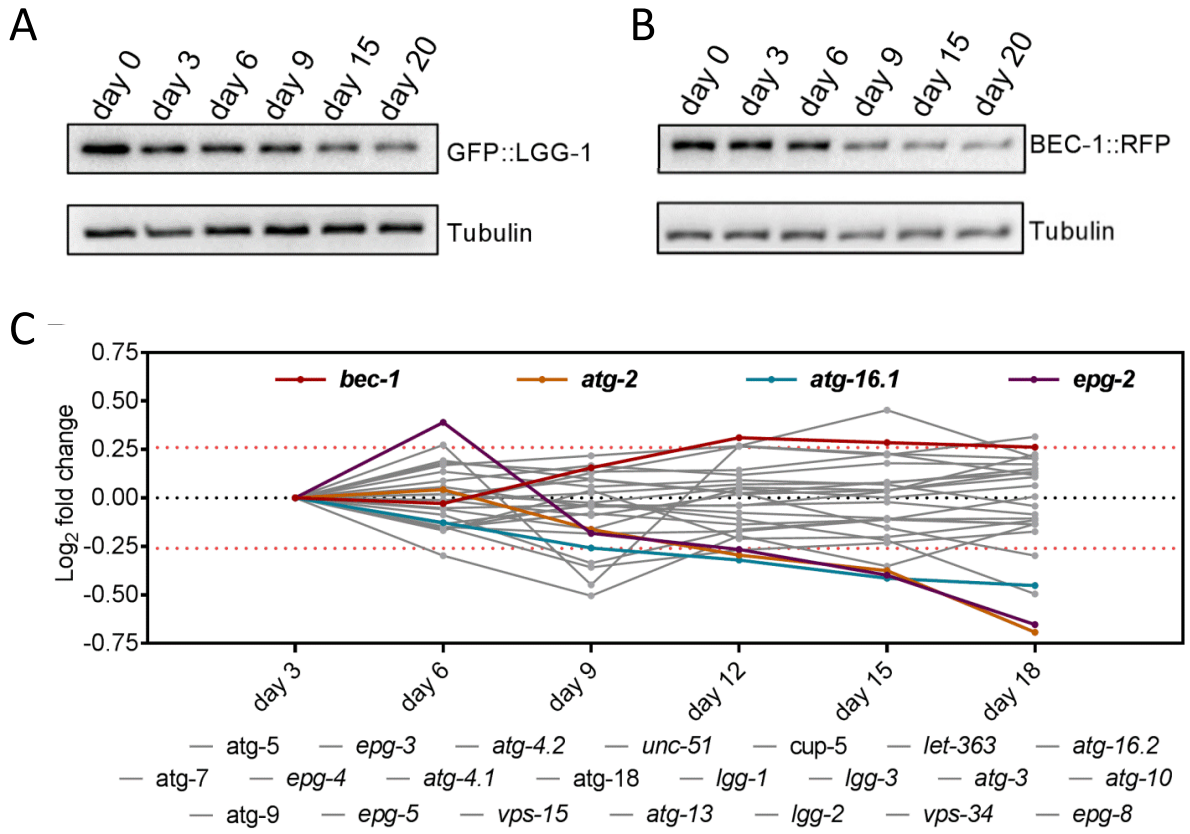

Figure 27: Age-associated changes to key autophagy genes on protein and mRNA level. (A) Representative western blot of GFP::LGG-1 levels across lifespan shows a decrease in LGG-1 protein levels as the worms ages. (B) Representative western blot of BEC-1::RFP levels across lifespan shows a decrease in BEC-1 protein levels as the worms ages. (C) RNA sequencing results of different autophagy genes across *C. elegans* lifespan. Log_2 fold change for the expression of each gene is plotted compared to day 3 values. Genes that show a greater change than +/- 20% (indicted as doted orange line) across three time-points are highlighted in colour and genes that do not exceed this threshold are depicted in grey. The overall abundance most autophagy genes does not markedly change at the mRNA level across lifespan.

This observation implies an increased autophagosome formation or dysfunctional autophagosomal recycling that depletes GFP::LGG-1 and BEC-1::RFP protein pools while mRNA levels of these genes are not diminished with age. Transcriptional upregulation of autophagy genes with age may be indicative of an increased induction of autophagy in post-reproductive worms. However, our sequencing results did not show a systemic upregulation of

autophagy genes (Figure 27C), which is in line with a recent proteomic study of ageing *C. elegans* (Walther et al., 2015). Of note, aged worms displayed a ~20% increase in *bec-1* mRNA levels (Figure 27C) that could hint at increasing autophagic nucleation events with age.

Next, we monitored GFP::LGG-1 foci levels in aged worms upon genetic inactivation of the individual steps of the autophagic flux. To this end we treated day 9-old worms with RNAi targeting *pha-4*, *unc-51, bec-1*, *atg-7*, *epg-5,* and *cup-5*. The inactivation of genes that govern the early autophagic flux, including vesicle nucleation and maturation, led to a significant reduction of GFP::LGG-1 positive foci (Figure 28). Conversely, the inactivation of *epg-5* and *cup-5* that are respectively essential for lysosomal fusion and degradation, respectively, did not significantly alter the GFP::LGG-1 foci numbers (Figure 28). When autophagy is functioning, the inactivation of *epg-5* and *cup-5* should

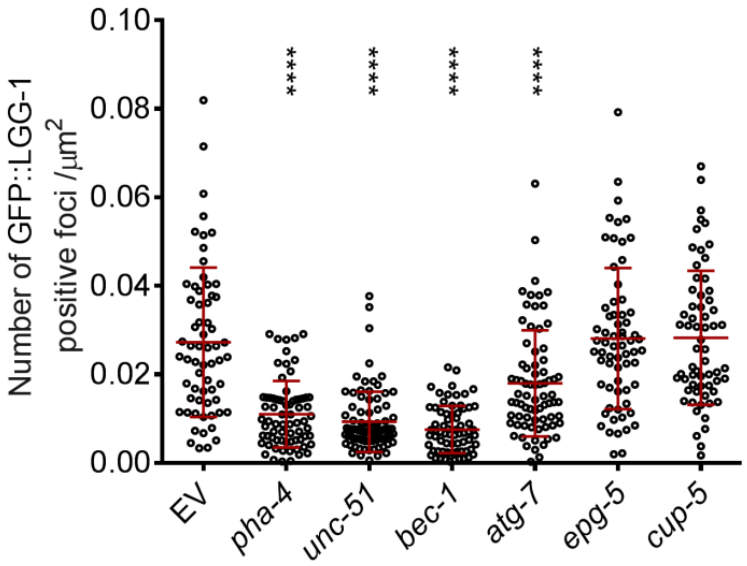

Figure 28: Day 9 inhibition of early autophagy genes decrease autophagic structures whereas the inhibition of late autophagy genes show no effect. Blot shows day 15 quantification of GFP::LGG-1 foci in the hypodermis of worms that *rrf-3(pk1426); lgg-1p::GFP::lgg-1* worms that were RNAi treated against different autophagy genes from day 9.

lead to an increase of autophagic numbers because their absence hinders autophagsome turnover (Tian et al., 2010; Sun et al., 2011). Thus, the observed lack of accumulation suggests a block of the late autophagic flux that results in an inefficient completion of the autophagic cascade. Once the autophagosome fuses with the lysosome to form the autolysosome, Atg8/LC3/LGG-1 reporter proteins are degraded by autolysosomal hydrolases (Klionsky et al., 2016). The fluorescent reporter protein GFP is more resistant to lysosomal hydrolases and will not be degraded if the autolysosomal degradation is inefficient. For that reason, the presence of undigested free GFP that derives from the GFP::LGG-1 fusion protein can be used as a measure for unproductive autolysosomal degradation (Figure 29A) (Klionsky et al., 2016). Interestingly, we observed a strong increase in the free GFP/GFP::LGG-1 ratio across *C. elegans* ageing (Figure 29A). These results imply that age-associated increases in autophagic structures are predominantly marked by free GFP, indicating a challenged autophagic system later in life. Throughout lifespan, we obtained similar results with worms expressing the autophagic reporter

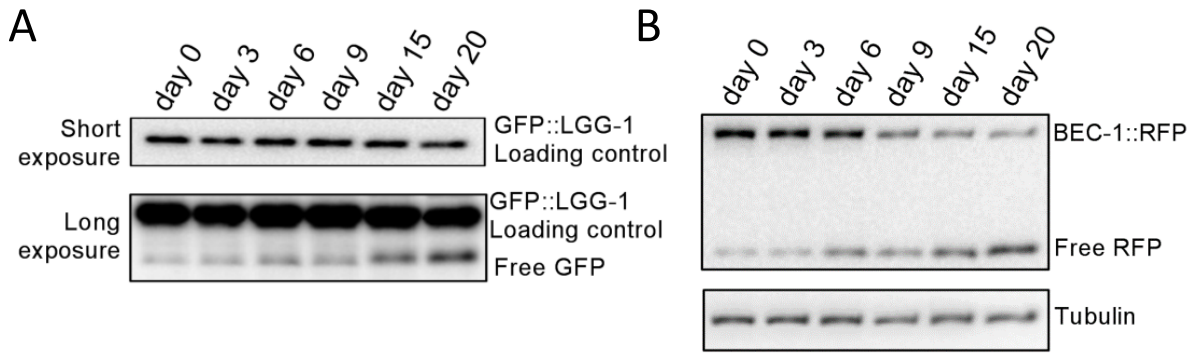

Figure 29: Cleaved fluorescent reporter proteins of autophagic makers increase with age. (A) Representative western blot of free GFP degradation product of GFP::LGG-1 increases relative to the GFP::LGG-1 protein pool. (B) Representative western blot of free RFP degradation product of BEC-1::RFP increases relative to the BEC-1::RFP protein pool.

protein BEC-1::RFP, which corroborates the previous findings (Figure 29B). We attribute the much stronger accumulation of the free RFP moiety over time as the worm ages to the fact that RFP is much more stable in acidic conditions compared to GFP (Shaner et al., 2005). Importantly, the increasing abundance of free GFP moiety from GFP::LGG-1 can either indicate an increase or a blockage in overall autophagy.

To discriminate between these options, we pharmacologically inhibited lysosomal degradation via chloroquine treatment in young and old worms (Figure 30A). Chloroquine is a lysosomotropic agent that inhibits lysosomal enzymes required for maintenance of a low lysosomal pH (Rutz et al., 2004; Shintani and Klionsky, 2004). This neutralization of the lysosomal pH in turn inhibits autolysosomal degradation. Young animals that were exposed to chloroquine showed an increase in free GFP that mirrored the rise observed in aged non-treated worms. However, chloroquine treatment did not further increase the level of free GFP in aged worms. Following, we genetically perturbed the lysosomal acidification through inactivation of the vacuolar ATPase subunit VHA-15 (Figure 30B). In line with the chloroquine effects in aged animals, we also did not detect an increase in free GFP upon inhibition of *vha-15* from day 9 (Figure 30C). Conversely, we observed a strong increase in free GFP upon *vha-15* inactivation in young animals (Figure 30D). Together, these findings indicate a dysfunction of the late autophagy flux at the step of cargo degradation in aged worms. It has been previously shown that blocking autophagy leads to the accumulation of the adaptor protein SQST-1/p62, which recognizes and loads cargo into the autophagosome for degradation. Intriguingly, we detected that SQST-1::GFP protein levels strongly increase in ageing worms (Figure 31A). However, we did not detect a matched increase in

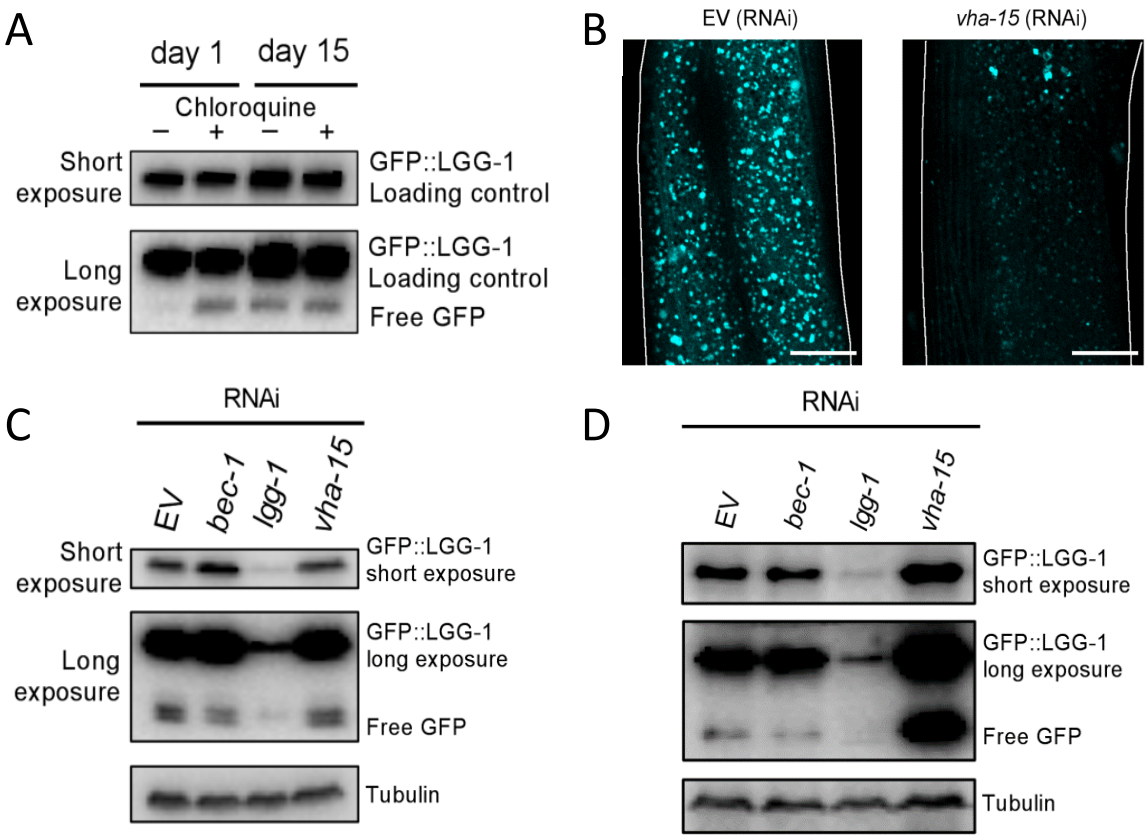

Figure 30: The late autophagic flux is dysfunctional in aged worms. (A) Representative western blot of free GFP degradation product of GFP::LGG-1 in young and old worms upon chloroquine treatment. Free GFP is balanced to GFP::LGG-1 full size protein levels. Protein was detected with anti GFP antibody. (B) LysoTracker staining of day 15 old worms upon RNAi treatment targeting vha-15 from day 9. Scale bar represents 20 µm. (C) Representative western blot of free GFP degradation product of GFP::LGG-1 in aged day 15 old worms that were exposed to RNAi treatment from day 9. Free GFP and GFP::LGG-1 full size protein were detected with anti GFP antibody and were balanced using an anti tubulin antibody.(D) Representative western blot of free GFP degradation product of GFP::LGG-1 in young day 4 old worms that were exposed to RNAi treatment from the first day of adulthood. Free GFP and GFP::LGG-1 full size protein were detected with anti GFP antibody and were balanced using an anti tubulin antibody.

its mRNA expression levels (Figure 31B). Together with the described increase in autophagic structures in aged animals (Figure 26B), this further argues for the presence of dysfunctional autophagy during aging. Additionally, we observed that inactivating *bec-1* in aged worms did not markedly increase SQST-1 levels (Figure 31C), whereas genetic inactivation of autophagy in young

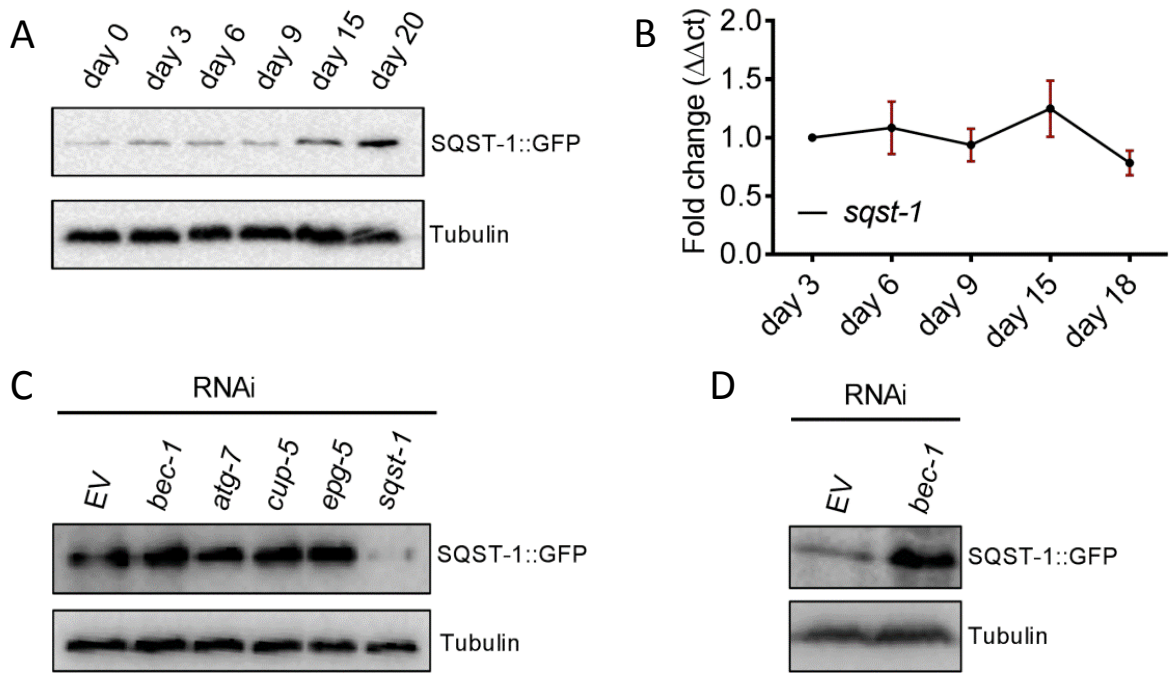

Figure 31: SQST-1 protein levels accumulate with age due to a dysfuntional autophagic system. (A) Representative western blot of SQST-1::GFP protein levels across aging. (B) qPCR quantification of relative mRNA levels (ΔΔCt) of sqst-1 across lifespan. (C) Representative western blot of SQST-1::GFP at day 15 upon RNAi knockdown of different autophagy genes from day 9. (D) Representative western blot of SQST-1::GFP at day 4 upon *bec-1* RNAi from first day 0; For all blots SQST-1::GFP was detected with anti GFP antibody anti tubulin antibody was used for balancing.

worms did strongly increase SQST-1 protein (Figure 31D). This further indicates a dysfunction of late-life autophagy. Further, perturbation of the lysosome through inactivation of the vacuolar ATPases *vha-15* and *vha-13* significantly reduced lifespan in young worms (Figure 32A). However, the same perturbation in day 9-old animals via the inactivation of *vha-15*, *vha-13*, *epg-5*, and *cup-5* did not affect lifespan (Figure 32B).

This observation substantiates our previous results and indicates a dysfunction of the lysosomal degradation machinery in aged worms. Taken together, our findings suggest two possible mechanisms by which post-

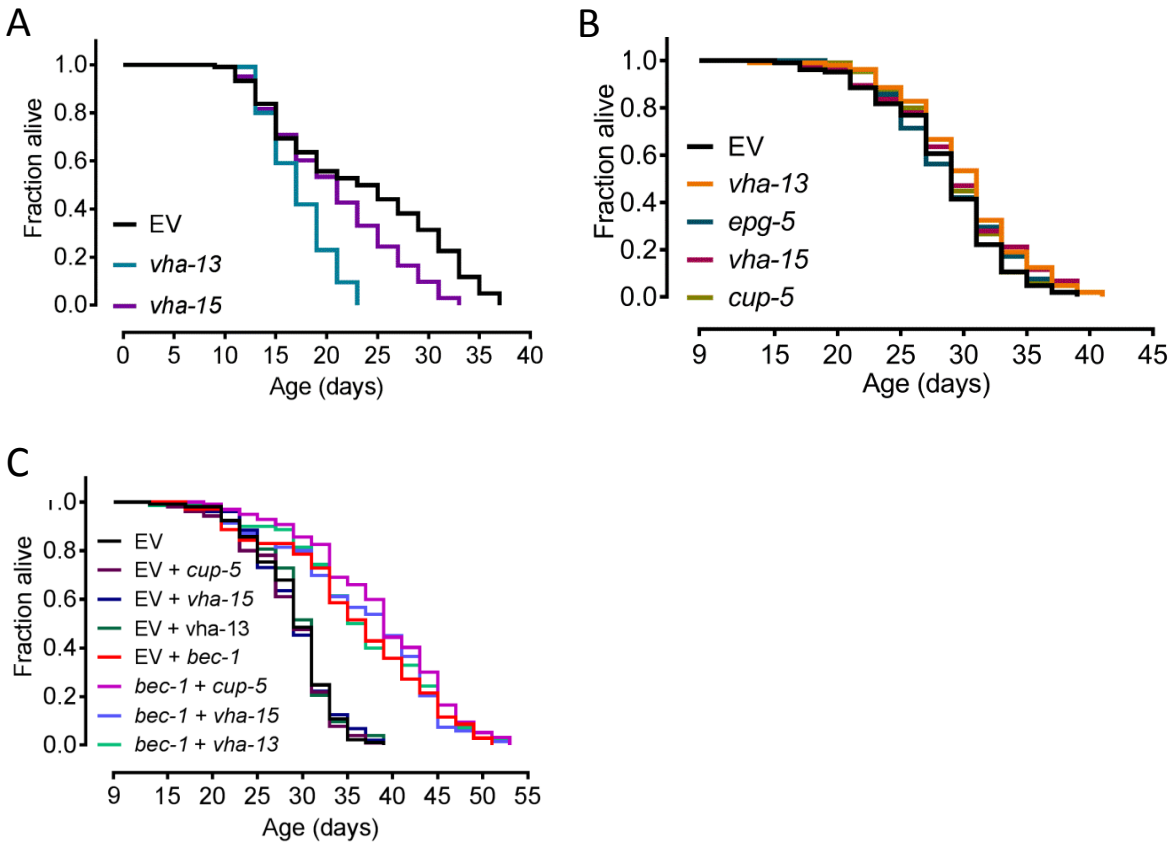

Figure 32: Autolysosomal genes are not required for post-reproductive lifespan or lifespan extension through *bec-1* inactivation. (A) Inactivation of *vha-13* and *vha-15* via RNAi from the first day of adulthood shortens lifespan. (B) Day 9 inactivation of different genes required for autolysosomal function does not effect post-reproductive lifespan. (C) Combinatorial day 9 RNAi targeting *bec-1* and autolysosomal genes does not reduce *bec-1* mediated longevity. - Lifespan assay was carried out in *rrf-3(pk1426)* worms; statistics are shown in supplemental tables 4 to 6.

reproductive inhibition of autophagic vesicle nucleation could be beneficial. It is conceivable that reduced nucleation events alleviate the pressure on the autophagic system and thereby restore productive autophagy. Alternatively, the inhibition of early autophagosome nucleation stops detrimental effects that arise from a dysfunctional autophagic machinery. To test for a restoration of functional autophagy through the inhibition of vesicle nucleation, we investigated whether *bec-1* mediated lifespan extension requires functional autolysosomal degradation. To this end, we simultaneously inactivated *bec-1*

and either *cup-5*, *vha-13,* or *vha-15* from day 9 (Figure 32C). Unexpectedly, this combinatorial inactivation did not reduce the *bec-1* mediated longevity. This shows that the lifespan extension though post-reproductive inhibition of autophagic vesicle nucleation does not require functional autolysosomal degradation. Thus, the post-reproductive inactivation of *bec-1* does not appear to restore functional autophagy. Instead, its lifespan-extending properties likely arise through the inhibition of harmful consequences of impaired late stage autophagy.

Neuronal inhibition of vesicle nucleation extends lifespan

After identifying AP effects of *pha-4* and *bec-1* in *rrf-3* mutants, we investigated whether this phenotype also holds true for WT worms. It was intriguing that post-reproductive inactivation of genes that govern the early autophagic flux increased lifespan to a lesser extent in WT animals than previously observed for *rrf-3* mutants (Figure 33). Day 9 longevity effects of

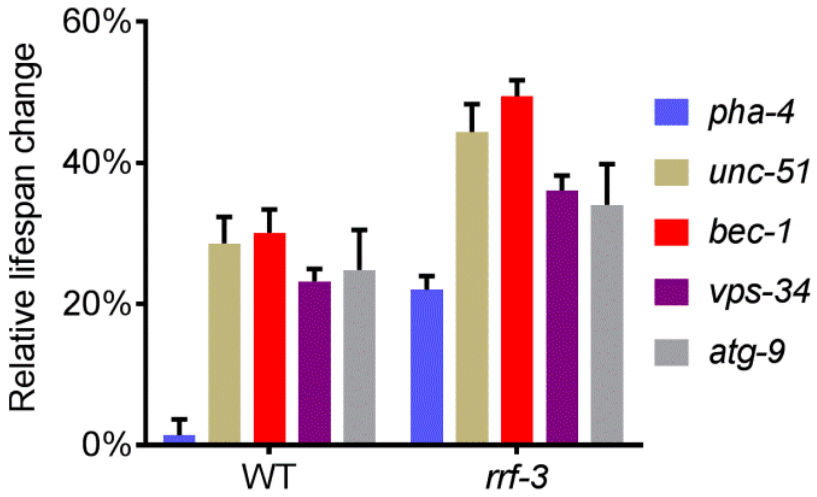

Figure 33: Relative change in MTL upon post-reproductive RNAi in WT and *rrf-3* mutants. Bars show mean of at least three independent experiments +/- SEM. . - Lifespan assay was carried out in WT and *rrf-3(pk1426)* worms, respectively; statistics are shown in supplemental table 7.

bec-1, vps-34, unc-51, and *atg-9* RNAi in WT were roughly half as strong, extending MTL by approximately 30%. Lifespan extension mediated through post-reproductive inactivation of *pha-4* was even more strongly reduced, leading to no detectable lifespan extension upon day 9 inactivation of *pha-4* in WT worms. This interstrain longevity discrepancy may be due to an increased overall RNAi efficiency in *rrf-3* mutants (Simmer et al., 2002). Hence, we compared day 9 RNAi knockdown effectiveness between WT and *rrf-3* mutants via qPCR. As expected, we observed a reduced knockdown efficiency in WT compared to *rrf-3* worms at day 12. However, this effect equalized by day 15 (Figure 34).

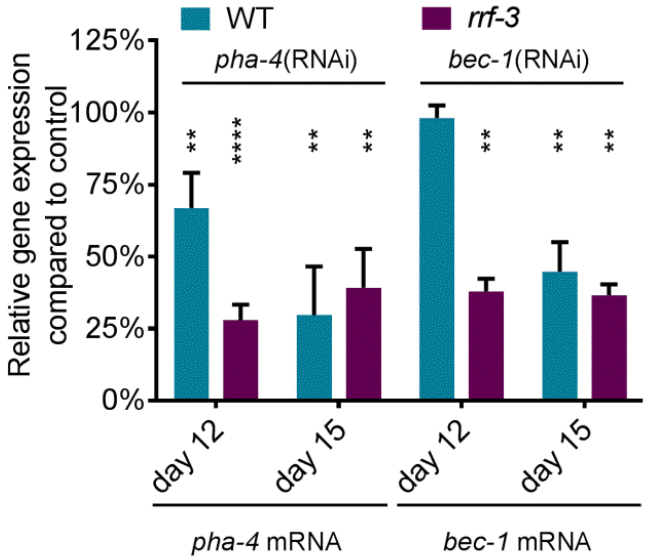

Figure 34: Relative *pha-4* and *bec-1* gene expression upon post-reproductive inactivation in WT and *rrf-3* mutants. Graph displays mRNA levels measured by qPCR at day 12 and day 15 upon day 9 RNAi treatment. (Data created by Jonathan Byrne)

In addition to enhanced global RNAi efficiency, *rrf-3* mutants are known to exhibit a neuronal RNAi hypersensitivity (Simmer et al., 2002). In contrast, WT worms are largely refractory to RNAi in the nervous system (Timmons et al., 2001). We showed that this neuronal hypersensitivity also persists in aged

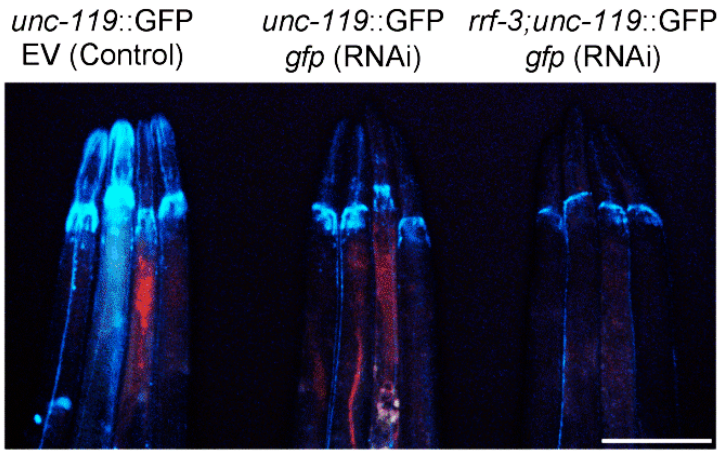

Figure 35: Expression of neuron specific UNC-119::GFP reporter protein upon RNAi inactivation in RNAi hypersensitive *rrf-3* mutants and in WT worms. Representative fluorescent microscopy picture comparing UNC-119::GFP reporter protein abundance upon day RNAi knockdown in head neurons of WT and rrf-3 mutant worms. Scale bar represents 200 µm.

rrf-3 mutants (Figure 35). We did so by employing the neuronal reporter *unc-119::gfp*, which we inactivated in the *rrf-3* mutant background as well as in control WT worms. This treatment led to a much stronger neuronal reduction of UNC-119::GFP in the RNAi hypersensitive background and prompted us to investigate a neuronal contribution to our observed longevity phenotypes.

During *C. elegans* RNAi feeding, interfering dsRNA enters cells via the channel protein SID-1 (Winston, 2002; Li et al., 2015). Neuronal cells lack this transporter protein and therefore are mostly resistant to RNAi feeding mediated gene inactivation (Timmons et al., 2001). In contrast, mutants with an enhanced RNAi response (such as the *rrf-3* mutant) or mutant worms that express *sid-1* in the neurons, show an enhanced neuronal sensitivity to RNAi feeding (Calixto et al., 2010). In order to examine the effects of neuron-specific inactivation of the autophagic vesicle nucleation complex on post-reproductive longevity, we employed the *sid-1(-); unc-119p::sid-1(+)* mutant strain (Figure 36).

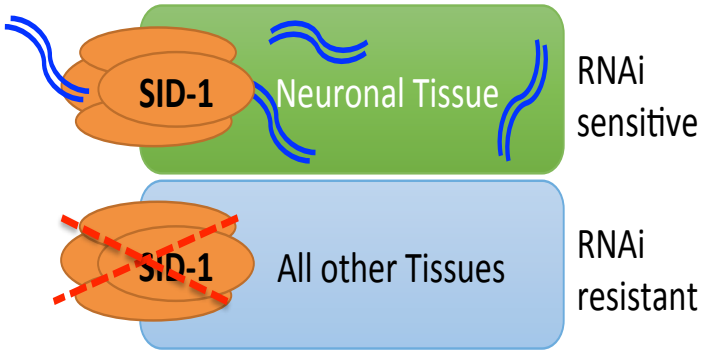

Figure 36: Model of SID-1 coordinated uptake of ingested dsRNA in *sid*(-) mutants that express *sid*(+) from a neuron-specific promoter. The channel protein SID-1 allows ingested dsRNA (blue lines) to diffuse into and between cell in order to mediate RNAi. Therefore, RNAi via feeding of dsRNA expressing bacteria is not effective in worms with a sid-1 loss of function mutation [sid-1(pk3321)]. Neurons are generally refractory to feeding RNAi as they do not express sid-1. Mutants that express sid-1 under the control of a neuron-specific promoter are rendered sensitive to neuronal RNAi [unc-119p::sid-1]. Double mutants with dysfunctional sid-1 in all tissues that carry functional sid-1 from a neuronal promoter [sid-1(pk3321); unc-119p::sid-1] are refractory to RNAi in all tissues except the neurons, which are rendered RNAi sensitive.

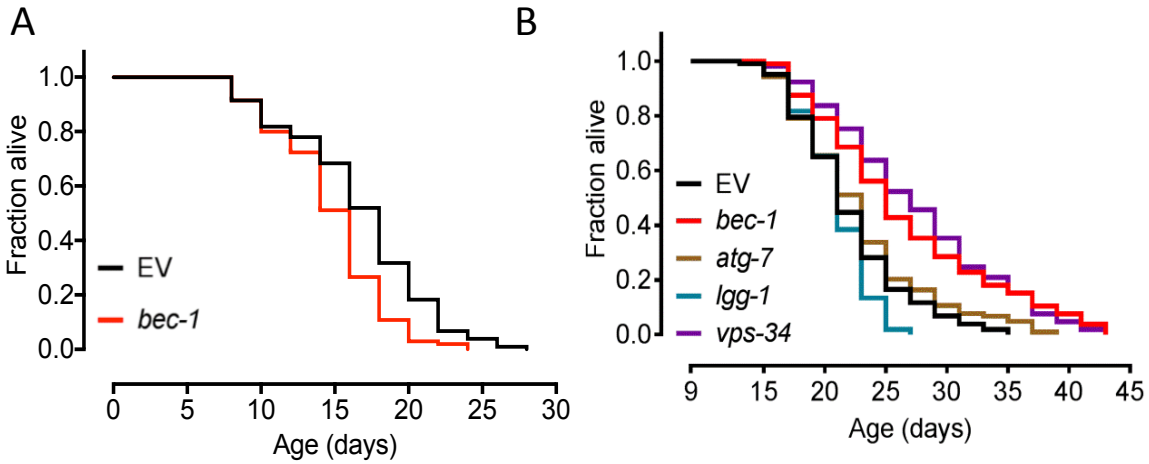

Figure 37: Neuron-specific inactivation of early *bec-1* shows AP, whereas late autophagy flux genes do not extend lifespan via the neurons. MTL effects upon day 9 RNAi against different genes of the autophagic flux in *sid-1*(pk3321); *unc-119p::sid-1* worms from (A) day 0 of adulhood and (B) day 9 of adulhood. - statistics are shown in supplemental table 8 and 9.

These mutant worms are hypersensitive to RNAi in neurons but refractory in all other tissues (Calixto et al., 2010). We first tested whether or not the inactivation of *bec-1* results in reduced longevity when inhibited in the nervous system. Indeed, neuron-specific inactivation of this key autophagy gene in young animals led to a significant decrease in lifespan (Figure 37A). Interestingly, neuron-specific inactivation of *bec-1* and *vps-34* from day 9 led to a strong MTL extension of up to 57% (Figure 37B). As previously observed for *rrf-3* mutants, day 9 inhibition of *atg-7* in the neurons did not affect lifespan, whereas the inactivation of *lgg-1* reduced MTL (Figure 37B). These results suggest that the observed post-reproductive longevity effects in *rrf-3* mutants are primarily mediated through neurons. To test effects mediated by other tissues we used *rde-1* mosaic mutants. Once dsRNA enters the cell through the SID-1 channel, the argonaut protein RDE-1 is required to achieve dsRNA mediated gene knockdown (Tabara et al., 1999). In this way, tissue-

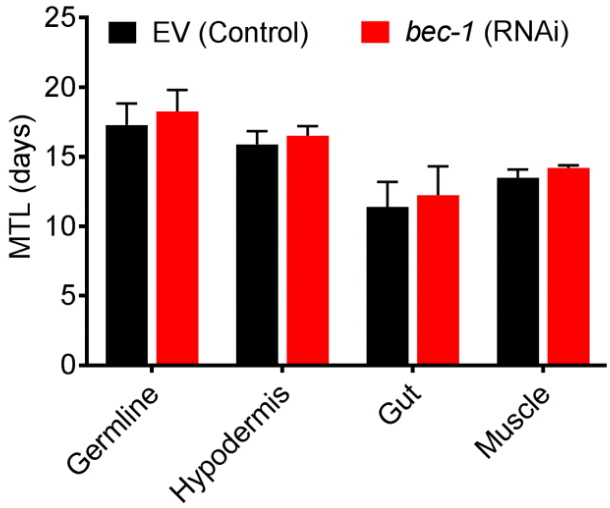

Figure 38: Tissue specific inactivation of *bec-1* from day 9 in the germline, hypodermis, gut, or in muscles has no significant lifespan effects. Tissue specific knockdown was initiated via RNAi feeding from day 9 in mutants that are refractory to RNAi in all tissues but *rde-1(ne219); nhx-2p::rde-1* (gut), *rde-1(ne219); lin-26p::rde-1* (hypodermis), *rde-1(ne300); myo-3::RDE*-1 (muscle), or *rde-1(ne219); lag-2p::rde-1* (germline niche). - statistics are shown in supplemental tables 9.

specific *rde-1* mosaic allows for RNAi mediated gene knockdown exclusively in one specific tissue, whereas other tissues are not affected (Qadota et al., 2007). Tissue-specific inactivation of *bec-1* in the germline niche, muscle, gut, or hypodermis did not significantly impact the lifespan of post-reproductive *C. elegans* (Figure 38). These observations suggest that enhanced neuronal RNAi is likely the main contributor to the extended longevity that was observed in *rrf-3* mutants, whereas other tissues may only have minor combinatorial effects on lifespan. In summation, our data implies that post-reproductive inhibition of the autophagic nucleation complex extends lifespan primarily through the neurons.

Neuronal inhibition of vesicle nucleation extends healthspan

Next, we investigated the effects of post-reproductive neuronal inactivation of autophagic vesicle nucleation on *C. elegans* healthspan. To this end, we

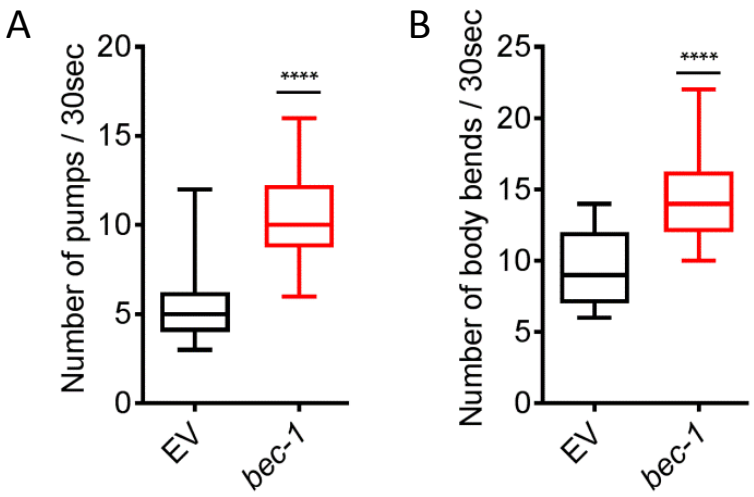

Figure 39: Improved healthspan upon post-reproductive inactivation of *bec-1* specifically in the neurons. (A) Quantification of pharynx pumping at day 20 upon day inactivation of *bec-1* in *sid-1*(pk3321); *unc-119p::sid-1* worms. (B) Quantification of movement by scoring of body bends at day 20 upon day inactivation of *bec-1* in *sid-1*(pk3321); *unc-119p::sid-1* worms. - Box plots extends from 25 to 75 percentiles and the line is plotted at the median; whiskers indicating the absolute measurement range. (Data created by Johannes Geisinger)

inactivated *bec-1* from day 9 in *sid-1(-); unc-119p::sid-1(+)* mutants and monitored the influence on two widely used indicators of healthspan, namely the pharyngeal pumping rate of body lateral bends (Onken and Driscoll, 2010; Leiser et al., 2011).

Neuron-specific inactivation of *bec-1* resulted in improved mobility and an increased pharyngeal pumping rate (Figure 39, A and B). Moreover, we observed that the same treatment led to a more youthful muscle structure and reduced sarcopenia in aged worms (Figure 40). Intriguingly, we did observe similar effects when inactivating *bec-1* from day 9 specifically in the muscles (Figure 41). As such, the inhibition of the vesicle nucleation complex through *bec-1* in the musculature did not improve pharyngeal pumping, mobility, or age-related sarcopenia. Hence, it appears that the post-reproductive inhibition of *bec-1* in neurons gives a cell non-autonomous improvement in global health and muscle integrity.

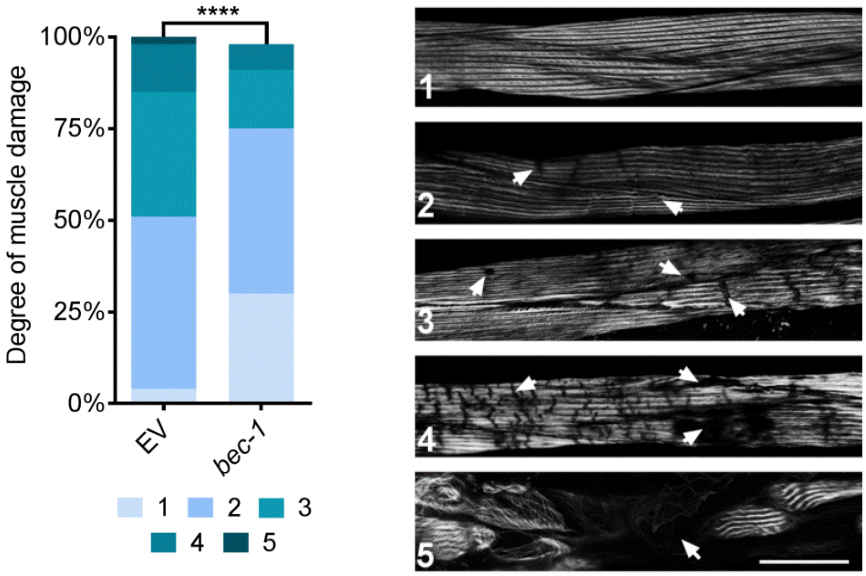

Figure 40: Neuron-specific inactivation of *bec-1* in post-reproductive worms reduces muscle degeneration. Quantification of age-related sarcopenia at day 20 upon day 9 inactivation of bec-1 in *sid-1*(pk3321); *unc-119p::sid-1* worms. Microscopic pictures represent five-point scale that was used to quantify the degree of muscle damage. White arrows indicate sites of muscle damage. Scale bar represents 30 µm (**** = p<0.0001).

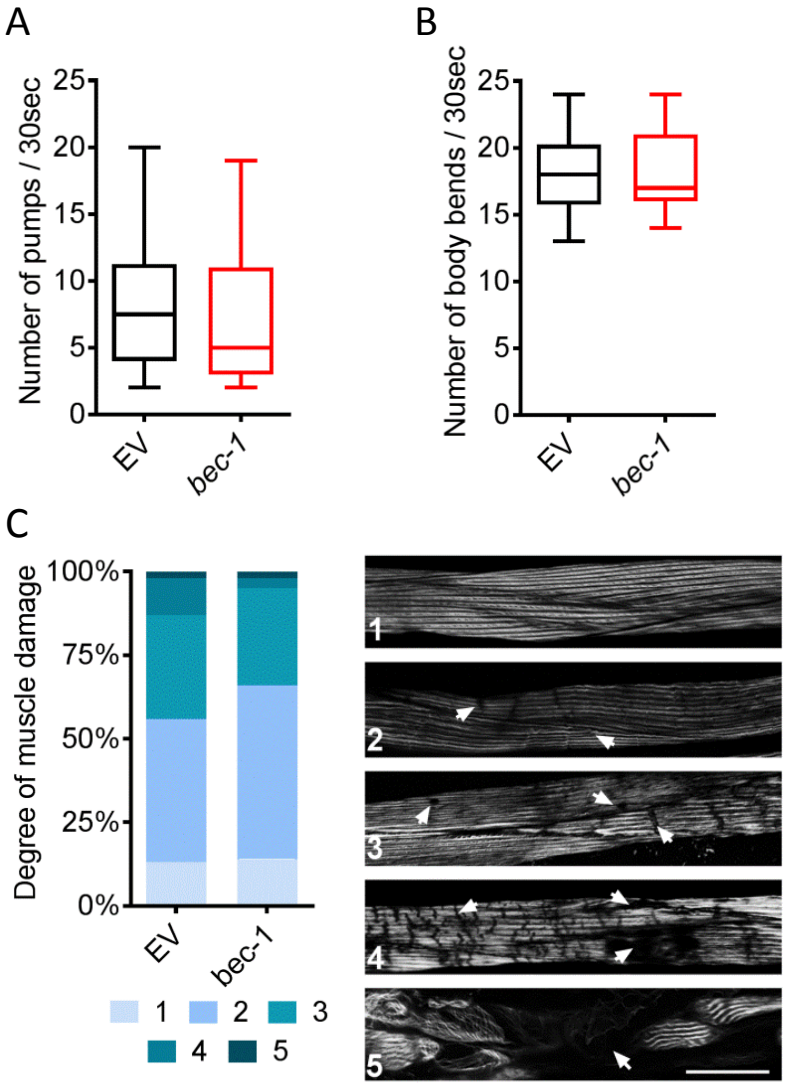

Figure 41: Muscle-specific inactivation of bec-1 in post-reproductive worms does not improve healthspan or sarcopenia. (A) Quantification of pharynx pumping at day 20 upon day inactivation of *bec-1* in *myo-3::RDE-1* worms that experience muscle-specific RNAi. (B) Quantification of movement by scoring of body bends at day 20 upon day inactivation of *bec-1* in in *myo-3::RDE-1* worms that experience muscle-specific RNAi. (C) Quantification of age-related sarcopenia at day 20 upon day 9 inactivation of bec-1 in *myo-3::RDE-1* worms that experience muscle-specific RNAi.. Microscopic pictures represent five-point scale that was used to quantify the degree of muscle damage with a 63x magnification. - White arrows indicate sites of muscle damage. Scale bar represents 30 µm (**** = p<0.0001). Box plots extends from 25 to 75 percentiles and the line is plotted at the median; whiskers indicating the absolute measurement range.

Neuronal inhibition of vesicle decreases neurodegeneration

Next, we examined if the inhibition of the early autophagic flux impacts age-related neurodegeneration in *C. elegans*. We did so by imaging the longitudinal neuronal network, using the neuronal reporter UNC-119::GFP. In RNAi hypersensitive *rrf-3* mutant worms that carry the *unc-119::gfp* reporter construct, we observed that *bec-1* inactivation from day 9 led to a marked decrease in neurodegeneration by day 20 of adulthood (Figure 42). Afterwards, we quantified the degree of axonal degeneration by employing a three-point scale, measuring the amount of neuronal bubbling and gaps within the axonal structures (Figure 43). This quantification identified a highly significant neuroprotection phenotype in worms that were treated with *bec-1* RNAi from day 9 of adulthood.

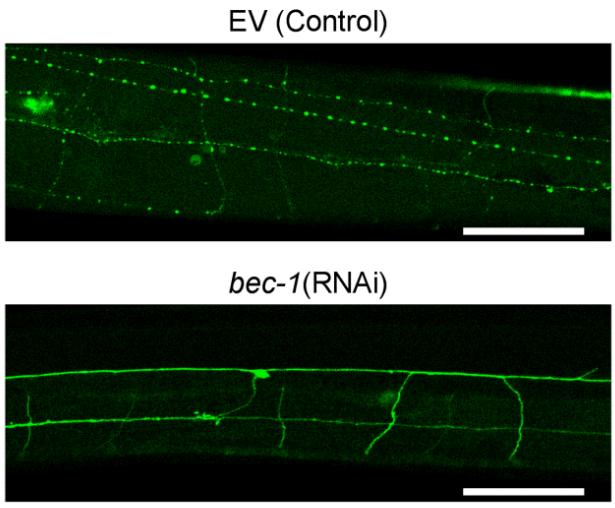

Figure 42: Neuron-specific inactivation of bec-1 in post-reproductive worms ameliorates age-associated neurodegeneration. Representative microscopy images depicting the longitudinal axonal network in the mid-body region or *rrf-3(pk1426); unc-119::gfp* worms at day 20 upon day 9 RNAi targeting bec-1. Images were taken at a 40x magnification and the scale bar represents 50 µm.

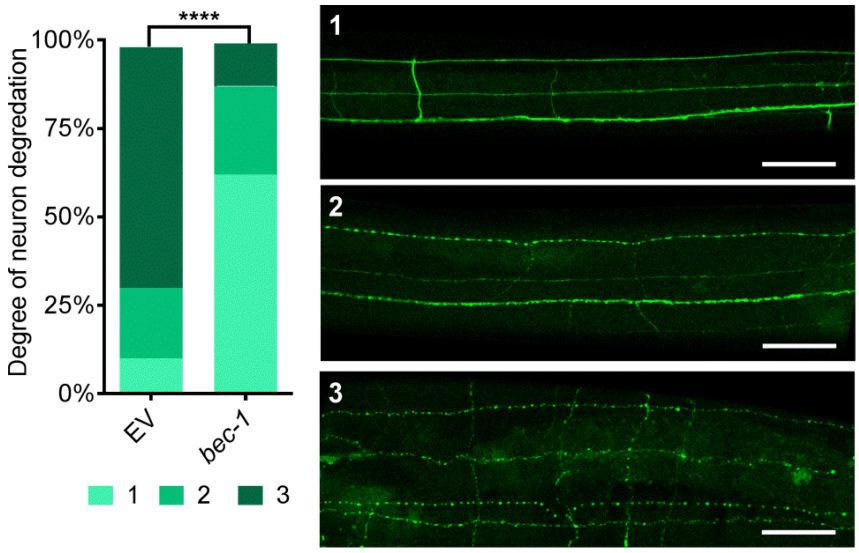

Figure 43: Quantification of age-related neurodegeneration at day 20 upon day 9 inactivation of bec-1 in *unc-119p::GFP; rrf-3(pk1426)* worms. Microscopic pictures represent three-point scale used to quantify the degree of neuronal damage by judging the amount of neuronal bubbling and axonal gaps with a 40x magnification. Scale bar represents 40 µm (**** = p<0.0001).

Discussion

Post-reproductive longevity screens for AP genes

Many prevalent and severe age-associated diseases such as cancer and neurodegenerative disorders have a genetic basis (Kulminski et al., 2016), which should have been selected against during evolution. However, the AP theory of ageing predicts that genes with detrimental effects late in life can be selected for if they promote fitness in early life. Thought-provokingly, recent genome-wide association studies (GWAS) in humans have shown that disease risks associated with a given allele are highly sensitive to chronological age (Kulminski et al., 2016; Rodríguez et al., 2017). Specifically, these studies show that certain alleles are linked to disease risks in an antagonistic fashion since they are protective against an early onset of a disease while promoting its late-

life progression. While research on short-lived model organisms such as *C. elegans* and *Drosophila melanogaster* have led to the discovery of many mutations that alter lifespan (Aigaki et al., 2002; Ni and Lee, 2010), these studies largely ignored late-life genetic effects. In line with the AP hypothesis of ageing, many longevity pathways that are modulated from early life reduce overall fitness of the mutant animal (Van Voorhies et al., 2006). In this way, it has been shown that long-lived IGF-I receptor mutant worms are quickly outcompeted and become rapidly extinct when co-cultured with WT worms (Jenkins et al., 2004). Hence it seems as though there is a species-specific trade-off between organismal fitness and longevity. This predicament may be overcome if genes that are needed for fitness in early life are specifically inhibited in late life, when natural selection is inefficient, to diminish their detrimental effects. Since the formulation of the AP theory of ageing sixty years ago, it is only recently that genetic tools have been available to experimentally test this approach. To the best of our knowledge we here present the first genetic screen that specifically inhibits genes after reproduction, within the evolutionary selection shadow, to identify novel genes that behave according to the AP theory of ageing. With this approach, we identified 30 previously unknown longevity genes that increase lifespan upon post-reproductive inactivation. These findings not only show that AP is a ubiquitous modulator of lifespan but may also lend insights into the progression of age-associated diseases. Five per cent of the 800 RNAi clones that were post-reproductively screened in our non-automated 24 well system showed longevity effects of which over 80% had not been previously described to extend lifespan. The here developed automated AP screen using 96-transwell plates should allow for a genome-wide screening for late-life

longevity in the future. Such a screening would target roughly 20,000 coding genes and should, if the rate of hits would be comparable to our 24-well screen, lead to the identification of hundreds of AP genes; this could substantially advance understanding of the ageing process.

Status of the autophagic flux in late-life

The current view on autophagy is predominated by its advantageous cytoprotective and longevity-promoting effects. In contrast, our findings suggest that this view needs to be adjusted when looking at the aged organism. We here show that the inactivation of key autophagy genes shortens lifespan when inactivated until day one of adulthood. In contrast, the inactivation of these genes resulted in lifespan extension with progressing age. Specifically, we showed that post-reproductive inhibition of genes that are involved in the process of autophagosome formation strongly extends *C. elegans'* lifespan and health span. In order to investigate how these genes modulate lifespan conversely over ageing we investigated the status of the autophagic flux as the animals get older. We observed functional autolysosomal degradation in young worms which could be disrupted either genetically or pharmacologically. In contrast, autolysosomal degradation becomes ineffective in aged worms, as measured via the accumulation of the free GFP moiety from GFP::LGG-1. Notably, this malfunctioning process could not be further impaired in aged worms though genetic or pharmacological perturbations. Further, blocking late stages of the autophagic flux should interrupt the turnover of autophagosomal vesicles and lead to an accumulation of autophagic structures. Conversely, we observed no further increase in autophagic structures upon genetic inhibition of late stage

autophagy. This indicates a blocked autophagic flux at the degradation step in aged worms, which leads to the accumulation of dysfunctional autophagosomes. Notably, similar observations have previously been made in hepatocytes of ageing mice (Terman, 1995; Del Roso et al., 2003). These studies show that autophagic-proteolytic response as well as the elimination of autophagic vacuoles slow down during aging. This malfunction of the autophagic flux appears to result in a decline of functional autophagy. This is evidenced by the age-associated accumulation of the SQSTM1/p62 ortholog SQST-1, which recognizes and loads cargo for degradation into the autophagosome. This finding is corroborated by our observation that the accumulation of SQST-1 strongly increases upon inactivation of key autophagy genes in young but not in old worms. Overall, our findings reveal that autophagy becomes dysfunctional as *C. elegans* ages and shows defects specifically at the step of autolysosomal degradation.

In line with a late-life dysfunction of the autolysosomal degradation, the perturbation of the lysosome through inactivation of the vacuolar ATPases *vha-15* and *vha-13* significantly reduced lifespan in young worms (Figure 31A), while not affecting lifespan when inactivated in aged worms (Figure 31B). It is of interest that autolysosomal degradation has been previously described as dysfunctional in ageing neurons and cell culture models of neurodegenerative diseases (Cuervo and Dice, 2000; Larsen et al., 2002; Lynch and Bi, 2003; Boland et al., 2008; Sadasivan et al., 2010). In addition, brain sections of patients with neurodegenerative diseases display build-up of dysfunctional late autophagosomes and autolysosomes (Nixon, 2013).

Inhibition of autophagy nucleation mediates longevity

We show that only the inactivation of genes that mediate the early steps of the autophagic cascade result in longevity. Specifically, we demonstrate that this longevity effect depends on the inhibition of the BEC-1/VPS-34/EPG-8 autophagic nucleation complex, or its upstream regulators such as the transcription factor PHA-4, and the serine/threonine protein kinase UNC-51. In contrast, genes involved in later stages of autophagosomal maturation do not similarly extend lifespan when knocked down post-developmentally.

Notably, there is no clear correlation between the reduction of quantifiable GFP::LGG-1 puncta marking autophagic structures and post-reproductive longevity effects. As an example, the late-life inhibition of ATG-7 that is required for vesicle expansion (Levine and Klionsky, 2004) also significantly reduced quantifiable GFP::LGG-1 puncta without altering lifespan. Similarly, LGG-1/Atg8 regulates vesicle expansion and completion (Levine and Klionsky, 2004) but does not positively affect *C. elegans* lifespan when inactivated late in life. Hence, lifespan extending effects are coupled to the inhibition of the early event of vesicle nucleation, which implies that this process is harmful in the context of late-life dysfunctional autophagy.

Our data also indicates that the process of vesicle nucleation is potentially hyper-activated in late life. We observe that the early autophagic flux is still active post day 9, as we detected a reduction of autophagic structures following inactivation of the early autophagic flux and a decrease in free GFP and *bec-1* RNAi at day 9 (Figure 27, Figure 29C). Further, while cleaved RFP as well as GFP moieties increase with age, the respective full-size reporter proteins BEC-1::RFP and GFP::LGG-1 strongly decrease with age

(Figure 26, A and B). However, this is not mirrored by the endogenous mRNA expression of these genes (Figure 26C). In fact, we saw a ~20% increase in *bec-1* gene expression across aging. Together with the marked increase with age in GFP:LGG-1 foci, these results suggest an increased and possibly excessive autophagy induction late in life. It is also possible that the observed dysfunction of the late steps of the autophagic flux in aged worms triggers a compensatory mechanism, which results in increased vesicle nucleation.

Lifespan reduction due to LGG-1 pleiotropism

Day 9 inhibition of *lgg-1* led to strong lifespan reduction that was not observed for any other gene in the autophagic flux upon post-reproductive inhibition (Figure 21). Further, we observed a very sick and sluggish phenotype within two days of *lgg-1* RNAi feeding (data not shown). This negative phenotype was independent of the treatment time-point and hence did not exhibit an AP behaviour. Also, no other gene of the flux caused produced sick or sluggish worms upon day 9 inhibition. Interestingly, other genes needed for the function of LGG-1 in autophagy, such as ATG-7 and LGG-3 did not produce negative effects when inactivated post-reproductively. Further, day 9 inhibition of the LGG-1 homologue LGG-2, which acts synergistically to modulate lifespan through autophagy in early life (Alberti et al., 2010) did not decrease *C. elegans* lifespan. Our data show that there is a dysfunction in autolysosomal degradation with age. We show that further disruption of autophagy through inhibiting autophagic fusion/degradation via *epg-5, cup-5, vha-13,* and *vha-15* has no negative effect on lifespan. Thus, it is highly unlikely that inhibition of *lgg-1* could disrupt the autophagic process, and become the only member of this pathway to shorten lifespan. Importantly, *lgg-1* day 9

RNAi still exerts negative effects when autophagy is independently repressed through simultaneous *bec-1* inactivation (Figure 24). Combined, these findings demonstrate that LGG-1 has a critical role outside autophagy. Such a process could be the ER-associated degradation (ERAD) tuning process, which operates on LC-3 decorated membrane vesicles but is otherwise independent of autophagy (De Haan et al., 2010).

Neuronal contribution to observed longevity

Decreased autophagic activity is closely linked to ageing (Kaushik and Cuervo, 2015). We here show active, and possibly increased, autophagosome formation with blocked autophagic degradation in aged *C. elegans*. Autophagy can be a double-edged sword that promotes neuroprotection when functional (Ravikumar et al., 2004; Wang et al., 2009) but stimulates neurodegeneration when defective (Sanchez-Varo et al., 2012; Nixon, 2013). Notably, Alzheimer's, Parkinson's, and Huntington's diseases have often been linked to impairments of the late autophagic flux (Nixon, 2013). The exact mechanisms that connect a dysfunction of autophagic degradation and neurodegeneration are still largely elusive and seem to depend on the disease context. Amongst the proposed mechanisms are the following: defective retrograde transport, harmful accumulation of autophagosomes and autolysosomes, ineffective organelle clearance, increased ROS production, incomplete degradation as a source of cytotoxic products, and cell death through leakage of lysosomal enzymes (Nixon, 2013). It has also been reported that the inhibition of autophagosome formation counteracts neurodegeneration in diseases that show a pathological accumulation of autophagic vesicles (Yang et al., 2007; Lee and Gao, 2009). We show dysfunctional late-stage autophagy in aged *C. elegans*. In these aged

animals we observed that not only global but neuron-specific inactivation of autophagic vesicle nucleation strongly extends lifespan. Although further research must be done to describe the status of the autophagic flux in aged *C. elegans* neurons, our experiments imply that autophagy in the nervous system is as impaired as in the entire organism. Importantly, our data suggest that age-associated dysfunctional autophagy causes neurodegeneration, which is ameliorated by inhibiting early autophagosome formation (Figure 44). This process works through an as yet unidentified mechanism, which possibly inhibits the formation of toxic aggregates upon cargo loading or improves retrograde axonal transport. Both events can cause neurodegeneration through autophagy (Haung Yu et al., 2005; Boland et al., 2008). Our observed neuroprotection ultimately produces a systemic increase in health and lifespan (Figure 44), likely mediated though preserved neuronal signalling in aged worms.

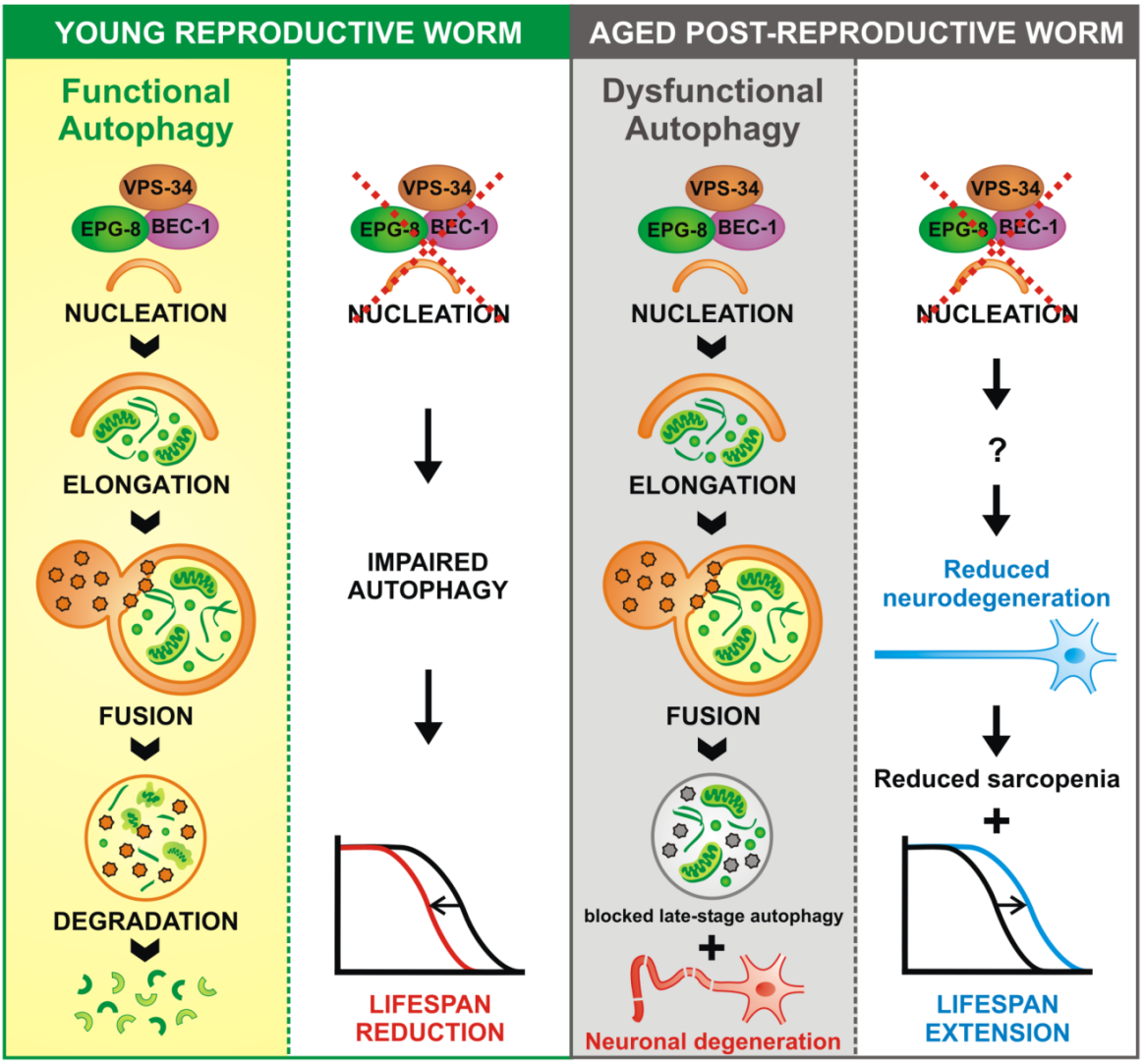

Figure 44: Schematic model representing age-associated antagonistic effects of neuronal autophagy in *C. elegans*. Young reproductive worms show functional autophagy that leads to a complete degradation and recycling of dysfunctional organelles, proteins, and other macromolecules. This process is beneficial to the organism as it maintains cellular homeostasis. Thus the inactivation of autophagy in young animals through knockdown of the autophagic nucleation complex leads to a reduction in lifespan (left panel). Conversely, aged post-reproductive worms exhibit dysfunctional autophagy that is associated with an incomplete degradation of autophagic cargo and the accumulation of stalled autolysosomes. We found that this age-associated dysfunction of the autophagic flux is linked to neurodegeneration and sarcopenia and that the inhibition of the early autophagic flux at the step of vesicle nucleation ameliorates these negative phenotypes. Through an unknown mechanism, the post-reproductive inhibition of the nucleation complex not only leads to improved muscle and neuronal structures but also increases lifespan through its neuron-specific inactivation.

Conclusion and Future Perspectives

The current view on autophagy is predominated by its advantageous cytoprotective and longevity-promoting effects. In contrast, our findings suggest that this view needs to be adjusted when looking at the aged organism. Minor lifespan extensions upon inactivation of autophagy genes in young adults have previously been reported (Hashimoto et al., 2009). Opposing this study, we observed lifespan shortening effects until day 1, while lifespan extension was only observed with progressing age. Specifically, we showed that post-reproductive inhibition of autophagosome formation in the neurons strongly extends lifespan and healthspan in *C. elegans*. This suggests a contrasting consequence of autophagy; it is beneficial and necessary for survival during development and early life but becomes increasingly dysfunctional and harmful late in life.

We believe genes responsible for autophagosome nucleation belong to a group of multiple genes that, through the absence of natural selection after reproduction, are dysregulated and harmful late in life. The AP genes could be at the root of many age-associated diseases and the rapid organismal decline at advanced ages. Hence it is important to identify these genes and their interactions late in life in order to fully understand how genes and gene networks impinge on the ageing process. High-throughput AP screens in *C. elegans* could represent the best route to rapidly identify genes that increase lifespan and healthspan upon late-life inactivation. From there we may want to investigate whether these insights hold through in mammalian model systems such as mice. If we can identify AP genes that are conserved within humans these genes could represent drug targets to treat many age-

associated diseases in a preventative manner. Today this is all the more important as we live in an increasingly ageing population, with age-associated disorders such as cardiovascular diseases, cancer, and neurodegenerative diseases on the rise.

Acknowledgements

[redacted]

[redacted]

[redacted]

Lastly I want to thank our funding sources that made this work possible. The research was supported by Boehringer Ingelheim Foundation and a Marie Curie Reintegration Grant (321683, Call FP7-PEOPLE-2012-CIG). The Large Particle Sorter (Biosorter®, Union Biometrica) used for our large-scale RNAi longevity screen was financed through the DFG Major Research Instrumentation Program (INST 247/768-1 FUGG). Some strains were provided by the CGC, which is funded by NIH Office of Research Infrastructure Programs (P40 OD010440).

Materials and Methods

C. elegans strains

C. elegans strains were maintained at 20°C using standard procedures (Brenner, 1974) unless indicted differently. The following strains were used in this study: WT (N2 Bristol), NL2099/*rrf-3(pk1426)*II, CB4037/*glp-1(e2141)*III, CF1814/*rrf-3(pk1426)*II; *daf-2(e1370)*III, TU3401/*sid-1(pk3321)*V; uIs69[*pCFJ90 (myo-2p::mCherry) + unc-119p::sid-1*]V, PD4251/ccIs4251 [*(pSAK2) myo-3p::GFP::LacZ::NLS + (pSAK4) myo-3p::mitochondrial GFP + dpy-20(+)*] I, VP303/kbIs7 [*nhx-2p::rde-1 + rol-6(su1006)*], NR222/kzIs9 [*(pKK1260) lin-26p::NLS::GFP + (pKK1253) lin-26p::rde-1 + rol-6(su1006)*], WM118/neIs9 [*myo-3::HA::RDE-1 + rol-6(su1006)*], JK4143/qIs57 [*lag-2p::GFP*] II. qIs140 [*lag-2p::rde-1 + (pRF4) rol-6(su1006)*], DP132/edIs6 [*unc-119::gfp + (pRF4) rol-6(su1006)*] IV. All strains were acquired from the *Caenorhabditis* Genetics Centre (CGC) at the University of Minnesota, except the following: QU34/izEx5[*pAy39.1, bec-1p::BEC-1::RFP*] was kindly provided by Alicia Meléndez (Queens College, Flushing, NY), BAT922/*rrf-3(pk1426)* II; adIs2122 [*lgg-1p::GFP::lgg-1 + rol-6(su1006)*], BAT1007/*rrf-3(pk1426)* II; bpIs151 [*sqst-1p::sqst-1::GFP + unc-76(+)*], BAT1032/*daf-16(mgDf47)* I; *daf-2(e1370)* III; *rrf-3 (pk1426)* II, BAT 1004/*rrf-3(pk1426)* II; edIs6 [*unc-119::gfp + (pRF4) rol-6(su1006)*] IV. *rrf-3* worms and all BAT strains were outcrossed to WT three times. Standard procedures for *C. elegans* strain maintenance were used (Brenner, 1974). All stock animals were maintained on nematode growth medium (NGM) plates and fed with EV expressing HT115 bacteria. Experimental animals were maintained in a liquid culture system as described in the following section.

Age synchronous liquid culture of C. elegans

NGM plus liquid media was prepared with 100 µg/ml Ampicillin and EV HT115 bacteria re-suspended to a final density of $3x10^9$ cells ml^{-1}. Cell culture flasks with breathable filter caps were filled to the following capacities: 75 cm^2 to a maximum of 50 ml, 175 cm^2 to a maximum of 100 ml and 300 cm^2 to a maximum of 200 ml, in order to provide optimal aeration. Capacities were determined by the desired worm load in each flask with a maximum density of 0.5 worms per µl per flask. Stock worms were washed from two 10 cm^2 NGM plates, sedimented and placed in a 100 ml cell culture flask. All procedures from this point were carried out under a laminar flow hood to avoid contamination. Worm cultures were placed at 20 °C in a shaking incubator at 40 rpm. Once dense with egg producing adults, they were harvested via bleaching using NaOCl treatment. Following, the harvested eggs were hatched and synchronized over night in M9 buffer without the addition of food. L1 worms were counted and placed back into culture at the appropriate density. Worms were maintained in this manner for a minimum of three and a maximum of eight generations at optimal conditions. For experimental samples, L1 worms were harvested from age synchronous adults at no later than day 1 of life. These offspring were allowed to grow until day 0 and were then subject to twice daily sedimentation to remove offspring.

The sedimentation protocol was as follows: Adult worms were allowed to settle in 50 ml Falcon tubes at a 1:1 ratio to the density of the liquid culture. Sedimentation proceeded for 5-10 minutes depending on the age of the worms, adult worms sediment faster than larvae. The supernatant containing L1-L3 worms was removed by aspiration. Worms were re-suspended in NGM

plus containing EV bacteria at a density of $1x10^9$ cell ml^{-1}. This was repeated at least six times. Worms were then carefully layered onto a 15 ml column of 36% Percoll with NGM in a 50 ml Falcon (Fabian and Johnson, 1994). Worms were allowed to settle through the Percoll for 10 minutes and the top two thirds of the Percoll containing: dead worms, bagging worms, and egg clumps was aspirated. Worms were washed a further three times with NGM plus before being transferred into a fresh food culture. Percoll sedimentation was performed twice daily for the first five days and then once daily thereafter. A final sedimentation of in 40% Percoll was performed on days where samples were extracted to eliminate any dead worms from the harvested worm pellet.

Automated AP screen using 96-transwell plates

A) Worm sorting on 96-transwell plates:

At day 9 of adulthood, 30 age-synchronized worms were sorted into each well of HTS Transwell®-96 well-permeable support plates with a large particle flow cytometer (Biosorter®, Union Biometrica). The wells were filled with 500 µl of M9 buffer with tween to dampen the impact, so that the worms were not damaged during the sorting process. Upon completion of the sort, M9 Buffer was removed through pressing the transwell membrane against a sterile cloth. Immediately afterwards, the transwell insert plate was transferred into a new receiver plate containing the RNAi feeding bacteria (see below).

B) RNAi feeding on 96-transwell plates:

Library was inoculated with a micro-plate 96 pin replicator (Boekel) into 96-round bottom deep well (2 ml) plates (Corning), containing 600 µl of Lennox LB medium. Cultures were incubated over night at 37°C degrees while shaking at 200 rpm. Next, the bacteria were induced by adding IPTG to a final

concentration of 4mM. The cultures were now induced for 1 hour while shaking (200 rpm) at 37°C. Following, the deep well plates containing the induced bacteria were spun down for 15 min at room temperature (3000 rpm). Next, the supernatant was discarded through quick inversion of the plate. Bacteria pellets were resuspended in 500 µl of NGM. Using a multichannel pipette, the resuspended RNAi feeding bacteria were transferred into two receiver plates with 210 µl per well receiver plate well. Next the transwell plate containing the worms was placed into the receiver feeding plate, exposing the worms to the RNAi feeding bacteria.

C) Washing of 96-transwell plates:

Every four days, the transwell plate was washed through pressing the transwell membrane against a sterile cloth. Using the a multichannel pipette, 300 µl of M9 buffer was added to each transwell and the plate was again pressed against a sterile cloth to remove the M9. This procedure removed the large majority of bacteria and debris from the wells, while the worms were still sitting on the membrane. The so cleaned transwell plate was now transferred to a new receiver plate containing freshly induced RNAi bacteria (see section above).

D) Imaging of 96-transwell plates:

Transwell plates images were acquired from below through the translucent membrane with a 1.25× objective using an AF7000 microscope (Leica) with an automated stage.

SYTOX dead staining in 96-transwell plates

SYTOX™ Orange Dead Cell Stain (Molecular Probes), which is a cell-permeable nucleic acid stain, was used to measure *C. elegans* survival in 96-transwell

plates. SYTOX™ Orange was added to each transwell to a final concentration of 4 µM and was incubated at 20°C for one hour before imaging. Images were acquired from below through the translucent membrane with a 1.25× objective using an AF7000 microscope and the dye was excited using a 532 nm green laser.

Movement scoring in 96-transwell plates

Movement scoring was carried out to measure *C. elegans* healthpan across aging. Every two days a short movie with 30 frames was acquired from below through the translucent membrane with a 1.25× objective using an AF7000 microscope (Leica) with an automated stage. Using ImageJ movement between each frame and the next is calculated through changes in subsequent pictures.

Body straightening scoring in 96-transwell plates

Body bending and straightening was used to measure *C. elegans* survival in 96-transwell plates. The WormToolbox image analysis pipeline for CellProfiler available via the open-source CellProfiler project was used to for image processing, worm untangling and straightening analysis as previously described by Gill and colleagues (Gill et al., 2003).

Lifespan assays

Worms were synchronized using liquid culture sedimentation. dsRNA expressing bacteria were grown overnight, seeded on NGM agar plates with 100 µg/ml Ampicillin and 1mM IPTG, and incubated at RT over night. Day 0 was determined with appearance of first internal eggs. A total of 105 - 140 animals were placed on 3 to 4 replicate plates with 35 worms per 6 cm plate.

Worms were picked to new plates and scored every two days. For double RNAi treatment, bacteria were diluted in a 1:1 ratio before being plated at 1x density. All assays were performed at 20 °C. For temperature sensitive *glp-1* mutant, worms were maintained restrictive temperature of 25 °C until day 0, when transferred to 20 °C. Lifespan assays indicated in supplementary table as "plate only", worms were maintained and synchronized only on plates. Worms were scored as alive until there was no movement after repeated prodding. Worms were censored when: crawled off plate, bagging, bursting, dropping on transfer, contamination, and burrowing. All RNAi clones used for lifespan assays are from the Ahringer libary and were sequence validated using the M13 forward primer.

Real-time quantitative PCR

Worms were grown in liquid culture as described. RNAi treatment commenced at day 0 or day 9. Samples were harvested at day 3 or day 12 and day 15 respectively. Total RNA was isolated from flash frozen samples of at least 100 age synchronised worms using Trizol extraction. cDNA synthesis was performed using First Strand cDNA Synthesis Kit (ThermoFisher) with 800 ng of RNA and oligo-dT primers. Quantitative PCR was performed in a ViiA™ 7 Real-Time PCR System (ThermoFisher) using SYBR® Green PCR Master Mix (Life technologies). Values were normalized to *cdc-42* and *pmp-3* as internal controls. Primers used are listed in supplementary Supplemental Table 12.

Western blotting

Worms were grown as described and transferred to respective RNAi treatments at day 9. For each time-point or knockdown condition: 200

synchronized animals were harvested, washed 3 times with M9 buffer and once with ddH_2O, and suspended in 2x standard Laemmli buffer via 10 minute boiling. The samples were subjected to standard SDS-PAGE and western blotting. Antibodies used were monoclonal mouse anti-GFP (Roche,1:10,000), mouse monoclonal [6G6] anti-RFP (Chromotek,1:1000), mouse monoclonal anti-α-Tubulin (Sigma, 1:10,000), rabbit monoclonal anti-ubiquitin (lys48-specific Apu2 clone; Millipore, 1:1000). Antibodies were diluted in PBST (5% milk powder, 0.1% Tween20) which was also used as blocking agent. For the timecourse analysis of cleaved GFP and RFP, worms were maintained in liquid culture as described and a portion of the culture was harvested at each timepoint following a 40% Percoll wash. This wash was repeated in the event that the cleaned worms contained less than 95% living worms. Each western blot is representative for similar results obtained in two independent biological replicates.

Pharynx imaging and analysis

Worms were grown as described and transferred to respective RNAi treatments at day 9. On day 20, 50 aged-synchronized worms from each knockdown condition were paralyzed using 0.5% NaAz and mounted on a 2% agar pad on a glass microscope slide. The images of the pharynges were acquired on a SP5 microscope (Leica) using the Differential Intense Contrast (DIC) filter and a 63x/1.4 NA Oil immersion objective. At least 30 whole worms per condition were imaged in each replicate with three technical replicates. Images were scored blind for pharynx degradation based on a three-point scale of damage related to changes in the structure of the corpus, isthmus or terminal bulb. Worms with no obvious damage to any of the three parts were

scored as 1, worms with damage to only one or two parts were scored 2, and worms with damage to all three parts were scored 3. For comparative analysis all worms were imaged at the same time, with the same settings and by the same user. This experiment was carried out in two independent biological replicates.

Muscle cell imaging and analysis

Worms were grown as described and transferred to respective RNAi treatments at day 9. On day 20, 30 aged-synchronized worms from each knockdown condition were incubated in fixation buffer (160 mM KCl, 100 mM Tris HCl pH 7.4, 40 mM NaCl, 20 mM Na_2EGTA, 1mM EDTA, 10 mM Spermidine HCl, 30 mM Pipes pH 7.4, 1% Triton-x-100, 50% Methanol) at room temperature for 1 hour rotating. Worms were washed twice with PBS and incubated in a 1:200 dilution of Phalloidin–Atto 565 (Sigma) in PBS-0.5% Triton-x-100 for 4 hours at room temperature rotating. Worms were then mounted on a 2% agar pad on a glass microscope slide. The 561 nm signals were acquired using a STED CW super-resolution microscope (Leica) and a 63x/1.4 NA Oil immersion objective. At least 40 images, comprising 2-4 cells, from 20 different worms were imaged per replicate with three technical replicates. Images were scored blind based on a five-point scale of muscle fiber degradation. Cells showing no obvious degradation were scored as 1, cells with kinks or striations were scored as 2, cells with small lesions combined with striations or other damage were scored 3, cells with muscle fiber breaks, gross striations and lesions were scored as 4, and cells where the muscle fibers were no longer intact were scored as 5. For comparative analysis, all worms were

imaged at the same time, with the same settings and by the same user. This experiment was carried out in two independent biological replicates.

Pharynx pumping assay

Worms were grown in liquid culture and transferred to respective RNAi treatments at day 9. On day 20, 50 aged-synchronized worms from each knockdown condition were transferred individually on an agar plate seeded with a bacterial lawn. The number of contractions in the terminal bulb of pharynx was scored during a 30 seconds period immediately upon transfer using a stereomicroscope. This experiment was carried out in two independent biological replicates.

Movement scoring/thrashing assay

Worms were grown as described and transferred to respective RNAi treatments at day 9. On day 20, 50 aged-synchronized worms from each knockdown condition were transferred individually in a 20 µL drop M9 buffer on a petri dish. After a 30 second recovery period, the numbers of body bends were scored during a 30 seconds period using a stereomicroscope. A body bend was defined as a change in the reciprocating motion of bending at the mid-body. This experiment was carried out in two independent biological replicates.

LGG-1::GFP microscopy

Worms were grown as described and transferred to respective RNAi treatments at day 9. On the day of analysis, 40 worms from each knockdown condition were paralyzed using 0.5% NaAz and mounted on a 2% agar pad on a glass microscope slide. GFP signals were acquired using a STED super-resolution microscope (Leica) at 100x magnifications. Images were taken of the hypodermis which was identified by locating the plane between the muscle and cuticle. At least 60 total regions were imaged from 50 different worms per replicate with two biological replicates. All images used for comparative quantifications were taken on the same day, with the same settings and by the same user.

Quantification of LGG-1::GFP foci

All GFP::LGG-1 foci were quantified using ImageJ according to standard procedures (Alberti et al., 2010; Palmisano and Meléndez, 2016). Each image was processed in the same manner. Briefly, the original image is examined and the hypodermis outlined and drawn to avoid other regions such as muscle or seam cells in young worms . Images are converted into a bit map following automatic threshold adjustment using the max entropy calculation to remove background. The region corresponding to the outlined hypodermis is selected for analysis Particles are analyzed in this selected region with the following criteria: particles were selected for quantification based on a size range of 0.2 - 4 μm^2 and with a circularity of 0 – 1. The outlines of the identified and counted particles are checked to avoid spurious counts. Images were not considered for quantification where the hypodermis was not clear or where foci were not

visible following thresholding. In total, at least 60 total regions were quantified from 30 different worm samples per condition.

Imaging and analysis of the axonal network

Worms were grown as described and transferred to respective RNAi treatments at day 9. On day 20, 100 aged-synchronized worms from each knockdown condition were paralyzed using 0.5% NaAz and mounted on a 2% agar pad on a glass microscope slide. GFP signal was acquired using a STED super-resolution microscope (Leica) at magnifications of 40x. Head regions of at least 100 different worms were imaged per knockdown condition and replicate. Axonal degeneration was scored on a three-point scale based on the amount of visible bubbling and neuron integrity. Scoring system: type 1 (intact axon without visible bubbling, kinks, or gaps); type 2 (slightly damaged axon, medium amount of bubbling, occasional kinks, very few to no gaps); type 3 (largely disrupted axon, high amount of bubbling, and frequent gaps). All images used for comparative quantifications were taken on the same day, with the same settings and by the same user. This experiment was carried out in two independent biological replicates.

Chloroquine treatment

To pharmacologically inhibit the lysosome, animals were treated with chloroquine diphosphate salt (Sigma-Aldrich). Briefly, worms were grown as described in liquid culture until day 14 and subsequently incubated with 20 mM chloroquine or DMSO vehicle control for 24 hours. The drug treatment

was performed in M9 liquid medium supplemented with EV HT115 bacteria at a density of $1x10^9$ cell ml^{-1} while shaking at 20 °C. The worms were harvested at day 15, following a 40% Percoll wash. This wash was repeated in the event that the cleaned worms contained less than 95% living worms.

Statistics

All statistical analysis was performed with Graph Prism 6. p-values for lifespan curves were calculated using the Log-Rank (Mantel Cox) test. MTL was calculated as the mean remaining lifespan of the worms from the day of first treatment. p-values for quantification of GFP::LGG-1 foci were calculated using the non-parametric Mann Whitney U test. p-values for: muscle health, pharynx integrity, and neuronal integrity were calculated using a Chi-square test with two tails and 95% confidence interval. p-values for: qPCRs, body bend counts, pharynx pumping, and chymotrypsin assay were calculated using a two tailed t-test. Significance was scored as follows for all experiments: **** $p<0.0001$, *** $p<0.001$, ** $p<0.01$, * $p<0.05$.

Lysotracker staining

Worms were grown as described and transferred to respective RNAi treatments at day 9. On day 15, 30 aged-synchronized worms were picked into M9 containing food and stained with 5 nM LysoTracker® Deep Red (Molecular Probes L12492) for 3 hours at room temperature in a rotating. Worms were paralyzed by 0.5% NaAz and mounted on a 2% agar pad on a glass microscope slide. 488 nm, 561 nm or 633 nm signals were acquired using a STED CW

super-resolution microscope (Leica) and a 63x/1.4 NA Oil immersion objective. At least 10 whole worms were imaged per condition.

RNA sequencing

Worms were grown in liquid culture as described. Worms were harvested at day 3, day 6, day 9, day 12, day 15 and day 18 following sedimentation in 40% Percoll. 200 worms were collected and flash frozen in 400 µl of Trizol. RNA extraction and cDNA synthesis was carried out following the manufacturer's instruction. 60 NGS libraries were prepared using Illumina's TruSeq stranded Total RNA LT Sample Prep Kit following Illumina's standard protocol (Part # 15031048 Rev. E). The ribozero steps of the protocol for rRNA depletion were carried out manually, while the following steps of library preparation were performed using the Bravo Automated Liquid Handling Platform (Agilent). Libraries were prepared from a starting amount of 500 ng of total RNA and amplified in 11 PCR cycles. Libraries were profiled in a High Sensitivity DNA chip on a 2100 Bioanalyzer (Agilent technologies) and quantified using the Qubit dsDNA HS Assay Kit, in a Qubit 2.0 Fluorometer (Life technologies). 15 libraries were pooled together in equimolar ratio (60 libraries into 4 pools), and each pool was sequenced on 2 HiSeq 2500 lanes of a High Output run, single-read for 51 cycles plus 7 cycles for the index read. The libraries were sequenced on a HiSeq2500 with a read length of 51 bp single read. Base calling and demultiplexing were performed using bcl2fastq (version 1.8.4). Reads were mapped against C. elegans genome assembly WBcel235 (ENSEMBL release 84) using STAR (Dobin et al., 2013) (version 2.5.1b, additional parameters: --outFilterMultimapNmax 10 --outFilterMismatchNmax 2 --

alignIntronMin 21 --sjdbOverhang 50). Strand specific read counts per gene were generated using featureCounts (Love et al., 2014) (version 1.4.6-p2 subread package). Differentially expressed genes were determined using DESeq2 (Liao et al., 2014) (version 1.12.3) with an FDR cutoff of 1% and default filtering criteria. Samtools (Quinlan and Hall, 2010) (version 1.3), BEDTools (Kent et al., 2010) (version 2.25) and UCSC tools (Li et al., 2009) were used to generate coverage tracks.

Statistics

All statistical analysis was performed with Graph Prism 6. p-values for lifespan curves were calculated using the Log-Rank (Mantel Cox) test. MTL was calculated as the mean remaining lifespan of the worms from the day of first treatment. p-values for quantification of GFP::LGG-1 foci were calculated using the non-parametric Mann Whitney U test. p-values for: muscle health, pharynx integrity, and neuronal integrity were calculated using a Chi-square test with two tails and 95% confidence interval. p-values for: qPCRs, body bend counts, pharynx pumping, and chymotrypsin assay were calculated using a two tailed t-test. Significance was scored as follows for all experiments: **** $p<0.0001$, *** $p<0.001$, ** $p<0.01$, * $p<0.05$.

Supplemental Tables

RNAi treatment	Treated MTL +/- SD	EV Control MTL +/- SD	Mean Change of MTL	*p*-Value
bec-1	26.417 +/- 0.425	18.962 +/- 1.339	39.32%	< 0.0001
bec-1	26.765 +/- 1.212	17.619 +/- 0.408	51.91%	< 0.0001
bec-1	31.153 +/- 1.662	19.171 +/- 0.807	62.50%	< 0.0001
vps-34	26.171 +/- 0.566	18.661 +/- 0.926	40.24%	< 0.0001
vps-34	25.491 +/- 2.037	19.121 +/- 1.026	33.31%	< 0.0001
vps-34	25.549 +/- 1.545	18.962 +/- 1.339	34.74%	< 0.0001
epg-8	24.857 +/- 1.200	19.257 +/- 0.181	29.08%	< 0.0001
epg-8	24.796 +/- 3.179	18.661 +/- 0.926	32.88%	< 0.0001
epg-8	25.517 +/- 0.602	19.121 +/- 1.026	33.45%	< 0.0001
epg-8	25.647 +/- 1.778	18.962 +/- 1.339	35.25%	< 0.0001

Supplemental Table 1: Lifespan effect in *rrf-3(pk1426)* worms given as Mean Treated Lifespan (MTL) from day 9 of adulthood. Table refers to Figure 21 and shows the relative MTL change compared to the EV control upon day 9 RNAi feeding targeting *bec-1, vps-34,* and *epg-8*, which encode for proteins that build up the autophagic vesicle nucleation complex; for each assay 105 worms were treated. Data used in Figure 21 is highlighted in grey.

RNAi treatment	Mean Change of MTL	SEM	n
pha-4	22.02%	1.952	10
unc-51	44.38%	3.945	3
atg-13	45.26%	5.864	4
bec-1	49.40%	2.305	20
vps-34	36.10%	2.112	3
epg-8	32.67%	1.297	4
atg-9	34.03%	5.810	3
atg-4	1.89%	0.6217	4
atg-7	5.75%	2.254	7
lgg-1	-13.98%	0.272	5
lgg-2	0.19%	4.331	4
lgg-3	12.41%	2.474	5
epg-5	4.13%	2.501	3
cup-5	1.95%	1.167	4

Supplemental Table 2: Lifespan effect in *rrf-3(pk1426)* worms given as Mean Treated Lifespan (MTL) change from day 9 of adulthood compared to EV control. Table refers to Figure 22 and shows the relative MTL change compared to the EV control upon day 9 RNAi feeding targeting different genes of the autophagic flux; n indicated number of independent lifespan assays; for each assay 105 worms were treated.

RNAi treatment	Treated MTL +/- SD	EV Control MTL +/- SD	Mean Change of MTL	*p*-Value
EV + *bec-1*	30.095 +/- 1.590	20.438 +/- 0.397	47.25%	< 0.0001
EV + *bec-1*	24.386 +/- 1.245	16.900 +/- 0.694	44.30%	< 0.0001
bec-1 + *lgg-1*	21.791 +/- 0.235	20.438 +/- 0.397	6.62%	0.0048
bec-1 + *lgg-1*	20.152 +/- 0.981	16.900 +/- 0.694	19.24%	< 0.0001
bec-1 + *lgg-1*	17.983 +/- 0.480	18.902 +/- 0.241	-4.86%	0.1652
bec-1 + *lgg-1*	18.922 +/- 1.543	18.661 +/- 0.926	1.40%	0.0463

Supplemental Table 3: Lifespan effect in *rrf-3(pk1426)* worms given as Mean Treated Lifespan (MTL) from day 9 of adulthood. Table refers to Figure 25 and shows the relative MTL change compared to the EV control upon day 9 RNAi double feeding targeting *bec-1* and *lgg-1*; for each assay 105 worms were treated. Data used in Figure 25 is highlighted in grey.

RNAi treatment	Treated MTL +/- SD	EV Control MTL +/- SD	Mean Change of MTL	*p*-Value
vha-13	18.261 +/- 0.082	23.553 +/- 1.452	-22.47%	< 0.0001
vha-13	17.483 +/- 0.199	25.639 +/- 0.479	-31.81%	< 0.0001
vha-13	17.229 +/- 0.474	23.318 +/- 0.989	-26.11%	< 0.0001
vha-15	21.419 +/- 0.576	23.553 +/- 1.452	-9.06%	0.0022
vha-15	20.981 +/- 0.397	25.639 +/- 0.479	-18.17%	< 0.0001
vha-15	20.788 +/- 0.133	23.318 +/- 0.989	-10.85%	0.0002

Supplemental Table 4: Lifespan effect in *rrf-3(pk1426)* worms given as Mean Treated Lifespan (MTL) from day 0 of adulthood. Table refers to Figure 32A and shows the relative MTL change compared to the EV control upon day 0 RNAi feeding targeting genes that govern autolysosomal degradation (*vha-15* and *vha-13*); for each assay 105 worms were treated. Data used in Figure 32A is highlighted in grey.

RNAi treatment	Treated MTL +/- SD	EV Control MTL +/- SD	Mean Change of MTL	*p*-Value
vha-13	21.067 +/- 0.453	19.565 +/- 0.913	7.68%	0.0238
vha-15	20.492 +/- 0.605	19.565 +/- 0.913	4.74%	0.084
epg-5	20.804 +/- 1.247	19.088 +/- 0.445	8.99%	0.0028
epg-5	29.095 +/- 0.150	19.565 +/- 0.913	2.71%	0.4817
epg-5	19.302 +/- 0.646	19.171 +/- 0.807	0.68%	0.7206
cup-5	19.371 +/- 0.364	19.088 +/- 0.445	1.48%	0.9427
cup-5	20.362 +/- 0.402	19.565 +/- 0.913	4.07%	0.4615
cup-5	19.562 +/- 0.520	19.788 +/- 0.564	-1.14%	0.6263
cup-5	19.821 +/- 0.051	19.171 +/- 0.807	3.39%	0.6153

Supplemental Table 5: Lifespan effect in *rrf-3(pk1426)* worms given as Mean Treated Lifespan (MTL) from day 9 of adulthood. Table refers to Figure 32B and shows the relative MTL change compared to the EV control upon day 9 RNAi feeding targeting genes that govern autolysosomal degradation (*vha-15*, *vha-13, epg-5, and cup-5*); for each assay 105 worms were treated. Data used in Figure 32B is highlighted in grey.

RNAi treatment	Treated MTL +/- SD	EV Control MTL +/- SD	Mean Change of MTL	*p*-Value
EV + *bec-1*	26.692 +/- 0.222	17.897 +/- 0.468	49.14%	< 0.0001
EV + *bec-1*	25.566 +/- 2.094	19.281 +/- 0.393	32.60%	< 0.0001
EV + *bec-1*	26.886 +/- 1.286	19.788 +/- 0.564	35.87%	< 0.0001
EV + *bec-1*	22.913 +/- 0.799	17.638 +/- 0.593	29.91%	< 0.0001
EV + *bec-1*	28.569 +/- 1.284	18.968 +/- 1.031	50.62%	< 0.0001
EV + *bec-1*	23.115 +/- 0.810	16.238 +/- 0.744	42.35%	< 0.0001
EV + *bec-1*	27.486 +/- 1.382	19.088 +/- 0.445	44%	< 0.0001
EV + *vha-15*	18.495 +/- 0.257	17.897 +/- 0.468	3.34%	0.937
EV + *vha-15*	19.204 +/- 0.417	19.281 +/- 0.393	-0.40%	0.7858
EV + *vha-15*	20.001 +/- 0.260	19.788 +/- 0.564	1.08%	0.9366
EV + *vha-15*	18.774 +/- 0.395	18.968 +/- 1.031	-1.02%	0.966
EV + *vha-13*	18.845 +/- 0.130	18.968 +/- 1.031	-0.65%	0.8139
EV + *vha-13*	17.736 +/- 1.088	16.238 +/- 0.744	9.23%	0.0941
EV + *vha-13*	20.222 +/- 1.073	19.788 +/- 0.564	2.19%	0.6262
EV + *cup-5*	19.562 +/- 0.520	19.788 +/- 0.564	-1.14%	0.6263

EV + *cup-5*	16.390 +/- 0.071	16.711 +/- 0.611	-1.92	0.5489
EV + *cup-5*	19.488 +/- 0.871	19.088 +/- 0.445	0.021	0.2254
bec-1 + *vha-15*	27.518 +/- 0.776	19.788 +/- 0.564	39.06%	< 0.0001
bec-1 + *vha-15*	26.081 +/- 0.299	19.281 +/- 0.393	35.27%	< 0.0001
bec-1 + *vha-15*	27.752 +/- 1.210	17.897 +/- 0.468	55.07%	< 0.0001
bec-1 + *vha-15*	28.816 +/- 0.438	18.968 +/- 1.031	51.92%	< 0.0001
bec-1 + *vha-13*	28.249 +/- 0.808	18.968 +/- 1.031	48.93%	< 0.0001
bec-1 + *vha-13*	27.686 +/- 0.543	19.788 +/- 0.564	39.91%	< 0.0001
bec-1 + *vha-13*	22.410 +/- 3.101	16.238 +/- 0.744	38.01%	< 0.0001
bec-1 + *cup-5*	29.269 +/- 0.640	18.968 +/- 1.031	54.31%	< 0.0001
bec-1 + *cup-5*	29.654 +/- 0.498	19.788 +/- 0.564	49.86%	< 0.0001
bec-1 + *cup-5*	24.048 +/- 0.739	17.638 +/- 0.593	36.34%	< 0.0001
bec-1 + *cup-5*	28.485 +/- 0.914	19.088 +/- 0.445	49.23%	< 0.0001

Supplemental Table 6: Lifespan effect in *rrf-3(pk1426)* worms given as Mean Treated Lifespan (MTL) from day 9 of adulthood. Table refers to Figure 32C and shows the relative MTL change compared to the EV control upon day 9 RNAi double feeding targeting *bec-1* and genes that govern autolysosomal degradation (*vha-15*, *vha-13*, and *cup-5*); for each assay 105 worms were treated. Data used in Figure 32C is highlighted in grey.

Strain	RNAi treatment	Treated MTL +/- SD	EV Control MTL	Mean Change of MTL	*p*-Value
WT	*pha-4*	13.781 +/- 0.453	12.790 +/- 0.421	7.75%	0.0935
WT	*pha-4*	12.203 +/- 0.571	12.212 +/- 0.444	-0.07%	0.857
WT	*pha-4*	12.838 +/- 0.444	12.114 +/- 0.491	5.98%	0.3994
WT	*bec-1*	15.650 +/- 0.666	12.790 +/- 0.421	22.36%	< 0.0001
WT	*bec-1*	16.184 +/- 0.719	12.114 +/- 0.491	33.60%	< 0.0001
WT	*bec-1*	16.629 +/- 0.797	13.712 +/- 0.494	21.27%	0.0004
WT	*vps-34*	16.756 +/- 1.544	13.712 +/- 0.494	22.20%	< 0.0001
WT	*vps-34*	14.357 +/- 0.423	11.176 +/- 0.059	28.46%	< 0.0001
WT	*vps-34*	18.052 +/- 0.531	14.853 +/- 0.088	21.54%	0.0001
WT	*vps-34*	15.430 +/- 0.629	12.790 +/- 0.421	20.64%	< 0.0001
WT	*atg-9*	16.515 +/- 0.100	13.712 +/- 0.494	20.44%	0.0008
WT	*atg-9*	17.511 +/- 0.633	14.853 +/- 0.088	17.90%	0.001
WT	*atg-9*	15.453 +/- 0.947	11.176 +/- 0.059	36.13%	< 0.0001
WT	*unc-51*	15.214 +/- 1.229	11.176 +/- 0.059	36.13%	< 0.0001
WT	*unc-51*	17.091 +/- 0.652	13.712 +/- 0.494	24.64%	< 0.0001

WT	*unc-51*	18.561 +/- 0.304	14.853 +/- 0.088	24.96%	< 0.0001
rrf-3 (pk1426)	*pha-4*	20.821 +/- 1.129	18.226 +/- 0.928	14.24%	< 0.0001
rrf-3 (pk1426)	*pha-4*	21.796 +/- 0.948	18.661 +/- 0.926	16.80%	< 0.0001
rrf-3 (pk1426)	*bec-1*	29.024 +/- 0.890	19.565 +/- 0.913	48.35%	< 0.0001
rrf-3 (pk1426)	*bec-1*	30.002 +/- 0.539	18.226 +/- 0.928	64.61%	< 0.0001
rrf-3 (pk1426)	*bec-1*	26.924 +/- 0.600	19.133 +/- 0.756	40.72%	< 0.0001
rrf-3 (pk1426)	*bec-1*	27.124 +/- 1.151	18.657 +/- 0.244	45.38%	< 0.0001
rrf-3 (pk1426)	*bec-1*	21.537 +/- 0.015	14.808 +/- 0.336	45.44%	< 0.0001
rrf-3 (pk1426)	*bec-1*	28.368 +/- 2.096	18.661 +/- 0.926	52.02%	< 0.0001
rrf-3 (pk1426)	*bec-1*	26.506 +/- 0.486	19.121 +/- 1.026	38.62%	< 0.0001
rrf-3 (pk1426)	*vps-34*	26.171 +/- 0.566	18.661 +/- 0.926	40.24%	< 0.0001
rrf-3 (pk1426)	*vps-34*	25.491 +/- 2.037	19.121 +/- 1.026	33.31%	< 0.0001
rrf-3 (pk1426)	*vps-34*	25.549 +/- 1.545	18.962 +/- 1.339	34.74%	< 0.0001
rrf-3 (pk1426)	*atg-9*	26.438 +/- 0.230	18.661 +/- 0.926	41.68%	< 0.0001
rrf-3 (pk1426)	*atg-9*	23.571 +/- 2.163	19.222 +/- 1.716	22.63%	< 0.0001
rrf-3 (pk1426)	*atg-9*	25.903 +/- 0.160	18.800 +/- 0.657	37.78%	< 0.0001

rrf-3 (pk1426)	*unc-51*	27.683 +/- 1.209	18.226 +/- 0.928	51.89%	< 0.0001
rrf-3 (pk1426)	*unc-51*	27.434 +/- 1.603	19.222 +/- 1.716	42.72%	< 0.0001
rrf-3 (pk1426)	*unc-51*	25.358 +/- 0.583	18.305 +/- 0.135	38.53%	< 0.0001

Supplemental Table 7: Lifespan effect in WT and *rrf-3(pk1426)* worms, respectively, given as Mean Treated Lifespan (MTL) from day 9 of adulthood. Table refers to Figure 33 and shows the relative MTL change compared to the EV control upon day 9 RNAi feeding targeting genes that govern early autophagosome formation (*pha-4*, *unc-51, bec-1, vps-34 and epg-9*); for each assay 105 worms were treated.

Treatment start	RNAi treatment	Treated MTL +/- SD	EV Control MTL +/- SD	Mean Change of MTL	*p*-Value
day 0	*bec-1*	14.539 +/- 0.586	16.257 +/- 0.943	-10.57%	0.0062
day 0	*bec-1*	15.375 +/- 0.293	16.876 +/- 1.058	-8.89%	0.0032
day 0 (Fig. 37A)	*bec-1*	14.543 +/- 0.304	16.655 +/- 0.481	-12.68%	< 0.0001
day 9	*bec-1*	15.152 +/- 1.440	11.754 +/- 0.784	28.91%	< 0.0001
day 9	*bec-1*	18.228 +/- 0.516	11.581 +/- 0.380	57.40%	< 0.0001
day 9 (Fig. 37B)	*bec-1*	17.505 +/- 0.856	13.033 +/- 0.648	34.31%	< 0.0001
day 9	*bec-1*	17.048 +/- 0.591	12.857 +/- 0.399	32.60%	< 0.0001
day 9	*bec-1*	19.216 +/- 0.802	13.676 +/- 0.367	40.51%	< 0.0001
day 9	*bec-1*	18.368 +/- 0.132	14.457 +/- 0.047	27.05%	< 0.0001
day 9	*bec-1*	19.549 +/- 0.611	14.686 +/- 0.474	33.13%	< 0.0001
day 9	*vps-34*	14.845 +/- 0.591	11.754 +/- 0.784	26.30%	< 0.0001
day 9	*vps-34*	18.143 +/- 0.486	11.581 +/- 0.380	56.66%	< 0.0001
day 9 (Fig. 37B)	*vps-34*	18.438 +/- 1.261	13.033 +/- 0.648	41.47%	< 0.0001
day 9	*vps-34*	17.531 +/- 0.522	12.857 +/- 0.399	36.35%	< 0.0001
day 9	*vps-34*	18.677 +/- 1.230	13.676 +/- 0.367	36.57%	< 0.0001

day 9	*lgg-1*	10.676 +/- 0.117	11.754 +/- 0.784	-9.17%	0.0107
day 9	*lgg-1*	10.133 +/- 0.448	11.581 +/- 0.380	-12.50%	0.0015
day 9 (Fig. 37B)	*lgg-1*	12.003 +/- 0.252	13.033 +/- 0.648	-7.90%	0.012
day 9	*lgg-1*	11.962 +/- 0.350	12.857 +/- 0.399	-6.96%	0.0066
day 9	*atg-7*	12.619 +/- 0.189	11.754 +/- 0.784	7.36%	0.0974
day 9	*atg-7*	11.657 +/- 0.450	11.581 +/- 0.380	0.66%	0.9997
day 9 (Fig. 37B)	*atg-7*	13.811 +/- 0.222	13.033 +/- 0.648	5.97%	0.1654
day 9	*atg-7*	14.495 +/- 0.569	12.857 +/- 0.399	12.74%	0.0088

Supplemental Table 8: Lifespan effect in *sid-1*(pk3321); *unc-119p::sid-1* worms given as Mean Treated Lifespan (MTL) from day 0 and day 9 of adulthood, respectively. Table refers to Figure 37 and shows the relative MTL change compared to the EV control upon day 9 RNAi feeding targeting genes that govern different stages of the autophagic flux (*bec-1*, *vps-34, atg-7, and lgg-1*); for each assay 105 worms were treated. Data used in Figure 37 is highlighted in grey.

Strain	RNAi treatment	Treated MTL +/- SD	EV Control MTL	Mean Change of MTL	*p*-Value
rde-1(-);nhx-2p::rde-1	*bec-1*	13.541 +/- 0.220	12.722 +/- 0.190	6.44%	0.0153
rde-1(-);nhx-2p::rde-1	*bec-1*	13.124 +/- 0.467	12.610 +/- 0.097	4.08%	0.074
rde-1(-);nhx-2p::rde-1	*bec-1*	9.134 +/- 0.094	8.844 +/- 0.694	3.28%	0.7354
rde-1(-);nhx-2p::rde-1	*bec-1*	13.143 +/- 0.252	11.431 +/- 0.298	14.98%	< 0.0001
rde-1(-);lin-26p::rde-1 Day 9	*bec-1*	16.460 +/- 0.347	16.067 +/- 0.220	2.45%	0.4555
rde-1(-);lin-26p::rde-1 Day 9	*bec-1*	16.495 +/- 0.467	16.610 +/- 0.467	-0.69%	0.8694
rde-1(-);lin-26p::rde-1 Day 9	*bec-1*	15.690 +/- 0.794	14.578 +/- 0.559	7.63%	0.2902
rde-1(-);lin-26p::rde-1 Day 9	*bec-1*	17.397 +/- 0.292	15.752 +/- 0.268	10.44%	0.0004
rde-1(-);myo-3::HA::RDE-1	*bec-1*	13.933 +/- 0.230	13.571 +/- 0.612	2.67%	0.6453
rde-1(-);myo-3::HA::RDE-1	*bec-1*	14.369 +/- 0.630	13.962 +/- 0.230	2.92%	0.4538
rde-1(-);myo-3::HA::RDE-1	*bec-1*	14.298 +/- 1.187	12.657 +/- 1.190	12.97%	0.0147
rde-1(-);myo-3::HA::RDE-1	*bec-1*	14.167 +/- 4.095	13.810 +/- 0.190	2.59%	0.1484
rde-1(-);lag-2p::rde-1	*bec-1*	17.923 +/- 0.515	17.559 +/- 0.246	2.07%	0.7629
rde-1(-);lag-2p::rde-1	*bec-1*	19.940 +/- 0.366	18.683 +/- 0.493	6.73%	0.3075
rde-1(-);lag-2p::rde-1	*bec-1*	16.913 +/- 0.713	15.632 +/- 0.541	8.19%	0.0182

Supplemental Table 9: Lifespan effect in *rde-1(ne219); nhx-2p::rde-1* (gut), *rde-1(ne219); lin-26p::rde-1* (hypodermis), *rde-1(ne300); myo-3::RDE*-1 (muscle), or *rde-1(ne219); lag-2p::rde-1* (germline niche) worms, respectively, given as Mean Treated Lifespan (MTL) from day 9 of adulthood. Table refers to Figure 38 and shows the relative MTL change compared to the EV control upon day 9 RNAi feeding targeting *bec-1*; for each assay 105 worms were treated.

Primer Name	Forward	Reverse
cdc-42	CTGCTGGACAGGAAGATTACG	CTCGGACATTCTCGAATGAAG
pmp-3	GTTCCCGTGTTCATCACTCAT	ACACCGTCGAGAAGCTGTAGA
bec-1	TCAGGACGAGCTTCATTCGC	GCTCCAACAGGATCTCTAATAACA
pha-4	ACTATACGGCCATGAACGCT	TGGTGCCAGTGGTAAAACCAA
unc-51	CTATGTTGATCGCACAGACG	CTCCGTGCATTTGAGTAGGC
vps-34	TGTCGATTCTGCCTACCGGA	CGTTGTTCGATCTTGAAAATAGCC
atg-7	GTCAATTATCGCTTCATCAAACCG	TCCCAGATCTTTTCTGCTTCACT
cup-5	ACAGTTATCAAGGTATTTGGGACAG	CCGTCTGAGTAGCGATCCTT
epg-8	TTTACGAGGAGTTGAGAGCAGA	ATCTTCCGTTCGCTGAATTGT
atg-9	ACTGGGTGAAGGATTCGCTTAT	ATACCTCCTGCGTCACTTCAAC
atg-13	ACCAGAGATTGCTCCAGTAACA	CAGCTTCTCGGGAGGTAGAAC
ced-4	TGCTTTCGCAGTTGTGATGC	AAGAGCTCCACGTTTGCTGA
epg-5	TGCATTCCAGCTCTTGCTCA	GAACGCTGTGCTTGAGACTT
lgg-1	ACCCAGACCGTATTCCAGTG	TCGTGATGGTCCTGGTAGAGT
lgg-3	GCTTCCTTCATCTTGAAATTGCG	GGGATAGCGTCTCAAACGTGG
let-363	ACCACATCCAACAACGGTCA	TGAAATGGAGCAGGCTGAGG

Supplemental Table 10: List of PCR primers used to check gene knockdown following RNAi feeding.

References

Aigaki, T., Seong, K.H., and Matsuo, T. 2002. Longevity determination genes in Drosophila melanogaster. *Mech. Ageing Dev.* 123: 1531–1541.

Aitlhadj, L., and Stürzenbaum, S.R. 2010. The use of FUdR can cause prolonged longevity in mutant nematodes. *Mech. Ageing Dev.* 131: 364–365.

Alberti, A., Michelet, X., Djeddi, A., and Legouis, R. 2010. The autophagosomal protein LGG-2 acts synergistically with LGG-1 in dauer formation and longevity in C. elegans. *Autophagy* 6: 622–633.

Barth, H., Meiling-Wesse, K., Epple, U.D., and Thumm, M. 2001. Autophagy and the cytoplasm to vacuole targeting pathway both require Aut10p. *FEBS Lett.* 508: 23–28.

Bjørkøy, G., Lamark, T., and Johansen, T. 2006. p62/SQSTM1: A missing link between protein aggregates and the autophagy machinery. *Autophagy* 2: 138–139.

Boland, B., Kumar, A., Lee, S., Platt, F.M., Wegiel, J., Yu, W.H., and Nixon, R.A. 2008. Autophagy induction and autophagosome clearance in neurons: relationship to autophagic pathology in Alzheimer's disease. *J. Neurosci.* 28: 6926–6937.

Boya, P., Reggiori, F., and Codogno, P. 2013. Emerging regulation and functions of autophagy. *Nat. Cell Biol.* 15: 713–720.

Brenner, S. 1974. The genetics of Caenorhabditis elegans. *Genetics* 77: 71–94.

Budovskaya, Y. V., Stephan, J.S., Reggiori, F., Klionsky, D.J., and Herman, P.K. 2004. The Ras/cAMP-dependent Protein Kinase Signaling Pathway Regulates an Early Step of the Autophagy Process in Saccharomyces cerevisiae. *J Biol Chem.* 279: 20663–20671.

Budovskaya, Y. V, Stephan, J.S., Deminoff, S.J., and Herman, P.K. 2005. An evolutionary proteomics approach identifies substrates of the cAMP-

dependent protein kinase. *Proc Natl Acad Sci U S A* 102: 13933–13938.

Calixto, A., Chelur, D., Topalidou, I., Chen, X., and Chalfie, M. 2010. Enhanced neuronal RNAi in C. elegans using SID-1. *Nat. Methods* 7: 554–559.

Chang, Y.-Y., and Neufeld, T.P. 2009. An Atg1/Atg13 Complex with Multiple Roles in TOR-mediated Autophagy Regulation. *Mol. Biol. Cell* 20: 2004–2014.

Charlesworth, B. 1970. Selection in populations with overlapping generations. I. The use of Malthusian parameters in population genetics. *Theor. Popul. Biol.* 1: 352–370.

Charlesworth, B. 1973. Selection in Populations with Overlapping Generations. V. Natural Selection and Life Histories. *Am. Nat.* 107: 303–311.

Charlesworth, B. 1994. Evolution in age-structured populations. (Cambridge Univ. Press, London,U.K.).

Charlesworth, B., and Giesel, J.T. 1972. Selection in populations with overlapping generations. II. Relations between gene frequency and demographic variables. *Am. Nat.* 106: 388–401.

Charlesworth, B., and Williamson, J.A. 1975. Probability of survival of a mutant gene in an age-structured population and implications for evolution of life-histories. *Genet. Res.* 1–10.

Chen, D., Pan, K.Z., Palter, J.E., and Kapahi, P. 2007. Longevity determined by developmental arrest genes in Caenorhabditis elegans. *Aging Cell* 6: 525–533.

Cihan, E. 2014. C. elegans life cycle and developmental stages. figshare.

Cuervo, A.M., Bergamini, E., Brunk, U.T., Dröge, W., Ffrench, M., and Terman, A. 2005. Autophagy and aging: the importance of maintaining ‘clean’ cells. *Autophagy* 1: 131–140.

Cuervo, A.M., and Dice, J.F. 2000. When lysosomes get old. *Exp. Gerontol.* 35: 119–131.

Curran, S.P., and Ruvkun, G. 2007. Lifespan regulation by evolutionarily conserved genes essential for viability. *PLoS Genet.* 3: 0479–0487.

Dobin, A., Davis, C.A., Schlesinger, F., Drenkow, J., Zaleski, C., Jha, S., Batut, P., Chaisson, M., and Gingeras, T.R. 2013. STAR: Ultrafast universal RNA-seq aligner. *Bioinformatics* 29: 15–21.

Dorman, J.B., Albinder, B., Shroyer, T., and Kenyon, C. 1995. The age-1 and daf-2 genes function in a common pathway to control the lifespan of Caenorhabditis elegans. *Genetics* 141: 1399–1406.

Edney, E.B., and Gill, R.W. 1968. Evolution of senescence and specific longevity. *Nature* 220: 281–282.

Egan, D.F., Shackelford, D.B., Mihaylova, M.M., Gelino, S., Kohnz, R. a., Mair, W., Vasquez, D.S., Joshi, a., Gwinn, D.M., Taylor, R., et al. 2010. Phosphorylation of ULK1 (hATG1) by AMP-Activated Protein Kinase Connects Energy Sensing to Mitophagy. *Science (80-.).* 331: 456–461.

Eisenberg, T., Knauer, H., Schauer, A., Büttner, S., Ruckenstuhl, C., Carmona-Gutierrez, D., Ring, J., Schroeder, S., Magnes, C., Antonacci, L., et al. 2009. Induction of autophagy by spermidine promotes longevity. *Nat. Cell Biol.* 11: 1305–1314.

Fabian, T.J., and Johnson, T.E. 1994. Production of age-synchronous mass cultures of Caenorhabditis elegans. *J. Gerontol.* 49: B145–B156.

Fares, H., and Greenwald, I. 2001. Regulation of endocytosis by CUP-5, the Caenorhabditis elegans mucolipin-1 homolog. *Nat. Genet.* 28: 64–68.

Fielenbach, N., and Antebi, A. 2008. C. elegans dauer formation and the molecular basis of plasticity. *Genes Dev.* 22: 2149–2165.

Fisher, R.A. 1930. The genetical theory of natural selection.

Font-nieves, M., Navarro, X., Casas, C., Penas, C., Font-nieves, M., Forés, J., Petegnief, V., Planas, A., Navarro, X., and Casas, C. 2011. Autophagy, and BiP level

decrease are early key events in retrograde degeneration of motoneurons. *Cell Death Differ.* 18: 1617–1627.

Friedman, D.B., and Johnson, T.E. 1988. A mutation in the age-1 gene in Caenorhabditis elegans lengthens life and reduces hermaphrodite fertility. *Genetics* 118: 75–86.

Gelino, S., and Hansen, M. 2012. Autophagy - An Emerging Anti-Aging Mechanism. *J. Clin. Exp. Pathol.* S4: 6.

Gill, M.S., Olsen, A., Sampayo, J.N., and Lithgow, G.J. 2003. An automated high-throughput assay for survival of the nematode Caenorhabditis elegans. *Free Radic. Biol. Med.* 35: 558–565.

Guo, B., Huang, X., Zhang, P., Qi, L., Liang, Q., Zhang, X., Huang, J., Fang, B., Hou, W., Han, J., et al. 2014. Genome-wide screen identifies signaling pathways that regulate autophagy during Caenorhabditis elegans development. *EMBO Rep.* 15: 705–713.

De Haan, C.A.M., Molinari, M., and Reggiori, F. 2010. Autophagy-independent LC3 function in vesicular traffic. *Autophagy* 6: 994–996.

Haldane, J.B.. 1943. New paths in genetics (London: George Allen and Inwin).

Hall, D.H., and Altun, Z.F. 2012. Handbook of C. elegans Anatomy. In WormAtlas.

Hamilton, B., Dong, Y., Shindo, M., Liu, W., Odell, I., Ruvkun, G., and Lee, S.S. 2005. A systematic RNAi screen for longevity genes in C. elegans. *Genes Dev.* 19: 1544–1555.

Hamilton, W.D. 1966. The moulding of senescence by natural selection. *J. Theor. Biol.* 12: 12–45.

Hansen, M., Chandra, A., Mitic, L.L., Onken, B., Driscoll, M., and Kenyon, C. 2008a. A Role for Autophagy in the Extension of Lifespan by Dietary Restriction in C. elegans. *PLoS Genet.* 4: e24.

Hansen, M., Chandra, A., Mitic, L.L., Onken, B., Driscoll, M., and Kenyon, C. 2008b. A Role for Autophagy in the Extension of Lifespan by Dietary Restriction in C. elegans. *PLoS Genet.* 4: e24.

Hara, T., Nakamura, K., Matsui, M., Yamamoto, A., Nakahara, Y., Suzuki-Migishima, R., Yokoyama, M., Mishima, K., Saito, I., Okano, H., et al. 2006. Suppression of basal autophagy in neural cells causes neurodegenerative disease in mice. *Nature* 441: 885–889.

Hars, E.S., Qi, H., Ryazanov, A.G., Jin, S., Cai, L., Hu, C., and Liu, L.F. 2007. Autophagy regulates ageing in C. elegans. *Autophagy* 3: 93–95.

Hashimoto, Y., Ookuma, S., and Nishida, E. 2009. Lifespan extension by suppression of autophagy genes in Caenorhabditis elegans. *Genes to Cells* 14: 717–726.

Haung Yu, W., Cuervo, A.M., Kumar, A., Peterhoff, C.M., Schmidt, S.D., Lee, J.H., Mohan, P.S., Mercken, M., Farmery, M.R., Tjernberg, L.O., et al. 2005. Macroautophagy - A novel beta-amyloid peptide-generating pathway activated in Alzheimer's disease. *J. Cell Biol.* 171: 87–98.

He, C., and Klionsky, D.J. 2009. Regulation mechanisms and signaling pathways of autophagy. *Annu. Rev. Genet.* 43: 67–93.

Hosokawa, N., Hara, T., Kaizuka, T., Kishi, C., Takamura, A., Miura, Y., Iemura, S., Natsume, T., Takehana, K., Yamada, N., et al. 2009. Nutrient-dependent mTORC1 Association with the ULK1 – Atg13 – FIP200 Complex Required for Autophagy. *Mol. Biol. Cell* 20: 1981–1991.

Huang, C., Xiong, C., Kornfeld, K., and Gordon, J.I. 2004. Measurements of Age-Related Changes of Physiological Processes That Predict Lifespan of Caenorhabditis elegans. *Source Proc. Natl. Acad. Sci. United States Am.* 101: 8084–8089.

Huang, C., Yitzhaki, S., Perry, C.N., Liu, W., Giricz, Z., Mentzer, R.M., and Gottlieb, R.A. 2010. Autophagy induced by ischemic preconditioning is essential for

cardioprotection. *J. Cardiovasc. Transl. Res.* 3: 365–373.

Hughes, K.A., and Reynolds, R.M. 2005. Evolutionary and mechanistic theories of aging. *Annu Rev Entomol* 50: 421–445.

Ichimura, Y., Kirisako, T., Takao, T., Satomi, Y., Shimonishi, Y., Ishihara, N., Mizushima, N., Tanida, I., Kominami, E., Ohsumi, M., et al. 2000. A ubiquitin-like system mediates protein lipidation. *Nature* 408: 488–492.

Itakura, E., and Mizushima, N. 2010. Characterization of autophagosome formation site by a hierarchical analysis of mammalian Atg proteins. *Autophagy* 6: 764–776.

Jenkins, N.L., McColl, G., and Lithgow, G.J. 2004. Fitness cost of extended lifespan in Caenorhabditis elegans. *Proc. R. Soc. B Biol. Sci.* 271: 2523–2526.

Jenzer, C., Manil-Ségalen, M., Lefebvre, C., Largeau, C., Glatigny, A., and Legouis, R. 2014. Human GABARAP can restore autophagosome biogenesis in a C. elegans lgg-1 mutant. *Autophagy* 10: 1868–1872.

Jia, K., and Levine, B. 2007. Autophagy is required for dietary restriction-mediated life span extension in C. elegans. *Autophagy* 3: 597–599.

Jin, C., Li, J., Green, C.D., Yu, X., Tang, X., Han, D., Xian, B., Wang, D., Huang, X., Cao, X., et al. 2011. Histone demethylase UTX-1 regulates C. elegans life span by targeting the insulin/IGF-1 signaling pathway. *Cell Metab.* 14: 161–172.

Johansen, T., and Lamark, T. 2011. Selective autophagy mediated by autophagic adapter proteins. *Autophagy* 7: 279–296.

Kamath, R.S., Fraser, A.G., Dong, Y., Poulin, G., Durbin, R., Gotta, M., Kanapin, A., Le Bot, N., Moreno, S., Sohrmann, M., et al. 2003. Systematic functional analysis of the Caenorhabditis elegans genome using RNAi. *Nature* 421: 231–237.

Kametaka, S., Matsuura, A., Wada, Y., and Ohsumi, Y. 1996. Structural and functional analyses of APG5, a gene involved in autophagy in yeast. *Gene* 178: 139–143.

Kametaka, S., Okano, T., Ohsumi, M., and Ohsumi, Y. 1998. Apg14p and Apg6/Vps30p form a protein complex essential for autophagy in the yeast, Saccharomyces cerevisiae. *J. Biol. Chem.* 273: 22284–22291.

Kang, C., You, N.J., and Avery, L. 2007. Dual roles of autophagy in the survival of Caenorhabditis elegans during starvation. *Genes Dev.* 21: 2161–2171.

Kaushik, S., and Cuervo, A.M. 2015. Proteostasis and aging. *Nat. Med.* 21: 1406–1415.

Kent, W.J., Zweig, A.S., Barber, G., Hinrichs, A.S., and Karolchik, D. 2010. BigWig and BigBed: Enabling browsing of large distributed datasets. *Bioinformatics* 26: 2204–2207.

Kiefer, J.C., Smith, P.A., and Mango, S.E. 2007. PHA-4/FoxA cooperates with TAM-1/TRIM to regulate cell fate restriction in the C. elegans foregut. *Dev. Biol.* 303: 611–624.

Kihara, A., Noda, T., Ishihara, N., and Ohsumi, Y. 2001. Two distinct Vps34 phosphatidylinositol 3-kinase complexes function in autophagy and carboxypeptidase y sorting in Saccharomyces cerevisiae. *J. Cell Biol.* 153: 519–530.

Kim, J., Dalton, V.M., Eggerton, K.P., Scott, S. V, and Klionsky, D.J. 1999. Apg7p/Cvt2p is required for the cytoplasm-to-vacuole targeting, macroautophagy, and peroxisome degradation pathways. *Mol. Biol. Cell* 10: 1337–1351.

Kim, J., Kundu, M., Viollet, B., and Guan, K.-L. 2011. AMPK and mTOR regulate autophagy through direct phosphorylation of Ulk1. *Nat. Cell Biol.* 13: 132–141.

Kimura, S., Noda, T., and Yoshimori, T. 2007. Dissection of the autophagosome maturation process by a novel reporter protein, tandem fluorescent-tagged LC3. *Autophagy* 3: 452–460.

Kirisako, T., Ichimura, Y., Okada, H., Kabeya, Y., Mizushima, N., Yoshimori, T., Ohsumi, M., Takao, T., Noda, T., and Ohsumi, Y. 2000. The reversible modification

regulates the membrane-binding state of Apg8/Aut7 essential for autophagy and the cytoplasm to vacuole targeting pathway. *J. Cell Biol.* 151: 263–275.

Klass, M.R. 1983. A method for the isolation of longevity mutants in the nematode Caenorhabditis elegans and initial results. *Mech. Ageing Dev.* 22: 279–286.

Klionsky, D., Agholme, L., Agnello, M., Agostinis, P., Aguirre-ghiso, J.A., Ahn, H.J., Ait-mohamed, O., Brown, E.J., Brumell, J.H., Brunetti-pierri, N., et al. 2016. Guidelines for the use and interpretation of assays for monitoring autophagy. *Autophagy* 8: 445–544.

Knöferle, J., Koch, J.C., Ostendorf, T., Michel, U., Planchamp, V., Vutova, P., Tönges, L., Stadelmann, C., Brück, W., Bähr, M., et al. 2010. Mechanisms of acute axonal degeneration in the optic nerve in vivo. *Proc. Natl. Acad. Sci. U. S. A.* 107: 6064–6069.

Komatsu, M., Waguri, S., Ueno, T., Iwata, J., Murata, S., Tanida, I., Ezaki, J., Mizushima, N., Ohsumi, Y., Uchiyama, Y., et al. 2005. Impairment of starvation-induced and constitutive autophagy in Atg7-deficient mice. *J. Cell Biol.* 169: 425–434.

Kulminski, A.M., He, L., Culminskaya, I., Loika, Y., Kernogitski, Y., Arbeev, K.G., Loiko, E., Arbeeva, L., Bagley, O., Duan, M., et al. 2016. Pleiotropic Associations of Allelic Variants in a 2q22 Region with Risks of Major Human Diseases and Mortality. *PLoS Genet.* 12:.

Kumsta, C., Chang, J.T., Schmalz, J., and Hansen, M. 2017. Hormetic heat stress and HSF-1 induce autophagy to improve survival and proteostasis in C. elegans. *Nat. Commun.* 8: 14337.

Lapierre, L.R., Gelino, S., Meléndez, A., and Hansen, M. 2011. Autophagy and lipid metabolism coordinately modulate life span in germline-less C. elegans. *Curr. Biol.* 21: 1507–1514.

Lapierre, L.R., De Magalhaes Filho, C.D., McQuary, P.R., Chu, C.-C., Visvikis, O., Chang,

J.T., Gelino, S., Ong, B., Davis, A.E., Irazoqui, J.E., et al. 2013. The TFEB orthologue HLH-30 regulates autophagy and modulates longevity in Caenorhabditis elegans. *Nat. Commun.* 4: 2267.

Larsen, K.E., Fon, E. a, Hastings, T.G., Edwards, R.H., and Sulzer, D. 2002. Methamphetamine-induced degeneration of dopaminergic neurons involves autophagy and upregulation of dopamine synthesis. *J. Neurosci.* 22: 8951–8960.

Law, F., Seo, J.H., Wang, Z., DeLeon, J.L., Bolis, Y., Brown, A., Zong, W.-X., Du, G., and E. Rocheleau, C. 2017. The VPS-34 PI3 kinase negatively regulates RAB-5 during endosome maturation. *J. Cell Sci.* [Epub ahea:

Lee, H.C., Kubo, T., Kono, N., Kage-Nakadai, E., Gengyo-Ando, K., Mitani, S., Inoue, T., and Arai, H. 2012. Depletion of mboa-7, an enzyme that incorporates polyunsaturated fatty acids into phosphatidylinositol (PI), impairs PI 3-phosphate signaling in Caenorhabditis elegans. *Genes to Cells* 17: 748–757.

Lee, I.H., Cao, L., Mostoslavsky, R., Lombard, D.B., Liu, J., Bruns, N.E., Tsokos, M., Alt, F.W., and Finkel, T. 2008. A role for the NAD-dependent deacetylase Sirt1 in the regulation of autophagy. *Proc. Natl. Acad. Sci.* 105: 3374–3379.

Lee, J.-A., and Gao, F.-B. 2009. Inhibition of autophagy induction delays neuronal cell loss caused by dysfunctional ESCRT-III in frontotemporal dementia. *J. Neurosci.* 29: 8506–8511.

Lee, J.-Y., Koga, H., Kawaguchi, Y., Tang, W., Wong, E., Gao, Y.-S., Pandey, U.B., Kaushik, S., Tresse, E., Lu, J., et al. 2010a. HDAC6 controls autophagosome maturation essential for ubiquitin-selective quality-control autophagy. *EMBO J.* 29: 969–980.

Lee, J.H., Budanov, A. V., Park, E.J., Birse, R., Kim, T.E., Perkins, G.A., Ocorr, K., Ellisman, M.H., Bodmer, R., Bier, E., et al. 2010b. Sestrin as a Feedback

Inhibitor of TOR That Prevents Age-Related Pathologies. *Science (80-.).* 327: 1223–1228.

Lehmann, M. 2008. Roles of the FOXA transcription factor Fork head in autophagic developmental cell death. *Autophagy* 4: 713–714.

Leiser, S.F., Begun, A., and Kaeberlein, M. 2011. HIF-1 modulates longevity and healthspan in a temperature-dependent manner. *Aging Cell* 10: 318–326.

Levine, B., and Klionsky, D.J. 2004. Development by self-digestion: Molecular mechanisms and biological functions of autophagy. *Dev. Cell* 6: 463–477.

Li, H., Handsaker, B., Wysoker, A., Fennell, T., Ruan, J., Homer, N., Marth, G., Abecasis, G., and Durbin, R. 2009. The Sequence Alignment/Map format and SAMtools. *Bioinformatics* 25: 2078–2079.

Li, W., Koutmou, K.S., Leahy, D.J., and Li, M. 2015. Systemic RNA Interference Deficiency-1 (SID-1) Extracellular Domain Selectively Binds Long Double-stranded RNA and Is Required for RNA Transport by SID-1. *J. Biol. Chem.* 290: 18904–18913.

Liao, Y., Smyth, G.K., and Shi, W. 2014. FeatureCounts: An efficient general purpose program for assigning sequence reads to genomic features. *Bioinformatics* 30: 923–930.

Liu, Y., Schiff, M., Czymmek, K., Tallóczy, Z., Levine, B., and Dinesh-Kumar, S.P. 2005. Autophagy regulates programmed cell death during the plant innate immune response. *Cell* 121: 567–577.

Love, M.I., Huber, W., and Anders, S. 2014. Moderated estimation of fold change and dispersion for RNA-seq data with DESeq2. *Genome Biol.* 15: 550.

Luckinbill, L.S., Arking, R., Clare, M.J., Cirocco, W.C., and Buck, S.A. 1984. Selection for delayed senescence in Drosophila melanogaster. *Evolution* 38: 996–1003.

Lynch, G., and Bi, X. 2003. Lysosomes and Brain Aging in Mammals. *Neurochem. Res.*

28: 1725–1734.

Madeo, F., Zimmermann, A., Maiuri, M.C., and Kroemer, G. 2015. Essential role for autophagy in life span extension. *J. Clin. Invest.* 125: 85–93.

Majeski, A.E., and Fred Dice, J. 2004. Mechanisms of chaperone-mediated autophagy. *Int. J. Biochem. Cell Biol.* 36: 2435–2444.

Manil-Ségalen, M., Lefebvre, C., Jenzer, C., Trichet, M., Boulogne, C., Satiat-Jeunemaitre, B., and Legouis, R. 2014. The C.elegans LC3 Acts Downstream of GABARAP to Degrade Autophagosomes by Interacting with the HOPS Subunit VPS39. *Dev. Cell* 28: 43–55.

Mari, M., Griffith, J., Rieter, E., Krishnappa, L., Klionsky, D.J., and Reggiori, F. 2010. An Atg9-containing compartment that functions in the early steps of autophagosome biogenesis. *J. Cell Biol.* 190: 1005–1022.

Mathew, R., Karantza-Wadsworth, V., and White, E. 2007. Role of autophagy in cancer. *Nat. Rev. Cancer* 7: 961–967.

Matsunaga, K., Morita, E., Saitoh, T., Akira, S., Ktistakis, N.T., Izumi, T., Noda, T., and Yoshimori, T. 2010. Autophagy requires endoplasmic reticulum targeting of the PI3-kinase complex via Atg14L. *J. Cell Biol.* 190: 511–521.

Matsuura, A., Tsukada, M., Wada, Y., and Ohsumi, Y. 1997. Apg1p, a novel protein kinase required for the autophagic process in Saccharomyces cerevisiae. *Gene* 192: 245–250.

Maures, T.J., Greer, E.L., Hauswirth, A.G., and Brunet, A. 2011. The H3K27 demethylase UTX-1 regulates C. elegans lifespan in a germline-independent, insulin-dependent manner. *Aging Cell* 10: 980–990.

Medawar, P.B. 1946. Old age and natural death. *Mod. Quart.* 2: 30–49.

Medawar, P.B. 1952. An unsolved problem of biology. *Evol. Heal. Dis.* 24.

Meléndez, A., Tallóczy, Z., Seaman, M., Eskelinen, E.-L., Hall, D.H., and Levine, B. 2003.

Autophagy genes are essential for dauer development and life-span extension in C. elegans. *Science* 301: 1387–1391.

Mizushima, N. 2005. The pleiotropic role of autophagy: from protein metabolism to bactericide. *Cell Death Differ.* 12 Suppl 2: 1535–1541.

Mizushima, N. 2007. Autophagy : process and function. *Genes Dev.* 21: 2861–2873.

Mizushima, N., Noda, T., and Ohsumi, Y. 1999. Apg16p is required for the function of the Apg12p-Apg5p conjugate in the yeast autophagy pathway. *EMBO J.* 18: 3888–3896.

Mizushima, N., Noda, T., Yoshimori, T., Tanaka, Y., Ishii, T., George, M.D., Klionsky, D.J., Ohsumi, M., and Ohsumi, Y. 1998. A protein conjugation system essential for autophagy. *Nature* 395: 395–398.

Morselli, E., Maiuri, M.C., Markaki, M., Megalou, E., Pasparaki, a, Palikaras, K., Criollo, a, Galluzzi, L., Malik, S. a, Vitale, I., et al. 2010. Caloric restriction and resveratrol promote longevity through the Sirtuin-1-dependent induction of autophagy. *Cell Death Dis.* 1: e10.

Mortimore, G.E., and Pösö, a R. 1987. Intracellular protein catabolism and its control during nutrient deprivation and supply. *Annu. Rev. Nutr.* 7: 539–564.

Mueller, L.D. 1987. Evolution of accelerated senescence in laboratory populations of Drosophila. *Proc. Natl. Acad. Sci. U S A* 84: 1974–1977.

Von Muhlinen, N., Thurston, T., Ryzhakov, G., Bloor, S., and Randow, F. 2010. NDP52, a novel autophagy receptor for ubiquitin-decorated cytosolic bacteria. *Autophagy* 6: 288–289.

Nagai, J., Lin, C.Y., and Sabour, M.P. 1995. Lines of mice selected for reproductive longevity. *Growth, Dev. Aging* 59: 79–91.

Nah, J., Yuan, J., and Jung, Y.-K. 2015. Autophagy in Neurodegenerative Diseases: From Mechanism to Therapeutic Approach. *Mol. Cells* 38: 381–389.

Nakagawa, I., Amano, A., Mizushima, N., Yamamoto, A., Yamaguchi, H., Kamimoto, T., Nara, A., Funao, J., Nakata, M., Tsuda, K., et al. 2004. Autophagy defends cells against invading group A Streptococcus. *Science* 306: 1037–1040.

Nakai, A., Yamaguchi, O., Takeda, T., Higuchi, Y., Hikoso, S., Taniike, M., Omiya, S., Mizote, I., Matsumura, Y., Asahi, M., et al. 2007. The role of autophagy in cardiomyocytes in the basal state and in response to hemodynamic stress. *Nat Med* 13: 619–624.

Nazio, F., Strappazzon, F., Antonioli, M., Bielli, P., Cianfanelli, V., Bordi, M., Gretzmeier, C., Dengjel, J., Piacentini, M., Fimia, G.M., et al. 2013. mTOR inhibits autophagy by controlling ULK1 ubiquitylation, self-association and function through AMBRA1 and TRAF6. *Nat. Cell Biol.* 15: 406–416.

Ni, Z., and Lee, S.S. 2010. RNAi screens to identify components of gene networks that modulate aging in Caenorhabditis elegans. *Briefings Funct. Genomics Proteomics* 9: 53–64.

Nixon, R.A. 2013. The role of autophagy in neurodegenerative disease. *Nat Med* 19: 983–997.

Noda, T., Kim, J., Huang, W.P., Baba, M., Tokunaga, C., Ohsumi, Y., and Klionsky, D.J. 2000. Apg9p/Cvt7p is an integral membrane protein required for transport vesicle formation in the Cvt and autophagy pathways. *J. Cell Biol.* 148: 465–479.

Noda, T., and Ohsumi, Y. 1998. Tor, a phosphatidylinositol kinase homologue, controls autophagy in yeast. *J. Biol. Chem.* 273: 3963–3966.

Ogata, M., Hino, S., Saito, A., Kondo, S., Kanemoto, S., Taniguchi, M., Tanii, I., Shiosaka, S., Hammarback, J. a, Morikawa, K., et al. 2006. Autophagy Is Activated for Cell Survival after Endoplasmic Reticulum Stress Autophagy Is Activated for Cell Survival after Endoplasmic Reticulum Stress □. *Mol. Cell. Biol.*

24: 9220–9231.

Ogawa, M., Yoshimori, T., Suzuki, T., Sagara, H., Mizushima, N., and Sasakawa, C. 2005. Escape of intracellular Shigella from autophagy. *Science* 307: 727–731.

Onken, B., and Driscoll, M. 2010. Metformin induces a dietary restriction-like state and the oxidative stress response to extend C. elegans healthspan via AMPK, LKB1, and SKN-1. *PLoS One* 5:.

Palmisano, N.J., and Meléndez, A. 2016. Detection of autophagy in Caenorhabditis elegans using GFP::LGG-1 as an autophagy marker. *Cold Spring Harb. Protoc.* 2016: 68–75.

Panowski, S.H., Wolff, S., Aguilaniu, H., Durieux, J., and Dillin, A. 2007a. PHA-4/Foxa mediates diet-restriction-induced longevity of C. elegans. *Nature* 447: 550–555.

Panowski, S.H., Wolff, S., Aguilaniu, H., Durieux, J., and Dillin, A. 2007b. PHA-4/Foxa mediates diet-restriction-induced longevity of C. elegans. *Nature* 447: 550–555.

Partridge, L., Fowler, K., Sgrò, C.M., Geddes, G., As, F., and Response, A.C. 2000. Selection on age at reproduction in Drosophila melanogaster: female mating frequency as a correlated response. *Evolution (N. Y).* 54: 2152–2155.

Pattingre, S., Tassa, A., Qu, X., Garuti, R., Xiao, H.L., Mizushima, N., Packer, M., Schneider, M.D., and Levine, B. 2005. Bcl-2 antiapoptotic proteins inhibit Beclin 1-dependent autophagy. *Cell* 122: 927–939.

Pyo, J.-O., Yoo, S.-M., Ahn, H.-H., Nah, J., Hong, S.-H., Kam, T.-I., Jung, S., and Jung, Y.-K. 2013. Overexpression of Atg5 in mice activates autophagy and extends lifespan. *Nat. Commun.* 4:.

Qadota, H., Inoue, M., Hikita, T., Köppen, M., Hardin, J.D., Amano, M., Moerman, D.G., and Kaibuchi, K. 2007. Establishment of a tissue-specific RNAi system in C.

elegans. *Gene* 400: 166–173.

Quinlan, A.R., and Hall, I.M. 2010. BEDTools: A flexible suite of utilities for comparing genomic features. *Bioinformatics* 26: 841–842.

Rauser, C., and Mueller, L. 2009. Evolution of aging and late life. *… Evol.* 551–584.

Rauser, C.L., Tierney, J.J., Gunion, S.M., Covarrubias, G.M., Mueller, L.D., and Rose, M.R. 2006. Evolution of late-life fecundity in Drosophila melanogaster. *J. Evol. Biol.* 19: 289–301.

Ravikumar, B., Vacher, C., Berger, Z., Davies, J.E., Luo, S., Oroz, L.G., Scaravilli, F., Easton, D.F., Duden, R., O'Kane, C.J., et al. 2004. Inhibition of mTOR induces autophagy and reduces toxicity of polyglutamine expansions in fly and mouse models of Huntington disease. *Nat. Genet.* 36: 585–595.

Reggiori, F., Tucker, K.A., Stromhaug, P.E., and Klionsky, D.J. 2004. The Atg1-Atg13 complex regulates Atg9 and Atg23 retrieval transport from the pre-autophagosomal structure. *Dev. Cell* 6: 79–90.

Rodríguez, J.A., Marigorta, U.M., Hughes, D.A., Spataro, N., Bosch, E., and Navarro, A. 2017. Antagonistic pleiotropy and mutation accumulation influence human senescence and disease. *Nat. Ecol. Evol.* 1: 55.

Roggo, L., Bernard, V., Kovacs, A.L., Rose, A.M., Savoy, F., Zetka, M., Wymann, M.P., and Müller, F. 2002. Membrane transport in Caenorhabditis elegans: An essential role for VPS34 at the nuclear membrane. *EMBO J.* 21: 1673–1683.

Rose, M., and Charlesworth, B. 1980. A Test of Evolutionary Theories of Senescence. *Nature* 287: 141–142.

Rose, M.R. 1982. Antagonistic pleiotropy, dominance, and genetic variation. *Heredity (Edinb).* 48: 63–78.

Rose, M.R. 1984. Laboratory Evolution of Postponed Senescence in Drosophila melanogaster. *Evolution (N. Y).* 38: 1004–1010.

Rose, M.R. 1985. Life history evolution with antagonistic pleiotropy and overlapping generations. *Theor. Popul. Biol.* 28: 342–358.

Rose, M.R., Burke, M.K., Shahrestani, P., and Mueller, L.D. 2008. Evolution of ageing since Darwin. *J. Genet.* 87: 363–371.

Rose, M.R., and Charlesworth, B. 1981. Genetics of life history in Drosophila melanogaster. II. Exploratory selection experiments. *Genetics* 97: 187–196.

Rose, M.R., Drapeau, M.D., Yazdi, P.G., Shah, K.H., Moise, D.B., Thakar, R.R., Rauser, C.L., and Mueller, L.D. 2002. Evolution of late-life mortality in Drosophila melanogaster. *Evolution* 56: 1982–1991.

Rose, M.R., Rauser, C.L., Benford, G., Matos, M., and Mueller, L.D. 2007. Hamilton's forces of natural selection after forty years. *Evolution (N. Y).* 61: 1265–1276.

Del Roso, A., Vittorini, S., Cavallini, G., Donati, A., Gori, Z., Masini, M., Pollera, M., and Bergamini, E. 2003. Ageing-related changes in the in vivo function of rat liver macroautophagy and proteolysis. *Exp. Gerontol.* 38: 519–527.

Roth, B.L., Poot, M., Yue, S.T., and Millard, P.J. 1997. Bacterial viability and antibiotic susceptibility testing with SYTOX green nucleic acid stain. *Appl. Environ. Microbiol.* 63: 2421–2431.

Rual, J.F., Ceron, J., Koreth, J., Hao, T., Nicot, A.S., Hirozane-Kishikawa, T., Vandenhaute, J., Orkin, S.H., Hill, D.E., van den Heuvel, S., et al. 2004. Toward improving Caenorhabditis elegans phenome mapping with an ORFeome-based RNAi library. *Genome Res.* 14: 2162–2168.

Rubinsztein, D.C., Mariño, G., and Kroemer, G. 2011. Autophagy and aging. *Cell* 146: 682–695.

Ruck, A., Attonito, J., Garces, K.T., Núnez, L., Palmisano, N.J., Rubel, Z., Bai, Z., Nguyen, K.C.Q., Sun, L., Grant, B.D., et al. 2011. The Atg6/Vps30/Beclin 1 ortholog BEC-1 mediates endocytic retrograde transport in addition to autophagy in C.

elegans. *Autophagy* 7: 386–400.

Russell, R.C., Tian, Y., Yuan, H., Park, H.W., Chang, Y.-Y., Kim, J., Kim, H., Neufeld, T.P., Dillin, A., and Guan, K.-L. 2013. ULK1 induces autophagy by phosphorylating Beclin-1 and activating VPS34 lipid kinase. *Nat. Cell Biol.* 15: 741–750.

Rutz, M., Metzger, J., Gellert, T., Luppa, P., Lipford, G.B., Wagner, H., and Bauer, S. 2004. Toll-like receptor 9 binds single-stranded CpG-DNA in a sequence- and pH-dependent manner. *Eur. J. Immunol.* 34: 2541–2550.

Sadasivan, S., Zhang, Z., Larner, S.F., Liu, M.C., Zheng, W., Kobeissy, F.H., Hayes, R.L., and Wang, K.K.W. 2010. Acute NMDA toxicity in cultured rat cerebellar granule neurons is accompanied by autophagy induction and late onset autophagic cell death phenotype. *BMC Neurosci.* 11: 21.

Sanchez-Varo, R., Trujillo-Estrada, L., Sanchez-Mejias, E., Torres, M., Baglietto-Vargas, D., Moreno-Gonzalez, I., De Castro, V., Jimenez, S., Ruano, D., Vizuete, M., et al. 2012. Abnormal accumulation of autophagic vesicles correlates with axonal and synaptic pathology in young Alzheimer's mice hippocampus. *Acta Neuropathol.* 123: 53–70.

Schmid, D., and Münz, C. 2007. Innate and Adaptive Immunity through Autophagy. *Immunity* 27: 11–21.

Schmid, D., Pypaert, M., and Münz, C. 2007. Antigen-Loading Compartments for Major Histocompatibility Complex Class II Molecules Continuously Receive Input from Autophagosomes. *Immunity* 26: 79–92.

Scott, R.C., Schuldiner, O., and Neufeld, T.P. 2004. Role and regulation of starvation-induced autophagy in the Drosophila fat body. *Dev. Cell* 7: 167–178.

Settembre, C., Di Malta, C., Polito, V.A., Garcia Arencibia, M., Vetrini, F., Erdin, S., Erdin, S.U., Huynh, T., Medina, D., Colella, P., et al. 2011. TFEB links autophagy to lysosomal biogenesis. *Science* 332: 1429–1433.

Shaner, N.C., Steinbach, P.A., and Tsien, R.Y. 2005. A guide to choosing fluorescent proteins. *Nat. Methods* 2: 905–909.

Sheaffer, K.L., Updike, D.L., Mango, S.E., Friedman, J.R., Kaestner, K.H., Panowski, S.H., Wolff, S., Aguilaniu, H., Durieux, J., Dillin, A., et al. 2008a. The Target of Rapamycin pathway antagonizes pha-4/FoxA to control development and aging. *Curr. Biol.* 18: 1355–1364.

Sheaffer, K.L., Updike, D.L., Mango, S.E., Friedman, J.R., Kaestner, K.H., Panowski, S.H., Wolff, S., Aguilaniu, H., Durieux, J., Dillin, A., et al. 2008b. The Target of Rapamycin pathway antagonizes pha-4/FoxA to control development and aging. *Curr. Biol.* 18: 1355–1364.

Shintani, T., and Klionsky, D.J. 2004. Autophagy in health and disease: a double-edged sword. *Science* 306: 990–995.

Shintani, T., Mizushima, N., Ogawa, Y., Matsuura, A., Noda, T., and Ohsumi, Y. 1999. Apg10p, a novel protein-conjugating enzyme essential for autophagy in yeast. *EMBO J.* 18: 5234–5241.

Shintani, T., Suzuki, K., Kamada, Y., Noda, T., and Ohsumi, Y. 2001. Apg2p Functions in Autophagosome Formation on the Perivacuolar Structure. *J. Biol. Chem.* 276: 30452–30460.

Simmer, F., Tijsterman, M., Parrish, S., Koushika, S.P., Nonet, M.L., Fire, A., Ahringer, J., and Plasterk, R.H.A. 2002. Loss of the putative RNA-directed RNA polymerase RRF-3 makes C. elegans hypersensitive to RNAi. *Curr. Biol.* 12: 1317–1319.

Simonsen, A., Cumming, R.C., Brech, A., Isakson, P., Schubert, D.R., and Finley, K.D. 2008. Promoting basal levels of autophagy in the nervous system enhances longevity and oxidant resistance in adult Drosophila. *Autophagy* 4: 176–184.

Sokal, R.R. 1970. Senescence and Genetic Load: Evidence from Tribolium. *Science* 167:

1733–1734.

Stack, J.H., Herman, P.K., Schu, P. V, and Emr, S.D. 1993. A MEMBRANE-ASSOCIATED COMPLEX CONTAINING THE VPS15 PROTEIN-KINASE AND THE VPS34 PI 3-KINASE IS ESSENTIAL FOR PROTEIN SORTING TO THE YEAST LYSOSOME-LIKE VACUOLE. *Embo J.* 12: 2195–2204.

Stephan, J.S., Yeh, Y.-Y., Ramachandran, V., Deminoff, S.J., and Herman, P.K. 2009. The Tor and PKA signaling pathways independently target the Atg1/Atg13 protein kinase complex to control autophagy. *Proc. Natl. Acad. Sci. U. S. A.* 106: 17049–17054.

Sun, T., Wang, X., Lu, Q., Ren, H., and Zhang, H. 2011. CUP-5, the C. elegans ortholog of the mammalian lysosomal channel protein MLN1/TRPML1, is required for proteolytic degradation in autolysosomes. *Autophagy* 7: 1308–1315.

Suzuki, K., Kubota, Y., Sekito, T., and Ohsumi, Y. 2007. Hierarchy of Atg proteins in pre-autophagosomal structure organization. *Genes to Cells* 12: 209–218.

Tabara, H., Sarkissian, M., Kelly, W.G., Fleenor, J., Grishok, A., Timmons, L., Fire, A., and Mello, C.C. 1999. The rde-1 gene, RNA interference, and transposon silencing in C. elegans. *Cell* 99: 123–132.

Takacs-Vellai, K., Vellai, T., Puoti, A., Passannante, M., Wicky, C., Streit, A., Kovacs, A.L., and Müller, F. 2005. Inactivation of the autophagy Gene bec-1 triggers apoptotic cell death in C. elegans. *Curr. Biol.* 15: 1513–1517.

Tanida, I., Minematsu-Ikeguchi, N., Ueno, T., and Kominami, E. 2005. Lysosomal turnover, but not a cellular level, of endogenous LC3 is a marker for autophagy. *Autophagy* 1: 84–91.

Tanida, I., Tanida-Miyake, E., Komatsu, M., Ueno, T., and Kominami, E. 2002. Human Apg3p/Aut1p homologue is an authentic E2 enzyme for multiple substrates, GATE-16, GABARAP, and MAP-LC3, and facilitates the conjugation of hApg12p

to hApg5p. *J. Biol. Chem.* 277: 13739–13744.

Terman, A. 1995. The effect of age on formation and elimination of autophagic vacuoles in mouse hepatocytes. *Gerontology* 41: 319–326.

The C. elegans Sequencing Consortium 1998. Genome sequence of the nematode C. elegans: a platform for investigating biology. *Science (80-.).* 282: 2012–2018.

Tian, Y., Li, Z., Hu, W., Ren, H., Tian, E., Zhao, Y., Lu, Q., Huang, X., Yang, P., Li, X., et al. 2010. C. elegans Screen Identifies Autophagy Genes Specific to Multicellular Organisms. *Cell* 141: 1042–1055.

Timmons, L., Court, D.L., and Fire, A. 2001. Ingestion of bacterially expressed dsRNAs can produce specific and potent genetic interference in Caenorhabditis elegans. *Gene* 263: 103–112.

Tischler, J., Lehner, B., Chen, N., and Fraser, A.G. 2006. Combinatorial RNA interference in Caenorhabditis elegans reveals that redundancy between gene duplicates can be maintained for more than 80 million years of evolution. *Genome Biol.* 7: R69.

Toth, M.L., Sigmond, T., Borsos, E., Barna, J., Erdelyi, P., Takacs-Vellai, K., Orosz, L., Kovacs, A.L., Csikos, G., Sass, M., et al. 2008. Longevity pathways converge on autophagy genes to regulate life span in Caenorhabditis elegans. *Autophagy* 4: 330–338.

Tsukada, M., and Ohsumi, Y. 1993. Isolation and characterization of autophagy-defective mutants of Saccharomyces cerevisiae. *FEBS Lett.* 333: 169–174.

Uno, M., and Nishida, E. 2016. Lifespan-regulating genes in C. elegans. *Npj Aging Mech. Dis.* 2: 16010.

Viscomi, M.T., and D'Amelio, M. 2012. The 'Janus-Faced Role' of Autophagy in Neuronal Sickness: Focus on Neurodegeneration. *Mol. Neurobiol.* 46: 513–521.

Van Voorhies, W.A., Curtsinger, J.W., and Rose, M.R. 2006. Do longevity mutants

always show trade-offs? *Exp. Gerontol.* 41: 1055–1058.

Van Voorhies, W.A., and Ward, S. 1999. Genetic and environmental conditions that increase longevity in Caenorhabditis elegans decrease metabolic rate. *P. Nat. Acad. Sci. USA* 96: 11399–11403.

Wählby, C., Kamentsky, L., Liu, Z.H., Riklin-Raviv, T., Conery, A.L., O'Rourke, E.J., Sokolnicki, K.L., Visvikis, O., Ljosa, V., Irazoqui, J.E., et al. 2012. An image analysis toolbox for high-throughput C. elegans assays. *Nat. Methods* 9: 714–716.

Walther, D.M., Kasturi, P., Zheng, M., Pinkert, S., Vecchi, G., Ciryam, P., Morimoto, R.I., Dobson, C.M., Vendruscolo, M., Mann, M., et al. 2015. Widespread proteome remodeling and aggregation in aging C. elegans. *Cell* 161: 919–932.

Wang, C.W., Kim, J., Huang, W.P., Abeliovich, H., Stromhaug, P.E., Dunn, W.A., and Klionsky, D.J. 2001. Apg2 Is a Novel Protein Required for the Cytoplasm to Vacuole Targeting, Autophagy, and Pexophagy Pathways. *J. Biol. Chem.* 276: 30442–30451.

Wang, Q.J., Ding, Y., Kohtz, D.S., Mizushima, N., Cristea, I.M., Rout, M.P., Chait, B.T., Zhong, Y., Heintz, N., and Yue, Z. 2006. Induction of autophagy in axonal dystrophy and degeneration. *J Neurosci* 26: 8057–8068.

Wang, T., Lao, U., and Edgar, B.A. 2009. TOR-mediated autophagy regulates cell death in Drosophila neurodegenerative disease. *J. Cell Biol.* 186: 703–711.

Wang, Z., Miao, G., Xue, X., Guo, X., Yuan, C., Wang, Z., Zhang, G., Chen, Y., Feng, D., Hu, J., et al. 2016. The Vici Syndrome Protein EPG5 Is a Rab7 Effector that Determines the Fusion Specificity of Autophagosomes with Late Endosomes/Lysosomes. *Mol. Cell* 63: 781–795.

Wattiaux, J.M. 1968a. Cumulative Parental Age Effects in Drosophila subobscura. *Evolution (N. Y).* 22: 406–421.

Wattiaux, J.M. 1968b. Parental age effects in Drosophila pseudoobscura. *Exp. Gerontol.* 3: 55–61.

Wei, Y., Pattingre, S., Sinha, S., Bassik, M., and Levine, B. 2008. JNK1-Mediated Phosphorylation of Bcl-2 Regulates Starvation-Induced Autophagy. *Mol. Cell* 30: 678–688.

Weismann, A. 1891. Essays Upon Heredity and Kindred Biological Problems. *Oxford Clarendon Press* 1: 1–5.

Williams, G.C. 1957. Pleiotropy, Natural Selection, and the Evolution of Senescence. *Evolution (N. Y).* 11: 398–411.

Winston, W.M. 2002. Systemic RNAi in C. elegans Requires the Putative Transmembrane Protein SID-1. *Science (80-.).* 295: 2456–2459.

Wong, E., and Cuervo, A.M. 2010. Autophagy gone awry in neurodegenerative diseases. *Nat. Neurosci.* 13: 805–811.

Yamamoto, H., Kakuta, S., Watanabe, T.M., Kitamura, A., Sekito, T., Kondo-Kakuta, C., Ichikawa, R., Kinjo, M., and Ohsumi, Y. 2012. Atg9 vesicles are an important membrane source during early steps of autophagosome formation. *J. Cell Biol.* 198: 219–233.

Yang, P., and Zhang, H. 2011. The coiled-coil domain protein EPG-8 plays an essential role in the autophagy pathway in C. elegans. *Autophagy* 7: 159–165.

Yang, Y., Fukui, K., Koike, T., and Zheng, X. 2007. Induction of autophagy in neurite degeneration of mouse superior cervical ganglion neurons. *Eur. J. Neurosci.* 26: 2979–2988.

Yorimitsu, T., Zaman, S., Broach, J.R., and Klionsky, D.J. 2007. Protein Kinase A and Sch9 Cooperatively Regulate Induction of Autophagy in Saccharomyces cerevisiae. *Mol. Biol. Cell* 18: 4180–4189.

Yu, L., Wan, F., Dutta, S., Welsh, S., Liu, Z., Freundt, E., Baehrecke, E.H., and Lenardo,

M. 2006. Autophagic programmed cell death by selective catalase degradation. *Proc. Natl. Acad. Sci. U. S. A.* 103: 4952–4957.

Zhang, X., Li, L., Chen, S., Yang, D., Wang, Y., Zhang, X., Wang, Z., and Le, W. 2011. Rapamycin treatment augments motor neuron degeneration in SOD1(G93A) mouse model of amyotrophic lateral sclerosis. *Autophagy* 7: 412–425.

Zhang, Y., Yan, L., Zhou, Z., Yang, P., Tian, E., Zhang, K., Zhao, Y., Li, Z., Song, B., Han, J., et al. 2009. SEPA-1 Mediates the Specific Recognition and Degradation of P Granule Components by Autophagy in C. elegans. *Cell* 136: 308–321.

Zhong, M., Niu, W., Lu, Z.J., Sarov, M., Murray, J.I., Janette, J., Raha, D., Sheaffer, K.L., Lam, H.Y.K., Preston, E., et al. 2010. Genome-Wide Identification of Binding Sites Defines Distinct Functions for Caenorhabditis elegans PHA-4/FOXA in Development and Environmental Response. *PLoS Genet.* 6: e1000848.

Curriculum Vitae